NATIONAL ADVISORY COMMITTEE FOR AERONAUTICS

TECHNICAL NOTE

No. 1144

MEASUREMENTS OF THE PRESSURE DISTRIBUTION ON THE HORIZONTAL-TAIL SURFACE OF A TYPICAL PROPELLER-DRIVEN PURSUIT AIRPLANE IN FLIGHT

I - EFFECTS OF COMPRESSIBILITY IN STEADY STRAIGHT AND ACCELERATED FLIGHT

By Melvin Sadoff, William N. Turner, and Lawrence A. Clousing

Ames Aeronautical Laboratory
Moffett Field, Calif.

Washington

July 1947

NATIONAL ADVISORY COMMITTEE FOR AERONAUTICS

TECHNICAL NOTE NO. 1144

MEASUREMENTS OF THE PRESSURE DISTRIBUTION ON THE HORIZONTAL-TAIL SURFACE OF A TYPICAL PROPELLER-DRIVEN PURSUIT AIRPLANE IN FLIGHT

I - EFFECTS OF COMPRESSIBILITY IN STEADY STRAIGHT AND ACCELERATED FLIGHT

By Melvin Sadoff, William N. Turner, and Lawrence A. Clousing

SUMMARY

Pressure-distribution measurements were made in steady straight and accelerated flight over both sides of the horizontal-tail surface of a typical pursuit airplane up to a Mach number of 0.79. The results showed that a sharply increasing down-load was required to balance the increased diving moment of the wing-fuselage-propeller group at Mach numbers above about 0.70. There was little change, up to a Mach number of 0.65, of the tail-load gradient (rate of increase of tail load for a unit change in accelelation factor); beyond that Mach number, however, a rapid decrease of tail-load gradient to a Mach number of about 0.73 and then a very sharp increase up to a Mach number of 0.785 was noted. The root bending moments increased considerably on the right tail and decreased, to a lesser extent, on the left tail at the higher Mach numbers, resulting in increased fuselage torsional moments at high speeds. At the higher values of lift coefficient (0.5 to 0.8), there was little change of the lateral distance to the center of pressure up to a Mach number of about 0.73; at the highest speed and at low lift coefficients (0 to 0.1) the center of pressure was inboard approximately 3 feet on the left tail and 1.5 feet on the right tail as compared with the values at lower speeds. It appears that satisfactory quantitative data on total tail loads may be obtained from measurements at four stations, equally spaced along the entire tail span.

A comparison of experimental results with the calculated horizontal-tail loading, using modified current Army specifications, showed that the calculated compressibility corrections were small and, except at the critical down-load conditions, could be neglected. Because the variations in the tail-off moment coefficient at zero lift and in airplane stability were not predicted accurately by modified current methods at the higher Mach numbers, the computed tail loads, which showed good agreement with the experimental loads at lower speeds, failed to predict the changes in actual loading at the higher Mach numbers. The calculated root bending moments were unconservative as compared with the experimental values over most of the speed range except at the highest speeds where the actual center of pressure on the left and

right tail moved inboard of the calculated value. The calculated asymmetric loads and fuselage torsional moments were conservative as compared with the experimental values. The specified chordwise distribution of the balancing tail loads over the horizontal-tail surface was considerably in error under certain conditions, because the actual section angle of attack (contrary to what was assumed) was not constant across the tail span, and because the elevator angle was not taken into account in distributing the chordwise loads.

INTRODUCTION

Structural failures of the horizontal-tail surfaces of high-speed military aircraft have occurred recently, raising the question of whether current design requirements are adequate for predicting the maximum horizontal-tail loads that are likely to be encountered in flight.

To provide data as a basis for possible revision of existing design requirements, pressure-distribution measurements were made on the horizontal-tail surface of a representative pursuit-type airplane during various types of maneuvers in which it was thought critical loading conditions on the tail might be obtained.

This report, the first of several reports on horizontal-tail loads in steady straight and accelerated flight, sideslips, and abrupt maneuvers, covers the tail loads in steady straight and accelerated flight over a range of speeds, including those where compressibility effects may become important. The tail loading calculated according to slightly modified, current design requirements is compared with the experimental results, and an attempt is made to point out where and why the application of these requirements results in failure of the designer to predict the actual loads and their distribution over the horizontal-tail surface.

SYMBOLS

The symbols used in this report are as follows:

b_t horizontal-tail span, feet

M_r root bending moment (positive when clockwise as seen from the rear), foot-pounds

c local tail chord, feet

$\bar{c}$ wing mean aerodynamic chord, feet

$c_n c$ section load modulus, feet

d propeller diameter, feet

D wing drag, pounds

H free-stream total pressure

h_p pressure altitude, feet

l_t tail length (distance from airplane c.g. to one-third maximum chord point of tail), feet

M free-stream Mach number

M_p pitching moment (stalling moment is positive), foot-pounds

M_T torsional moment on fuselage due to horizontal-tail loading (positive when moment is clockwise as seen from rear), pound-feet

N_t air load on horizontal tail (positive when load is acting upward), pounds

p free-stream static pressure

p_o standard atmospheric pressure at sea level

p_l pressure on lower surface, pounds per square foot

p_u pressure on upper surface, pounds per square foot

P_{RES} resultant pressure coefficient, $[(p_l - p_u)/q]$

q free-stream dynamic pressure, pounds per square foot

S horizontal-surface area, square feet

T propeller thrust, pounds

V true airspeed, miles per hour

V_i correct indicated airspeed, miles per hour

W average airplane weight during test run, pounds

x horizontal distance from center of gravity to aerodynamic center of wing (positive when c.g. is aft of a.c. of wing), percent M.A.C.

x' horizontal distance from center of gravity to propeller plane (positive when c.g. is aft of propeller plane), feet

z vertical distance from center of gravity to aerodynamic center of wing (positive when c.g. is below a.c. of wing), percent M.A.C.

z' vertical distance from center of gravity to thrust line (positive when c.g. is above thrust line), feet

β sideslip angle (positive when right wing is forward), degrees

δ_e elevator angle (positive when trailing edge is down), degrees from thrust axis

ρ air density, slugs per cubic foot

C_L airplane lift coefficient (WA_Z/qS_w)

A_Z the ratio of the net aerodynamic force along the airplane Z-axis (positive when directed upward) to the weight of the airplane

C_{M_r} root bending-moment coefficient (M_r/qS_tb_t)

C_{D_w} wing drag coefficient (D/qS_w)

C_{M_p} pitching-moment coefficient $(M_p/qS_w\bar{c})$

$C_{M_{p_F}}$ fuselage pitching-moment coefficient

$$\left(\frac{\text{fuselage pitching moment}}{qS_w\bar{c}}\right)$$

$C_{M_{p_{NFP}}}$ pitching-moment coefficient due to normal force on propeller

$$\left(\frac{\text{pitching moment due to normal force on propeller}}{qS_w\bar{c}}\right)$$

C_{M_T} torsional-moment coefficient $(M_T/qS_t v_t)$, $(C_{M_{r_L}} + C_{M_{r_R}})$

C_{N_t} tail normal-force coefficient (N_t/qS_t)

T_c propeller-thrust coefficient $(T/\rho V^2 d^2)$

c_n section normal-force coefficient

$$\left(\frac{\text{tail-section normal force}}{qc} \right)$$

Subscripts

a-t airplane minus tail

L left

R right

o zero lift

t tail

w wing

DESCRIPTION OF AIRPLANE

The test airplane is a single-place, single-engine, interceptor-pursuit, low-wing monoplane driven by a tractor propeller and equipped with a retractable tricycle landing gear. Figures 1 and 2 are photographs of the airplane as instrumented for the flight tests. Figure 3 is a three-view drawing showing the general layout of the airplane. The specifications of the test airplane are as follows:

Airplane, general

Span	34.0 ft
Length	30.17 ft
Height	9.27 ft

Horizontal tail

Span	13.0 ft
Area	40.99 sq ft
Airfoil section	NACA approx. 0010 to 0006 (fig. 4)

Stabilizer setting (relative to the airplane longitudinal axis . 2.25°

Elevator area (including 4.3 sq ft of overhang balance) . . 16.89 sq ft

Nominal deflection	35° up, 15° down

Wing

Airfoil section, root	NACA 0015
Airfoil section, tip	NACA 23009
Area, total, including ailerons and section projected through fuselage	213.22 sq ft
Angle of incidence at root (relative to airplane longitudinal axis)	2.0°
Geometric washout	approx. 0.7°
Taper ratio	1.97:1
Mean aerodynamic chord	6.72 ft

Weight

Normal gross	7629 lb
As flown	7720 to 7340 lb

Center-of-gravity positions

Horizontal

Most forward design, gear up	0.232 M.A.C.
Normal gross weight, gear up	0.285 M.A.C.
As flown, gear up	0.303 M.A.C.

Vertical

Most forward design, gear up	0.106 M.A.C.
Normal gross weight, gear up	0.077 M.A.C.
As flown, gear up (approx.)	0.067 M.A.C.

Engine

Type . . . . . Allison, V-1710-85

Ratings, without ram:

	bhp	Manifold pressure (in. Hg)	rpm	Altitude (ft)	Time limit (min)
Take-off	1200	51.5	3000	Sea level	5
Military	1125	44.5	3000	15,500	15
Normal	1000	39.0	2600	14,000	None

Engine-propeller speed ratio 2.23:1

Propeller

Diameter . . . . . 11.58 ft
Type . . . . . Three-blade hollow-steel selective automatic pitch
Blade model A-20-156-17
Maximum pitch limits . . . . . 28° to 63°
Direction of rotation, as seen by pilot . . . . . Clockwise

The horizontal tail of the test airplane was not a production type as extra ribs were placed in the elevators to permit rigid installation of the orifices at the desired stations, and doubler plates were installed in the lower stabilizer surface to reinforce cutouts necessary for the installation of the orifices. Figure 5 is a simplified pictorial drawing showing the added reinforcing features in the horizontal tail of the test airplane.

INSTRUMENTATION

Standard NACA photographically recording instruments were used to measure, as a function of time, the following variables: indicated airspeed; pressure altitude; normal acceleration; engine manifold pressure; engine speed; angle of sideslip; rolling, yawing, and pitching velocities; elevator, aileron, and rudder positions and control forces; and resultant pressure distribution on the left and right horizontal-tail surfaces.

A freely swiveling airspeed head was mounted on the end of a boom extending approximately one chord length ahead of the leading edge of the right wing and located at a spanwise station about 7 feet inboard of

the wing tip. The recording static head was calibrated for position error by comparing the altitude-recorder readings with the known pressure altitude as the airplane was flown past a reference height at several speeds. The measured total pressure was assumed to be correct. As used in this report, indicated airspeed was computed from the formula by which standard airspeed meters are graduated. The formula, which gives true airspeed at standard sea-level conditions, may be written as follows:

$$V_i = 1703 \left[\left(\frac{H - p}{p_o} + 1 \right)^{0.286} - 1 \right]^{1/2}$$

A 60-cell pressure recorder, located in the rear section of the fuselage between the oil tank and the baggage compartment, was used to measure the resultant pressures over the horizontal tail at the locations listed in table I and shown in figure 6. In order to obtain accurate resultant pressures (the algebraic difference of the pressures at the bottom and top surfaces), the orifices were located, as nearly as structural details permitted, one above the other on a line perpendicular to the chord plane of the tail plane.

PRECISION

The precision with which the various quantities were believed to be measured in the tests is indicated in the following table:

Item	Estimated precision
Normal acceleration	±0.05g
Elevator angle	±.50°
Sideslip angle	±1.0°
Airspeed (to 200 mph)	±2½ percent
(above 200 mph)	±1½ percent
Altitude	±300 ft
Tail load (low speeds, unaccelerated flight)	±50 lb
(high speed, accelerated flight)	±100 lb

The pertinent pressure-measuring instruments were the airspeed recorder, the altitude recorder, and the multiple-cell manometer. The errors inherent in these pressure-measuring devices, and the possible sources of error in obtaining loads and moments from pressure-distribution measurements are discussed fully in reference 1. Other possible sources of error considered were the pressure-lag characteristics of the tail lines and the procedure of fairing pressures over the bulged elevator assuming no change in section along the tail span. The pressure-lag characteristics of typical horizontal-tail lines were investigated, and it was found that the lag was negligible for the rates of pressure change encountered in this investigation. Figure 7 presents photographs of the elevator-fabric bulging of the test airplane in flight at several values of indicated airspeed. No attempt was made to correct the elevator loads for fabric bulging.

FLIGHT PROGRAM

With the center of gravity located at 30.3 percent of the mean aerodynamic chord, 13 successful test runs were made so that, at a pressure altitude of 15,000 feet, a Mach number range of 0.30 up to about 0.80 was covered. In order to reach the required speed at the specified altitude in the higher Mach number tests (0.70 and above), it was necessary to dive the airplane from progressively higher altitudes, until finally in a dive approaching terminal velocity in which a Mach number of 0.79 was attained, it was found necessary to start the dive from the airplane service ceiling of about 32,000 feet. Five dives were made to Mach numbers of 0.70 and above, with the starting altitude for these dives varying from approximately 24,000 feet to about 32,000 feet. Duplicate tests were made, as nearly as possible, for both the power-on and the power-off conditions. The required test runs are listed in the following table:

Power condition	V_i (mph)	h_p (ft)	M	$A_{z_{max}}$
Power on (engine power setting of full throttle and 3000 rpm)	170	15,000	0.30	Stall
	230	15,000	.40	5
	290	15,000	.50	5
	350	15,000	.60	5
	410	15,000	.70	5
	440	15,000	.75	5
	470	15,000	.80	5
Power off (engine fully throttled, propeller in high pitch)	170	15,000	0.30	Stall
	230	15,000	.40	5
	290	15,000	.50	5
	350	15,000	.60	5
	410	15,000	.70	5
	440	15,000	.75	5

All these tests were performed by taking continuous records during a gradual pull-out, while the other conditions were held constant insofar as possible. The effects of pitching accelerations of the magnitude measured in these tests were small enough to warrant no further consideration.

Power-off tests were run with the engine fully throttled and the propeller in high-pitch setting. Power-on tests were run with an engine-power setting of full throttle and 3000 rpm. Curves taken from reference 2 showing the variation of brake horsepower (as determined by reference to engine-power charts) with pressure altitude, and propeller-blade angle and engine speed with true airspeed are shown in figures 8 and 9 for these power settings.

RESULTS

Inasmuch as the power-off tests were not carried to Mach numbers where major changes in tail loading due to compressibility were incurred, and since the results from these tests showed good agreement with the power-on results at high speeds up to the limit of the power-off tests, the power-off curves are not presented or discussed in this report. The differences due to power at low speeds were in the expected direction.

Variation of Horizontal-Tail Loads with Mach Number

Reduction of data.-- The resultant pressures for each orifice station were obtained at selected time points during each test run and plotted against tail chord to obtain the chordwise pressure distribution at each spanwise station. The unit span loads, obtained by mechanically integrating the chordwise pressure distributions, were plotted against tail span. From a consideration of the effect of fuselage wake on the dynamic pressure at the tail and the reduction in the tail chord due to the elevator cut-out, it was decided to fair a constant load over the fuselage equal to two-thirds of the average loading of the left and right most inboard stations. Integration of the spanwise-load curves gave the left, right, and total tail loads in pounds per unit dynamic pressure. For the time points at which the tail loads were obtained, the corresponding values of airplane lift coefficient and Mach number were determined. In figure 10 are presented typical chordwise and spanwise load distributions. Since the original data were not reduced so that pressure distributions could be presented for even values of Mach number and lift coefficient, plots most nearly approaching the selected values of lift coefficient and Mach number are presented for comparison. For these distributions, four lift coefficients, 0.1, 0.2, 0.4, and 0.8, were selected, while the Mach number values chosen were 0.30, 0.50, 0.65, 0.73, and 0.785.

In order to derive certain related curves showing compressibility effects on horizontal-tail loading, the basic data in coefficient form as determined from figure 10 and from similar figures for other Mach numbers and lift coefficients not shown in this report were plotted as a function of airplane lift coefficient for several Mach number groups. These groups were divided as follows:

Mach number group	Average Mach number
M = 0.20 to 0.40	0.30
M = .40 to .60	.50
M = .60 to .70	.65
M = .70 to .75	.725
M = .75 to .78	.765
M = .78 to .79	.785

The above Mach number ranges were selected to provide enough average Mach number points to define subsequent derived curves. Figure 11 presents the data for several of the groups noted above to show the relative experimental scatter of the data. The method of least squares was used to fit straight lines through these data since fairing through experimental data by eye tends to favor the end points.

Pressure distributions.- Several points of interest may be noted in figure 10. First, the spanwise loading curves show clearly how the down-loads on the tail increased rapidly at Mach numbers above about 0.70 with the greater part of this incremental load being carried by the right tail. (See figs. 10(a) to (d).) Second, a change in chordwise distribution at the highest Mach number (fig. 10(d)) was characterized by greater negative peak pressures (especially at the most inboard sections), by the peak pressures extending over a greater portion of the stabilizer chord, and by a decrease in the up-loads on the elevator. There are at least three factors which may have contributed to these changes in chordwise pressure distribution: (1) shock waves may have formed over a portion of the horizontal-tail surface, since the highest test Mach number (0.79) was considerably higher than the highest calculated critical Mach number (fig. 12 taken from reference 3); (2) an increase in up-elevator (which resulted in reduced up-loads on the elevator as well as a decrease in effective angle of attack of the tail) was needed to trim the airplane at the higher Mach numbers; and (3) a change in the tail angle of attack may have occurred at a constant value of lift coefficient at supercritical Mach numbers. This effect would result from a decrease in the wing lift-curve slope and a change in the wing span load distribution (reference 2) with resulting changes in downwash distribution at the tail. An additional point of interest in connection with the changed chordwise distributions is that the negative pressure peaks at the inboard stations (A_L and A_R) did not flatten out as they did at the outboard stations. Possible reasons for this are that a reduction in dynamic pressure occurred at the inboard stations due to the fuselage boundary layer, and the rate of change of downwash with airplane angle of attack was different at the inboard stations because of the presence of the fuselage.

Tail normal-force coefficient.- By cross-plotting the values of tail normal-force coefficients in figure 11 against Mach number, figure 13 was obtained. The variation of the tail normal-force coefficients with Mach number in the low to intermediate speed range ($M = 0.30$ to about 0.65) can be attributed mainly to the several effects of power. The curves presented in figure 13 also show very clearly the sharp change toward negative tail loads beyond a Mach number of 0.70. This rapid increase in down tail loads beyond the critical wing Mach number (0.69 for NACA 0015 section at $C_{L_W} = 0$) may be seen from reference 2

to be the result of shock waves forming on the upper surface of the wing; the resulting decrease in the negative pressure peaks over the forward portion of the wing and rearward movement of the center of pressure causes a sharp increase in the diving moment.

Horizontal-tail loads.- The variation of horizontal-tail loads with indicated airspeed was derived with acceleration factor as a parameter by using the values of tail-load coefficient given in figure 13. Figure 14 shows this variation for acceleration factors of 0, 1, 2, 4, and 6 at a pressure altitude of 15,000 feet. Although the change in balancing tail load in steady unaccelerated flight at indicated airspeeds from 160 to 400 miles per hour was less than 400 pounds, the change at indicated airspeeds from 400 to 460 miles per hour was over 1000 pounds. In a terminal velocity dive ($A_Z = 0$) with the airplane assumed to be traveling at its limiting speed (475 miles per hour indicated at critical altitude), extrapolation of the curve in figure 14(a) indicates a down tail load of about 2500 pounds. Although this is not in excess of the down-load for which the tail was designed (5290 lb from the manufacturer's analysis), it is considerably more than the design balancing tail load for the test airplane (-1670 lb).

The curves presented in figures 14(b) and 14(c) show the portion of the total tail load that the left and right tail carry.

In order to illustrate the effect of altitude on the onset of compressibility effects on tail loads, the values obtained in figure 13 were used to determine the variation of horizontal-tail loads with pressure altitude at constant values of indicated airspeed in steady unaccelerated flight ($A_Z = 1.0$). The results are presented in figure 15. From figure 15(a), it is apparent that, at an indicated airspeed of 250 miles per hour, compressibility has very little effect on tail loads over the entire altitude range of the test airplane. At indicated speeds of 350, 400, and 450 miles per hour, compressibility starts affecting the tail loads at about 20,000, 15,000 and 10,000 feet, respectively. The converging of the curves in figure 15(b) at a down-load of about 200 pounds at sea level is the result of the combined action of power (slipstream rotation) and the normal change in balancing tail load with indicated airspeed; compressibility effects would not enter the picture since the Mach number at 450 miles per hour indicated airspeed at sea level is only 0.59. The increase in down-loads at the medium to high pressure altitudes may again be seen to be greater for the right tail than for the left. (See figs. 15(b) and 15(c).)

Horizontal-tail-load gradient.- By plotting the slopes of the normal-force-coefficient curves in figure 11 as a function of Mach number, figure 16 was obtained. This figure presents the variation with Mach number of the rate of change of tail normal-force coefficient with

airplane lift coefficient. These curves are similar in shape to curves of tail-load gradient (defined as the change in tail load in pounds for a change in acceleration factor of 1.0) as a function of Mach number; therefore, in the following discussion the term "tail-load gradient" will be used with reference to either parameter. It is to be noted from figure 16 that the left tail-load gradient is higher than the right over the entire speed range. A possible reason for this difference at supercritical Mach numbers is that the left wing encounters supersonic local speeds slightly before the right wing with the resulting unsymmetrical change of downwash at the tail with airplane angle of attack. The difference in the left and right tail-load gradients at the lower Mach numbers may be attributed to power effects. The small variation with speed of the total, left, and right tail-load gradients up to a Mach number of 0.65 was probably the result of a change in power effects with speed. Above a Mach number of 0.65, a rapid decrease in the total tail-load gradient occurred until a minimum value was reached at a Mach number of about 0.73. The decrease indicates that the instability $\left[\left(dC_{M_p}/dC_L \right)_{a-t} \right]$ of the airplane with tail off decreased in this region, as the stabilizing moment slope of the tail in steady flight is equal to the destabilizing moment slope of the rest of the airplane. At Mach numbers above 0.73, the tail-load gradient increased sharply with Mach number, indicating rapidly increasing tail-off instability.

The total tail-load gradient in pounds per unit acceleration factor is shown in figure 17. From this figure and from figure 14(a), the balancing tail load for a given Mach number at any acceleration factor can be determined by the use of the following equation where each of the values corresponds to the particular Mach number being considered:

$$N_t = N_{t_o} + (dN_t/dA_Z)A_Z$$

Since the tests were not carried to the airplane limit design load factors, the application of the above formula to obtain balancing loads at the design positive or negative load factors may indicate balancing loads on the horizontal tail slightly different from those that would actually be obtained. However, it is believed that, for the purpose of comparing the experimental with the calculated loading at maximum positive and negative load factors (Discussion section), the error introduced by the extrapolation is small and the advantages gained by its use outweigh any possible objection.

Variation of Root Bending Moments and Fuselage Torsional Moments with Mach Number

Bending moment.— Because a trend toward high asymmetric loads on the horizontal tail was noted at high Mach numbers, an investigation was made into the possibility of critical bending moments on the tail and high torsional moments at the rear fuselage sections. In order to determine whether the increased down-loads on the tail at the higher Mach numbers were accompanied by a redistribution of these loads, the left and right tail bending moments about the root chord were obtained. These moments were then reduced to coefficient form and plotted as a function of lift coefficient as in figure 11. Cross-plotting the values of moment coefficient in these figures as a function of Mach number gave figure 18.

An inspection of the curves in figure 18(a) shows that there was little variation in $C_{M_{r_L}}$ as the Mach number increased, the most noticeable change occurring as the Mach number exceeded about 0.72 at the lower lift coefficients. (No doubt similar or perhaps more marked changes would have been noted at the higher lift coefficients if they had been obtained at correspondingly high Mach numbers.) In figure 18(b) the variation of $C_{M_{r_R}}$ in the lower Mach number range ($M = 0.30$ to 0.60) was due mostly to load changes resulting from the effects of power (slipstream rotation). At higher Mach numbers, the bending-moment changes arose from two effects: (1) the increase in the down-loads on the tail at a constant lift coefficient, and (2) a redistribution of these loads. In order to determine the change in the lateral distance to the center of pressure that occurred with Mach number, the values in figures 18(a) and (b) and 13(c) and (b) were used. Figure 19 shows the variation of the lateral distance to the center of pressure on the right and left tail with Mach number for airplane lift coefficients of 0.50 and 0.80. The curves for the lower values of lift coefficient were not included because they were too inconsistent due to both the small tail loads and the small bending moments. However, several of the highest Mach number points were included at the lower values of lift coefficient for both the left and right tail because the down-loads were sufficiently large to enable dependable values of center of pressure to be determined. In general, it can be concluded from figure 19 that there was little movement of the center of pressure on the right and left tail up to a Mach number of 0.73. At the highest test Mach number, however, the center of pressure was inboard about 3 feet on the left tail and approximately $1\frac{1}{2}$ feet on the right tail as compared with the values at lower speeds and higher lift coefficients.

Fuselage torsional moment.- The variation with Mach number of the fuselage torsional-moment coefficient is presented in figure 18(c). The convergence of the curves at a Mach number of 0.30 for the different lift-coefficient parameters, at a torsional-moment coefficient of about 0.020, is of interest. This fact indicates that the fuselage torsional moment at low speeds was proportional principally to propeller-torque coefficient. The general trend for the torsional moments to increase beyond a Mach number of about 0.65 is also of interest, and follows, of course, from the fact previously noted that the right side of the tail carried a greater part of the increased down-load at supercritical speeds. Figure 20 presents curves of left and right bending moments and torsional moments as a function of Mach number at an airplane lift coefficient of 0.10 to show the actual magnitude of the moment changes in foot-pounds.

Variation of Section Loads with Mach Number

Of paramount interest is the possibility that qualitative and perhaps quantitative information regarding the effect of compressibility on total horizontal-tail loads may be obtained from pressure-distribution measurements at several carefully selected spanwise stations instead of from complete measurements on the entire horizontal-tail surface. In order to show whether this possibility exists, the values of section normal-force moduli (section normal force divided by free-stream dynamic pressure) at four spanwise stations were obtained from figure 11 and, after conversion to coefficient form, plotted as a function of total tail normal-force coefficient. The results are presented in figure 21. Also shown in figure 21 is a comparison of the total normal-force coefficient with the individual section normal-force coefficients at zero lift over the test Mach number range. The important observations to be made from this figure are first, that except for station C on the left tail, the section coefficients at zero lift and high Mach numbers varied in substantially the same manner with Mach number as did the total tail-load coefficient. At the lower speeds, power effects resulted in large discrepancies, particularly for the outboard sections. Second, the approximate parallelism of the curves of c_n as a function of C_{N_t} indicates that, except for station C on the left tail, the section load gradients changed in about the same manner with Mach number as did the total tail-load gradient. Another point to be noted in figure 21 is that the inboard sections carried more of the increased load on the tail than did the outboard sections as the lift coefficient was increased at high Mach numbers. Figure 15(l) of reference 2 shows that there was a marked decrease in lift at the wing stations adjacent to the fuselage at a Mach number of 0.78 and a lift coefficient of 0.20. Consequently, a decrease in the rate of change of

downwash with lift coefficient directly behind this part of the wing resulted in larger load gradients for the inboard tail sections.

In order to determine whether quantitative information regarding the effects of compressibility on total tail loads can be obtained from measurements at only four stations, the average of the values of normal-force coefficient measured at these stations was plotted as a function of total tail normal-force coefficient at several values of Mach number. Also determined was the variation with Mach number of the average value of normal-force coefficient at zero lift for the four stations. The results presented in figure 22 show that the average of the section characteristics is in excellent agreement with the total tail characteristics over the Mach number range.

DISCUSSION

Tail Loads

The following discussion is devoted mainly to showing whether current design specifications are conservative in predicting the magnitude and distribution of balancing loads on the horizontal-tail surface at high speeds. This may be best accomplished by first discussing the significance of the experimental balancing tail loads obtained over the speed range of the test airplane at its maximum positive, zero, and maximum negative load factors, and then comparing these experimental loads calculated according to the methods set forth in current Army design specifications. (In order to permit a comparison of computed with experimental loading, it was necessary to waive the requirement in the Army specifications which stated that high-speed-tunnel data shall be used for airplanes operating at high Mach numbers.) The calculated loads were first determined assuming no compressibility effects; then compressibility corrections were made to the wing drag and to the wing pitching moment at zero lift to account for the effect of their change on the calculated balancing tail loads at high speeds. A detailed account of the methods used to calculate balancing tail loads assuming both incompressible and compressible flow is given in the appendix. The method of determining the experimental balancing tail loads at any speed and acceleration factor has already been discussed under Results.

Figure 23 presents the variation of calculated and experimental tail loads with indicated airspeed at the limit positive, zero, and limit negative load factors. There are several interesting observations to be made from this figure; one is that there are two points at which either maximum up-loads are obtained or a trend toward critical up-loads is apparent. The maximum up-load is obtained at about the

minimum speed at which the design positive load factor of the airplane can be attained, and a trend toward critical up-loads is obtained at the maximum test speed of the airplane. Although the maximum positive loads so obtained are considerably below the design critical load on the tail (5290 lb), it must be remembered that the momentary up-loads introduced by deflecting the elevators downward to pitch the airplane out of a dive pull-out, or to prevent the positive load factor of the airplane being exceeded, must be added to the balancing tail loads. This point should be emphasized, because it is entirely possible to visualize a case where, as the speed changes during a high Mach number dive pull-out, the compressibility effects on the wing pitching moment and on the airplane stability would result in an abrupt increment of stalling moment which would have to be countered quickly by deflecting the elevators downward to prevent the wings being overloaded.

In addition to the maneuvering loads that are introduced by abrupt deflections of the elevator, there is the possibility of excessive loads being encountered in a high-speed, high-g stall. Two important contributions to critical up-tail loads during a high-speed stall are first, the momentary loads immediately following the stall may be increased about 100 percent over the load just before the stall because of the abrupt decrease in downwash from the stalled wing and second, the fluctuating downwash from the stalled wings coupled with the increased energy in the higher-speed air stream might result in dynamic stresses which could lead to tail failure even though an airplane remained within the boundary prescribed by its speed-strength diagram. The possibility of stalling inadvertently at high speeds is increased by the fact that, for conventional airfoils, the value of maximum lift coefficient decreases rapidly with increasing Mach number. (See reference 4.) If, for a given airplane, an unusually rapid decrease does occur, it would be advisable to have the normal high-speed high-g balancing tail load less than half the design up-load because of the possibility of overloading the horizontal tail during a high-speed stall.

Another interesting observation to be made in figure 23 is that the maximum balancing down-loads will occur at the airplane maximum test speed and at the design negative load factor.

A comparison of the calculated with the experimental loads (fig. 23) shows that, at zero load factor, the computed loads are in excellent agreement with the experimental up to an indicated airspeed of about 420 miles per hour (0.72 Mach number). At progressively higher speeds, the actual down-loads increase much more rapidly than the calculated, until at the highest test speed, the computed loads (corrected for compressibility) underestimate the actual loads by over 700 pounds. Curves are presented in figure 24 showing the calculated and the experimental variation of

$\left(C_{M_{p_o}}\right)_{a-t}$ with Mach number. The change in the experimental value of $\left(C_{M_{p_o}}\right)_{a-t}$ up to a Mach number of 0.72 is the result of the thrust moment decreasing as the Mach number is increased above 0.3. Beyond a Mach number of 0.72, the effects of compressibility are predominant and are manifested by a sharp increase in the negative value of $\left(C_{M_{p_o}}\right)_{a-t}$. A comparison of the calculated curve (corrected for compressibility), with the experimental curve shows good agreement up to a Mach number of 0.75. At higher Mach numbers, however, the computed values of $\left(C_{M_{p_o}}\right)_{a-t}$ become increasingly unconservative. It should be noted at this point that, although the compressibility increment to the balancing down-load at high speeds may not be critical for airplanes having wings with little or no camber (such as the test airplane), it may be very critical for airplanes having wings with high negative moment coefficients at zero lift and low speed, since the adverse effects of compressibility would increase the initially large down-loads necessary to balance the airplane at high speeds (and zero lift).

At low and medium speeds the computed loads corresponding to maximum positive (7.33) and maximum negative (-3.0) load factors were about 10 percent lower than the actual loads. Since computed values of $\left(C_{M_{p_o}}\right)_{a-t}$ agree well with experimental values, this discrepancy must be due to the fact that the calculated destabilizing moments of the wing, the fuselage, and the propeller are too low. The discrepancy corresponds to an error in the estimation of the aerodynamic center (tail off) of about 1.2 percent mean aerodynamic chord in the low- and medium-speed ranges. At speeds where Mach number effects become important, the conventional methods used for accounting for compressibility failed completely to follow the variations in the actual tail loads. Thus, the rather rapid reduction of the experimental up-loads (corresponding to maximum positive load factor) beyond an indicated speed of 400 miles per hour and the sharp reversal toward increasing up-loads at an indicated speed of 440 miles per hour were not predicted by the calculated values. Similarly, the decrease in the actual down-loads (corresponding to maximum negative load factor) beyond an indicated speed of 360 miles per hour and the sharp drop toward larger negative loads at indicated speeds above 420 miles per hour were not predicted.

These discrepancies arise from the fact that the tail-off instability $\left[\left(dC_{M_p}/dC_L\right)_{a-t}\right]$ as well as the value of $\left(C_{M_{p_o}}\right)_{a-t}$ of the airplane were not predicted accurately at high Mach numbers. This is an important point since high-speed wind-tunnel tests have generally shown that, at very high Mach numbers, $\left(C_{M_{p_o}}\right)_w$ will rapidly change in a positive (stalling) direction after having reached a minimum negative value. If, at the same time, the aerodynamic center of the airplane continues to move rapidly forward (or tail-off instability increased), then a critical loading condition on the horizontal tail is indicated. Figure 25 compares the experimental curve of the aerodynamic center of the wing-fuselage-propeller group as a function of Mach number with the calculated curve. The experimental curve was derived from the curve of dC_{N_t}/dC_L as a function of Mach number in figure 16. The calculated aerodynamic center at a given Mach number was determined from the index tail-off stability of the airplane $\left[\left(dC_{M_p}/dC_L\right)_{a-t}\right]$ which was determined by computing the net destabilizing moment of the airplane minus tail by methods given in the appendix for two values of lift coefficient and assuming a linear variation of the moment coefficient with lift coefficient. It is interesting to compare the curves of tail-off aerodynamic center with a similar curve, also shown in figure 25, which is dependent on the shift in aerodynamic center on the wing only as the Mach number increases above 0.3. This effect was computed from wing pressure-distribution data presented in reference 2 for lift coefficients of 0.1, 0.2, and 0.5. A definite similarity in the shape of the experimental curves is shown.

A comparison of the calculated loads on one side of the tail with the experimental left and right tail loads is shown in figure 26. The calculated loads (assuming symmetrical loading) were determined by dividing by 2 the total loads in figure 23. Because of the positive asymmetry of the actual loads at all indicated speeds except between 330 and 390 miles per hour at zero load factor, and because of the positive asymmetry of the tail-load gradient, the left tail carried an increasing percentage of the total up-loads at high speeds and load factors, and the right tail carried a greater part of the total down-load at high speeds and zero or negative load factors. It follows that the computed loads for the left tail will, in general, be more unconservative than will those for the right tail. This is borne out by figure 26 which shows that the calculated up-loads are conservative as compared with the actual right tail loads and unconservative as compared with the

experimental left tail loads. At zero and maximum negative load factors, the calculated loads show good agreement with the experimental loads except at the highest speeds where they become unconservative.

Root Bending Moments

In order to show whether current design specifications are conservative in predicting the distribution of balancing loads over the horizontal-tail surface, the root bending moments were determined over the speed range of the airplane and at the maximum positive load factors. Bending moments at zero and negative load factors were not considered because they are not critical as far as maximum bending moments are concerned. The experimental bending moments were obtained by combining the values of tail load corresponding to the maximum positive load factor in figure 26 with the data in figure 27 which show the variation with M of the lateral distance to the center of pressure at the maximum positive load factor. Also shown in figure 27 is the calculated location of the lateral distance to the center of pressure obtained by determining the centroid of area of one side of the tail. The experimental and calculated bending-moment curves are presented as figure 28.

The experimental curves reveal that the critical bending moment on the left and right tail will occur at the minimum speed at which the design load factor can be obtained. At higher speeds the bending moments drop off, at first gradually, then more sharply as the speed is increased beyond the point where compressibility causes the center of pressure to shift inboard. Comparison of the calculated with the experimental results shows that the calculated bending moments are unconservative over most of the speed range much more for the left tail than for the right. This follows because the calculated loads are unconservative as compared with the experimental results on the left tail, and the calculated distance to the center of pressure is inboard of the experimental values on both the left and the right tail. At high speeds, the calculated bending moments tend toward conservatism mainly because the experimental center of pressure shifted inboard at high Mach numbers.

Asymmetric Loads

The experimental asymmetric loads derived from the curves in figure 26, corresponding to the maximum positive load factors, are shown in figure 29. These curves were chosen because the combination of left and right tail loads for these conditions resulted in the maximum experimental asymmetric loads. The calculated asymmetric loads were obtained by methods outlined in current Army specifications where it is specified

that the load over one side of the tail is equal to the maximum load for that side obtained from any conditions, while the load on the other side is the load from the foregoing condition multiplied by a factor $1-(n/7.33)$ where n is the limit maneuvering load factor for which the airplane is designed. For the purposes of this report, n is defined as a value which is limited by the stall at low and medium speeds and by structural considerations at high speeds.

Applying the methods given in the Army specifications with this interpretation resulted in the calculated curves shown in figure 29. A comparison of these curves with the experimental curves shows that the maximum calculated asymmetric load occurs at the minimum speed at which the design load factor can be reached The calculated values are very conservative over most of the speed range becoming less conservative at the highest speeds, particularly for the curve corrected for compressibility.

Torsional Moments

In order to investigate the accuracy with which the present design specifications predict torsional moments, the calculated and the experimental torsional moments were obtained for conditions giving the maximum experimental torsional moments at any speed, in this case the condition of maximum positive load factors. Since the torsional moment is defined as the left tail bending moment plus the right tail bending moment, it is evident that the experimental torsional moments can be derived from figure 28. The calculated torsional moments can be obtained from the values given in figure 29 and the calculated values of center of pressure given in figure 27. The curves so obtained are shown in figure 30. Again it is noted that the calculated values are conservative over the entire speed range, the margin of conservatism becoming less at very high speeds, particularly for the curve corrected for compressibility.

Chordwise and Spanwise Loading

In order to permit comparison with corresponding experimental data, calculations have been made of chordwise and spanwise loadings at four values of lift coefficient and Mach number. One point was chosen at a high value of lift coefficient and an intermediate Mach number to correspond to one of the conditions where critical loading of the tail in a positive direction was indicated. The other three points were taken at the highest Mach numbers (0.78 and above) and at lift coefficients corresponding to the maximum, an intermediate, and the lowest acceleration reached at these speeds. Figure 31 compares the experimental with the

calculated loading over the tail. The calculated load was distributed over the horizontal tail according to the methods specified in current Army design requirements.

Comparisons of the distributions in figure 31(a) shows that the calculated loading predicts the stabilizer leading-edge loads fairly well for the right but not for the left tail. The calculated elevator loads are of about the same magnitude as the experimental but they act in an opposite direction, since current design specifications do not require a consideration of elevator angles in designing the tail for balancing loads. It is also to be noted that the calculated spanwise loading underestimates the actual bending moments that exist on both the right and left tail. (This has already been noted previously.) In figure 31(b) the calculated load is so small that the chordwise loads are hardly discernible, and the resulting unit span loads were too small to be plotted. From this figure it can be seen that the actual load, even at maximum acceleration reached at this speed, is much larger, negatively, than that predicted. It can also be seen that the change in the direction of the experimental load across the span is not predicted. The predicting of this type of loading is, of course, difficult if not impossible by rational methods at the present time; but the importance of this type of loading should not be overlooked, since present design specifications may predict fairly accurately the total tail load at a given condition and still be critically unconservative in predicting actual bending moments, torsional moments, and chordwise load distributions. Figures 31(c) and (d) also show considerable disagreement between calculated and experimental loadings. The very high experimental negative unit-span loads at the inboard stations and the associated high down-loads at the stabilizer leading edge are completely misrepresented by the calculated loading. It appears from these data, therefore, that the use of current design requirements might lead to large and perhaps critical errors in designing the ribs, skin, leading edge, and spars of the horizontal tail.

CONCLUSIONS

From results of tests made on a typical propeller-driven pursuit airplane up to a Mach number of 0.79 and with the test center of gravity located at 30.3 percent of the mean aerodynamic chord, and from a comparison of the calculated tail loading, using modified current Army specifications, with the experimental loading, the following conclusions may be drawn:

1. Because of the effects of compressibility on the balancing tail loads at high Mach numbers, the design procedures which do not adequately account for these effects may yield balancing loads which

underestimate the actual values. For the test airplane, the compressibility increment increased the balancing down-load at zero load factor by over 150 percent at the highest test Mach number.

2. Extreme up-loads on the horizontal tail may develop in accelerated flight at medium and high speeds. In accelerated maneuvers at high Mach numbers, the very rapid increase in tail-off instability such as experienced by the test airplane, may lead to up-loads in excess of that for which the tail is designed.

3. Critical torsional moments on the rear fuselage sections and excessive tail bending moments may result because of the trend toward high asymmetric loading of the horizontal tail at high Mach numbers. For the test airplane, the effects of compressibility were to decrease the left tail and to increase the right-tail bending moments at the higher Mach numbers. At higher values of lift coefficient (0.5 to 0.8) there was little movement of the lateral distance to the center of pressure on the left or right tail up to a Mach number of 0.73. Beyond that Mach number at low lift coefficients (0 to 0.1), the center of pressure was inboard of the values at lower speeds particularly on the left tail.

4. It appears that pressure-distribution measurements at four stations (about equally spaced along the tail span, two on each side of the horizontal tail) would suffice to provide quantitative information applicable to the design of the whole horizontal-tail surface. On the test airplane, the effects of compressibility on total tail loads were shown qualitatively by results of pressure-distribution measurements at each of the stations except that on the left tail about 4 feet outboard of the fuselage center line.

5. The calculated compressibility increments used to correct the computed tail loads for the test airplane at high speeds were small and, except for the critical down-load conditions, could be neglected.

6. Because the variations in the tail-off moment coefficient at zero lift and in airplane stability were not predicted accurately by modified current methods at the higher Mach numbers, the computed tail loads, which showed good agreement with the experimental loads at lower speeds, failed to predict the changes in actual loading at the higher Mach numbers.

7. The calculated root bending moments were unconservative over most of the speed range as compared with the experimental values, except at the highest speeds where the actual center of pressure on the left and right tail moved inboard of the calculated value.

8. The maximum calculated asymmetric loads and fuselage torsional moments were conservative as compared with the maximum experimental values.

9. The specified chordwise distribution of the balancing tail loads over the horizontal-tail surface was considerably in error under certain conditions because the actual section angle of attack (contrary to what was assumed) was not constant across the tail span, and because the elevator angle was not taken into account in distributing the chordwise loads.

Ames Aeronautical Laboratory,
National Advisory Committee for Aeronautics,
Moffett Field, Calif., August 28, 1945.

REFERENCES

1. Pearson, H. A.: Pressure Distribution Measurements on an O-2H Airplane in Flight. NACA Rep. No. 590, 1937.

2. Clousing, Lawrence A., Turner, William N., Rolls, L. Stewart: Measurements in Flight of the Pressure Distribution on the Right Wing of a P-39N-1 Airplane at Several Values of Mach Number. NACA ARR No. 4K09, 1945.

3. Heaslet, Max A.: Critical Mach Numbers of Various Airfoil Sections. NACA ACR No. 4G18, 1944.

4. Nissen, James N., and Gadeburg, Burnett L.: Effect of Mach and Reynolds Numbers on the Power-Off Maximum Lift Coefficient Obtainable on a P-39N-1 Airplane as Determined in Flight. NACA ACR No. 4F28, 1944.

5. Anderson, Raymond F.: Determination of the Characteristics of Tapered Wings. NACA Rep. No. 572, 1936.

6. White, Maurice D.: Estimation of Stick-Fixed Neutral Points of Airplanes. NACA Wartime Rep. L-116 (Originally issued as NACA CB No. L5C01, 1945).

7. Ribner, Herbert S.: Notes on the Propeller and Slipstream in Relation to Stability. NACA Wartime Rep. L-25 (Originally issued as NACA ARR No. L4I12a, 1944).

APPENDIX

Computation of Balancing Tail Loads

With several modifications, the methods outlined in current Army design specifications were used to determine the calculated tail loads over a range of speeds and lift coefficients. The methods used to calculate balancing tail loads in this report differ from those specified in the Army requirements in the following particulars:

1. The tail-off moments of the airplane were determined by combining the moments of the component parts of the airplane for incompressible and compressible flow instead of from high-speed wind-tunnel tests as was specified. The moments likely to be changed considerably by compressibility effects were corrected by the best available methods.

2. In calculating balancing tail loads, the destabilizing moment due to the normal force on the propeller was taken into account in addition to the wing, fuselage, and propeller thrust moments specified in the current requirements. This destabilizing moment due to the propeller was included because, in some cases, the computed moment was almost 40 percent of the total destabilizing moment of the airplane.

3. The variation of thrust with indicated airspeed corresponding to the experimental engine power setting of full throttle and 3000 rpm was used instead of the specified normal-rated-power setting of 39 inches of mercury manifold pressure and 2600 rpm.

The equation specified by the Army for computing balancing tail loads may be rewritten as follows when the foregoing changes are incorporated:

$$N_t = \frac{\left[C_L x + C_{D_w} z + \left(C_{M_{p_o}} \right)_w + C_{M_{p_F}} + (T_c \rho V^2 d^2 z' / qS_w\bar{c}) + C_{M_{p_{NFP}}} \right] qS_w\bar{c}}{l_t}$$

The use of the above equation is illustrated in an example where the balancing tail load is determined at an indicated airspeed of 463 miles per hour at 15,000 feet (0.785 Mach number) and at the design positive load factor (7.33) of the airplane for both incompressible and compressible flow. The derivation of the various quantities that are to be combined in the preceding equation may best be illustrated by the use of the following table:

Item	Incompressible			Compressible		
	Value	Source reference	Remarks	Value	Source reference	Remarks
C_L	0.51	-------	Corresponds to foregoing conditions and wing loading of 35.7	0.51	-------	Same as incompressible
C_{D_w}	.024	Mfr's design criteria	Corresponds to lift coeffi-cient of 0.51	.106	Unpublished data	---------
$\left(C_{M_{p_o}}\right)_w$	-.004	5	----------	-.0073	Empirical formula	---------
$dC_{M_{p_F}}/dC_L$	.029	6	----------	.029	-------	Same as incompressible
$C_{M_{p_F}}$	.0106	-------	Corresponds to lift coeffi-cient of 0.51	.0106	-------	Same as incompressible
$dC_{M_{p_{NFP}}}/dC_L$	.0483	7	----------	.0483	-------	Same as incompressible
$C_{M_{p\ NFP}}$	.0177	-------	Corresponds to lift coeffi-cient of 0.51	.0177	-------	Same as incompressible
T_c	.004	-------	Corresponds I.A.S. 463 mph, prop. eff. 80 percent, bhp 1125	.004	-------	Same as incompressible

Substituting the values for incompressible flow from the preceding table into the equation gives

$$N_t = \left[(0.51 \times 0.046 - 0.024 \times 0.067 - 0.004) + 0.0106 - \frac{0.004 \times 0.00149 \times 565^2 \times 11.58^2 \times 0.855}{517 \times 213.2 \times 6.72} + 0.0177 \right] \frac{517 \times 213.2 \times 6.72}{15}$$

N_t = 2240 pounds as compared with the experimental load of 2300 pounds

The computed load assuming compressible flow is changed by the amount that $\left(C_{M_{p_o}}\right)_w$ and C_{D_w} change from their low-speed values due to compressibility. Substituting the corrected values of C_{D_w} and $\left(C_{M_{p_o}}\right)_w$ into the above equation gives

$$N_t = \left[(0.51 \times 0.046 - 0.106 \times 0.067 - 0.0073) + 0.0106 - \frac{0.004 \times 0.00149 \times 565^2 \times 11.58^2 \times 0.855}{517 \times 213.2 \times 6.72} + 0.0177 \right] \frac{517 \times 213.2 \times 6.72}{15}$$

N_t = 1808 pounds as compared with the experimental load of 2300 pounds

TABLE I.- ORDINATES AT PRESSURE ORIFICES ON HORIZONTAL TAIL OF TEST AIRPLANE

[All values are in percent of chord]

Orifice	Row A				Row B				Row C				Row D			
	Upper surface		Lower surface		Upper surface		Lower surface		Upper surface		Lower surface		Upper surface		Lower surface	
	Station	Ordinate	Station	Ordinate	Station	Ordinate	Station	Ordinate	Station	Ordinate	Station	Ordinate	Station	Ordinate	Station	Ordinate
Left side																
1	1.44	1.55	1.55	1.55	2.57	1.70	2.84	1.70	1.61	1.24	1.24	1.14	2.08	1.40	2.21	1.43
2	10.15	3.51	9.37	3.51	10.43	3.23	9.88	3.27	7.30	2.43	7.08	2.48	25.04	3.15	24.98	3.09
3	30.96	4.48	30.96	4.64	31.89	4.11	31.95	4.21	20.35	3.28	20.25	3.38	46.14	2.93	46.34	2.93
4	47.10	4.13	46.44	4.23	42.61	2.95	42.66	3.91	31.06	3.35	33.79	3.45	57.56	2.11	57.72	2.11
5	57.48	3.80	57.28	3.72	54.55	3.55	54.65	3.52	46.91	3.03	46.71	3.01	70.60	1.95	70.99	1.95
6	62.54	1.80	62.54	1.86	59.77	1.52	59.88	1.86	57.29	2.19	57.44	2.36	79.80	1.40	80.00	1.37
7	68.98	2.79	69.04	2.89	68.93	2.61	68.98	2.84	67.58	2.09	68.05	1.99	-----	----	-----	----
8	82.64	1.65	82.68	1.75	80.68	1.66	80.84	1.73	83.73	1.17	83.73	.99	-----	----	-----	----
Right side																
1	1.34	1.45	1.51	1.45	2.02	1.59	2.40	1.70	1.96	1.49	2.43	1.49	1.98	1.50	2.02	1.24
2	10.10	3.57	10.03	3.45	10.06	3.27	10.43	3.29	9.80	3.00	10.12	2.75	25.24	3.24	26.18	3.09
3	30.90	4.55	30.86	4.47	31.75	4.20	31.86	4.08	35.56	3.66	36.08	3.29	45.37	2.93	45.85	3.06
4	47.70	4.10	47.22	4.16	43.08	3.92	43.08	3.83	49.02	3.29	49.28	3.14	58.86	2.44	58.37	1.95
5	57.70	3.70	57.54	3.74	54.33	3.63	54.42	3.51	60.13	2.75	60.42	2.14	71.54	2.11	70.93	1.95
6	63.33	2.17	62.40	1.86	59.36	1.95	59.52	1.59	71.11	2.17	71.24	1.91	80.16	1.63	80.03	1.37
7	68.67	2.77	68.60	2.92	68.89	2.74	69.14	2.72	84.97	1.20	84.97	1.18	-----	----	-----	----
8	82.25	1.80	82.11	2.05	78.23	2.02	78.28	1.97	-----	----	-----	----	-----	----	-----	----
9	-----	----	-----	----	86.96	1.36	86.73	1.36	-----	----	-----	----	-----	----	-----	----

NATIONAL ADVISORY
COMMITTEE FOR AERONAUTICS

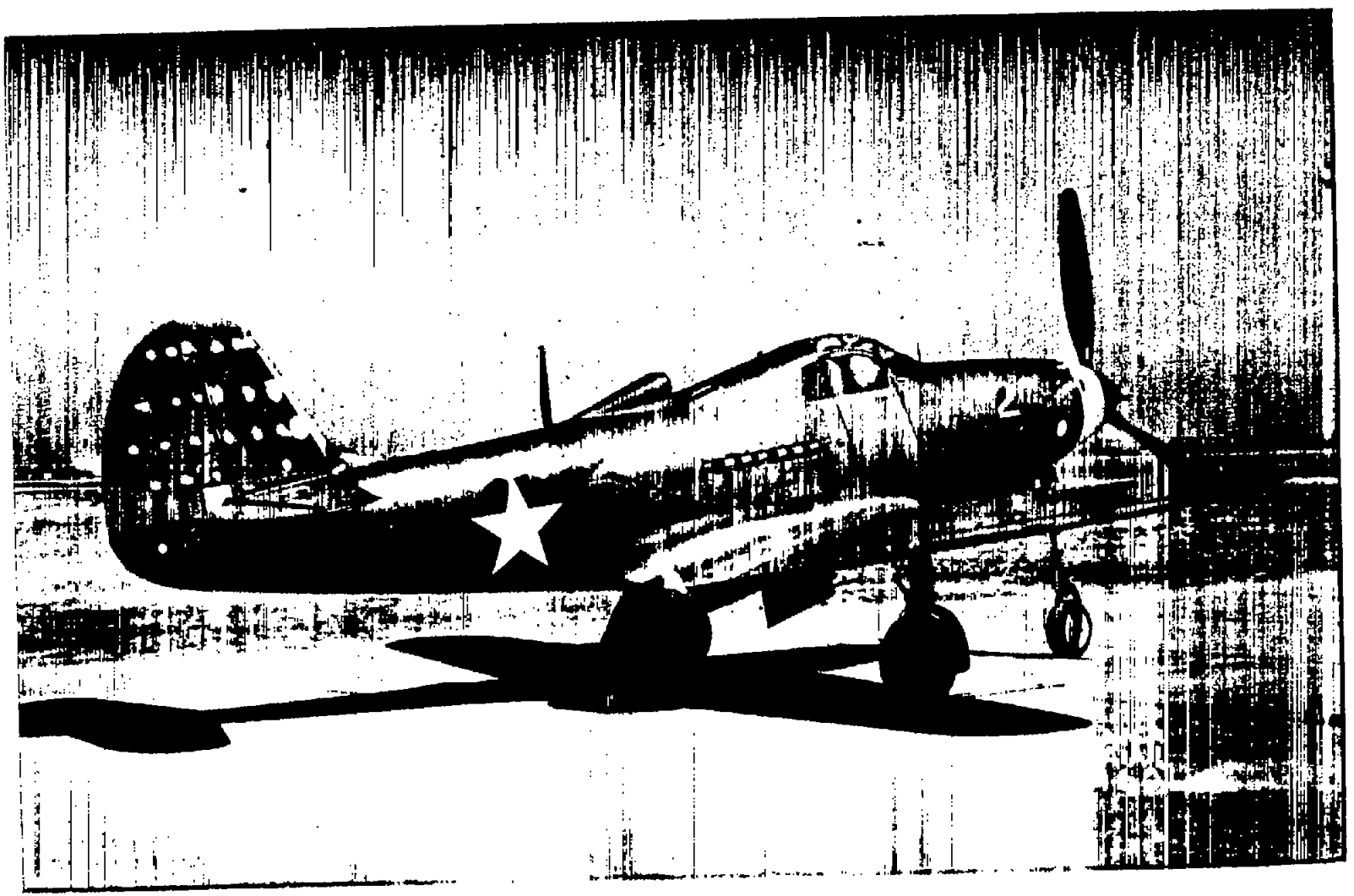

Figure 1.- Three-quarter rear view of test airplane.

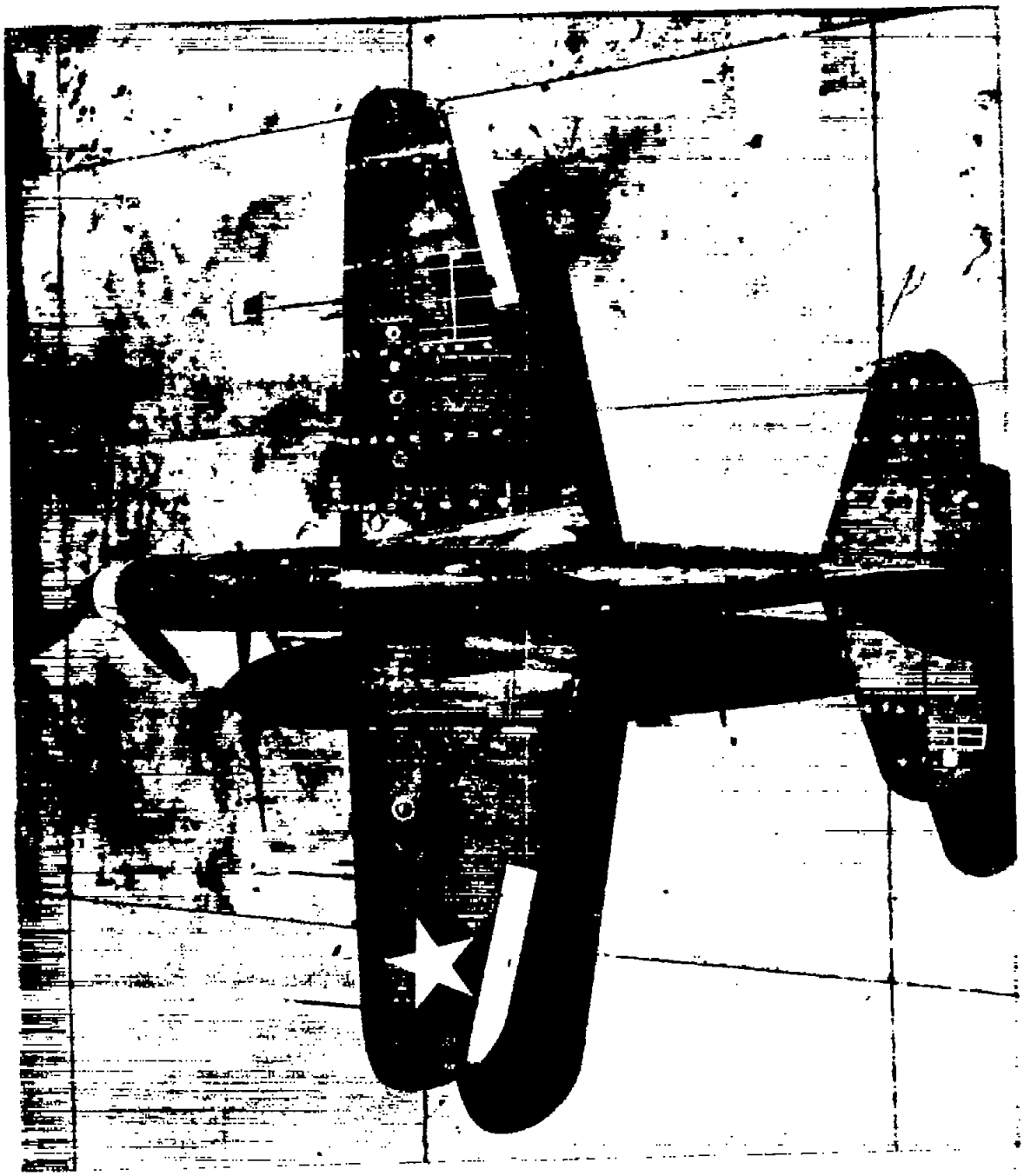

Figure 2.- Top view of the test airplane as instrumented for flight tests.

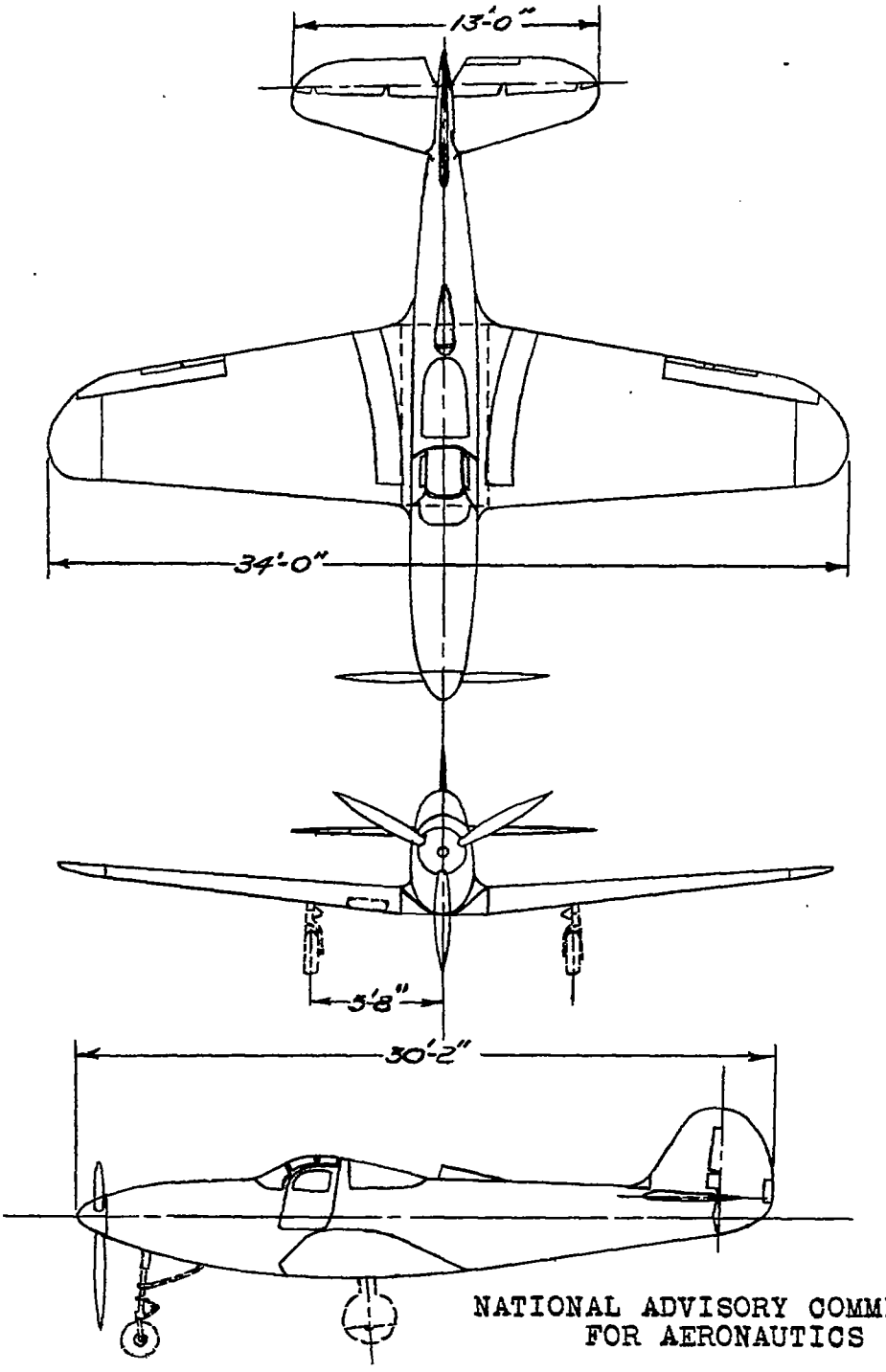

Figure 3.- Three-view drawing of the test airplane.

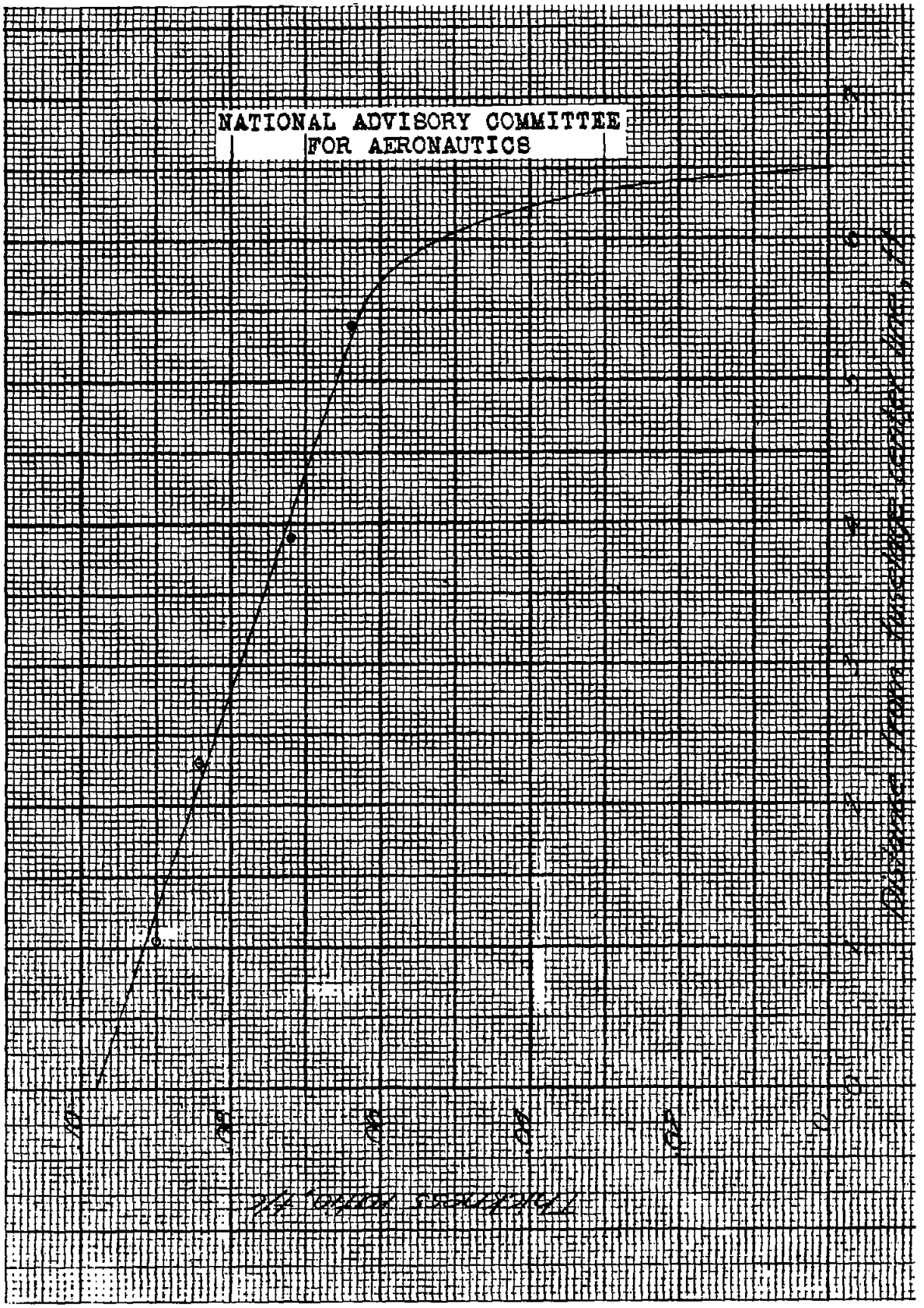

Figure 4.- Variation of thickness ratio along horizontal-tail semi-span of test airplane.

NATIONAL ADVISORY COMMITTEE
FOR AERONAUTICS

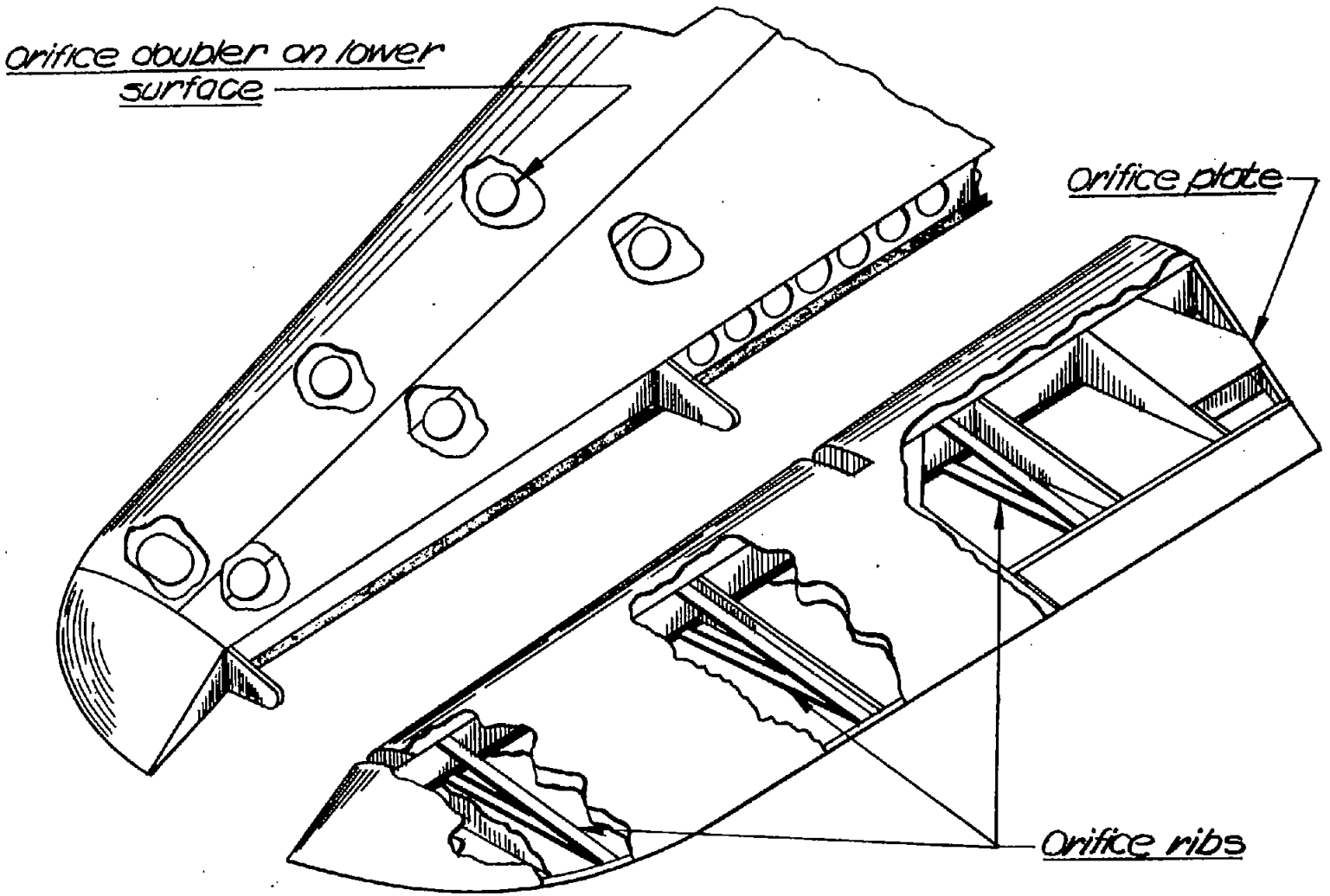

Figure 5.- Simplified pictorial sketch showing added reinforcements in test tail of test airplane.

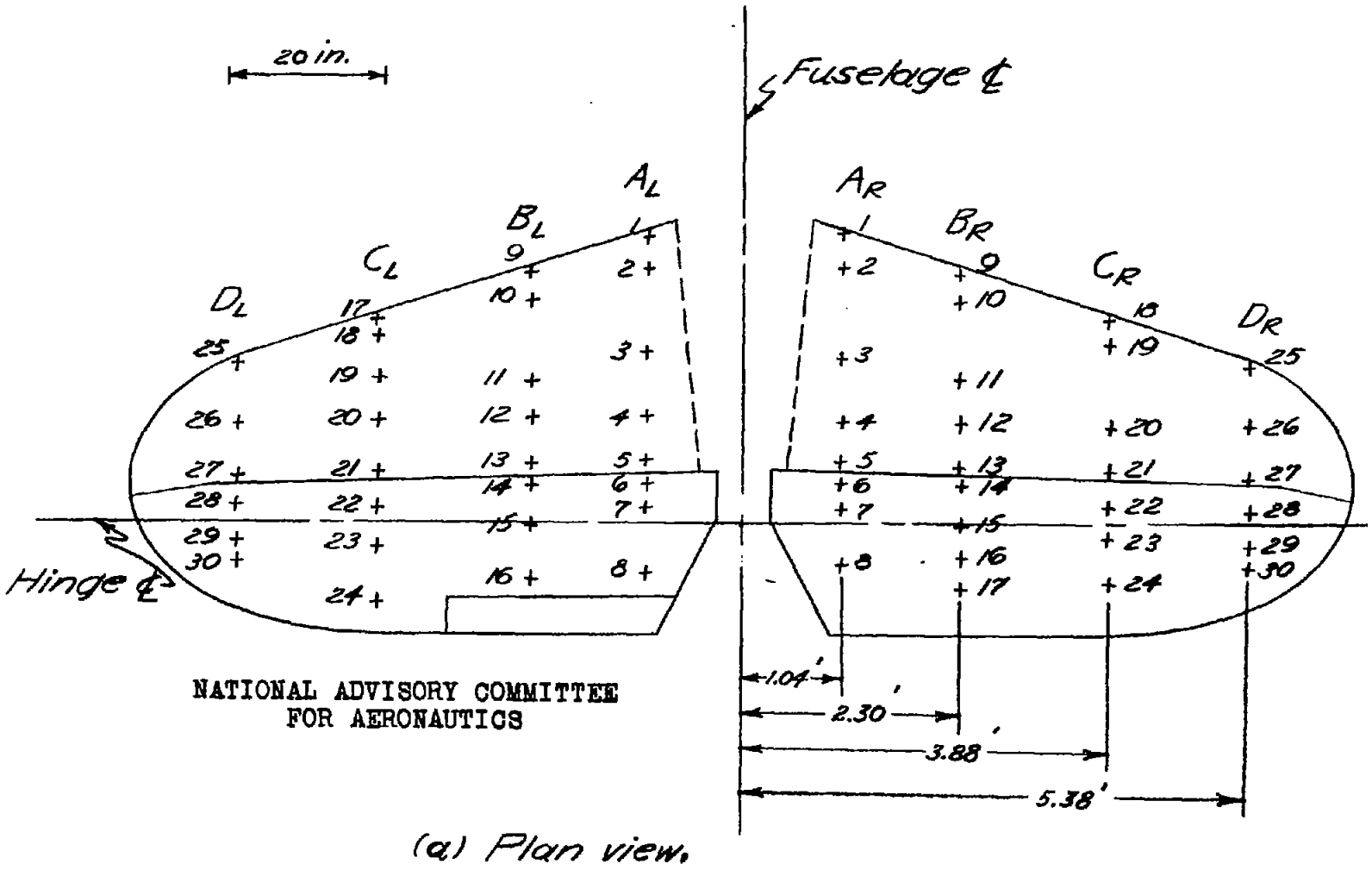

(a) Plan view.

Figure 6(a-c).- Orifice locations on horizontal tail of the test airplane.

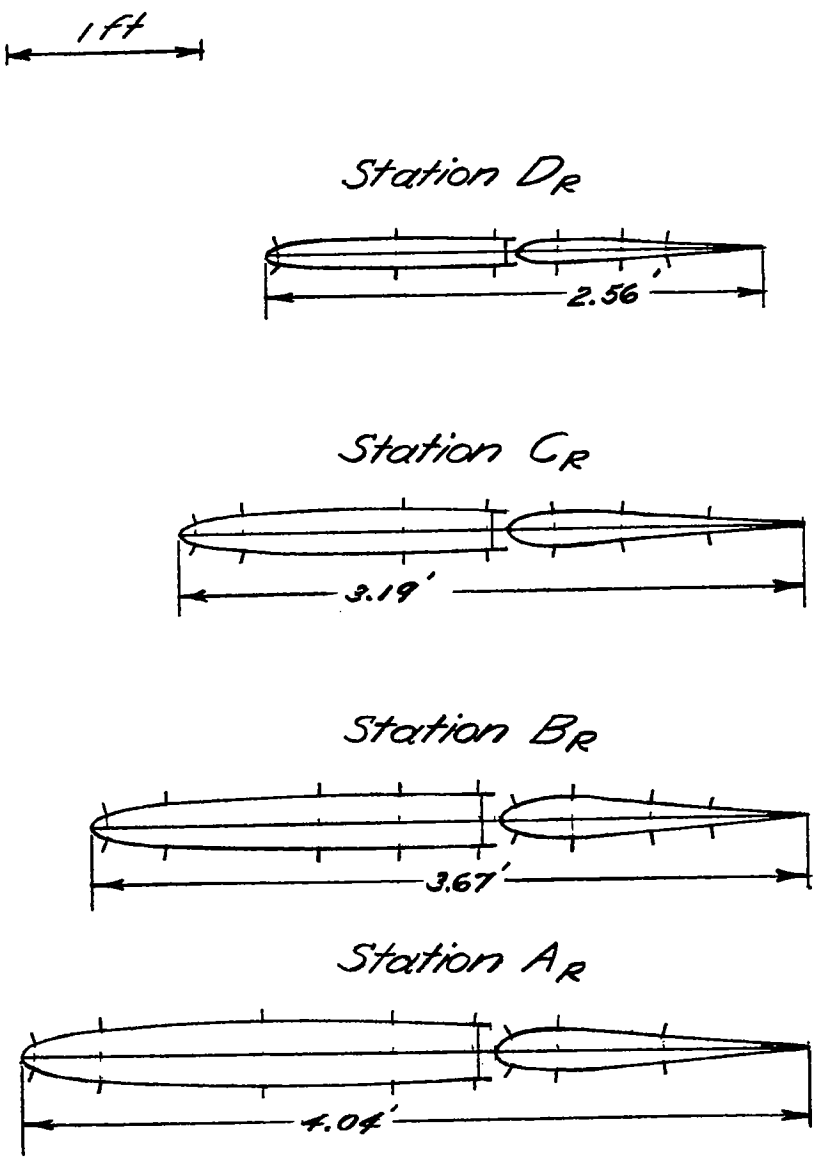

NATIONAL ADVISORY COMMITTEE
FOR AERONAUTICS

(b) Right tail sections.

Figure 6.- Continued.

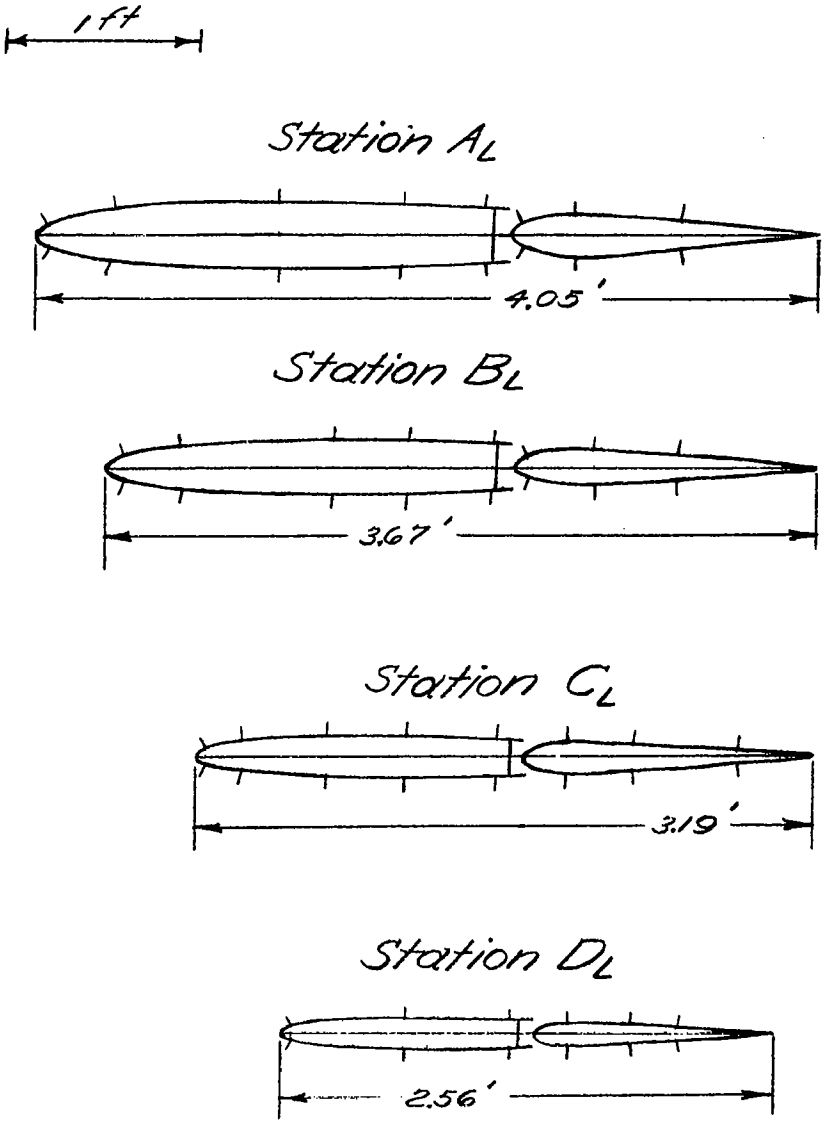

(c) Left tail sections.

Figure 6.- Concluded.

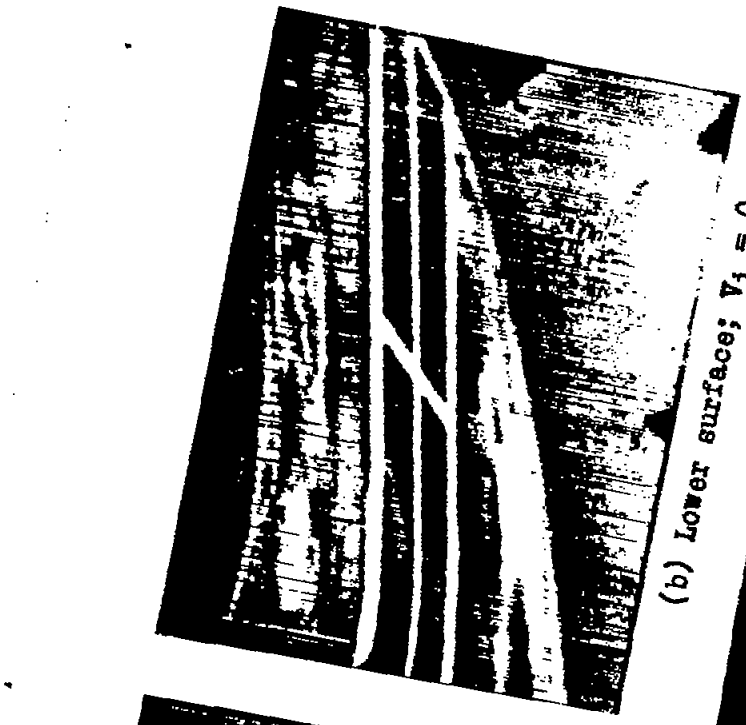

(a) Upper surface; $V_1 = 0$.

(b) Lower surface; $V_1 = 0$.

(c) Upper surface; $V_1 = 250$; $M = 0.55$; $\delta_e = 5.4^\circ$ down; $\Delta_Z = 0.30$.

(d) Lower surface; $V_1 = 250$; $M = 0.55$; $\delta_e = 5.4^\circ$ down; $\Delta_Z = 0.30$.

Figure 7(a-h).- Photographs of elevator-fabric distortion on the top and bottom surfaces of the left elevator of the test airplane at several values of indicated airspeed.

Fig. 7a,b,c,d

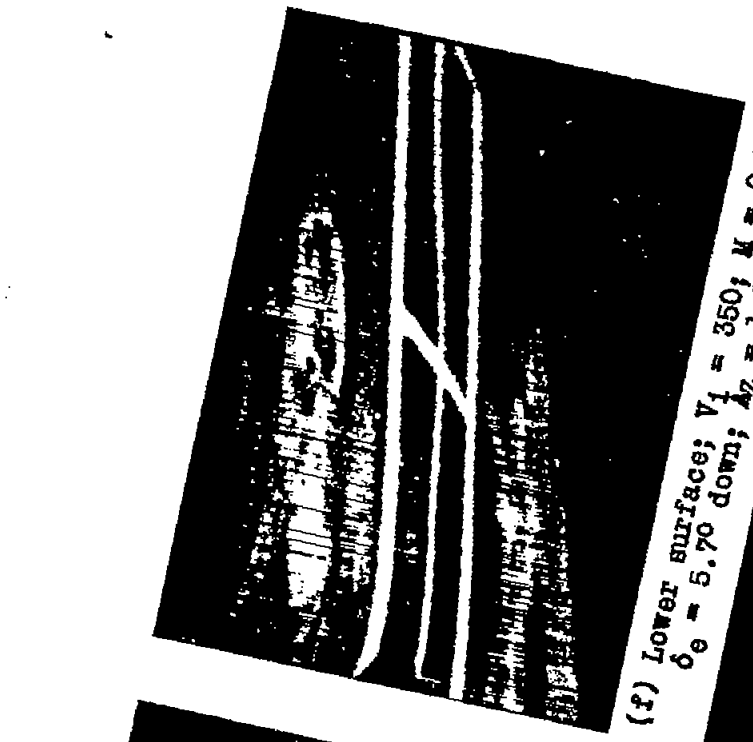

(e) Upper surface; V_1 = 350; M = 0.69; δ_e = 5.7° down; A_Z = 1.1.

(f) Lower surface; V_1 = 350; M = 0.69; δ_e = 5.7° down; A_Z = 1.1.

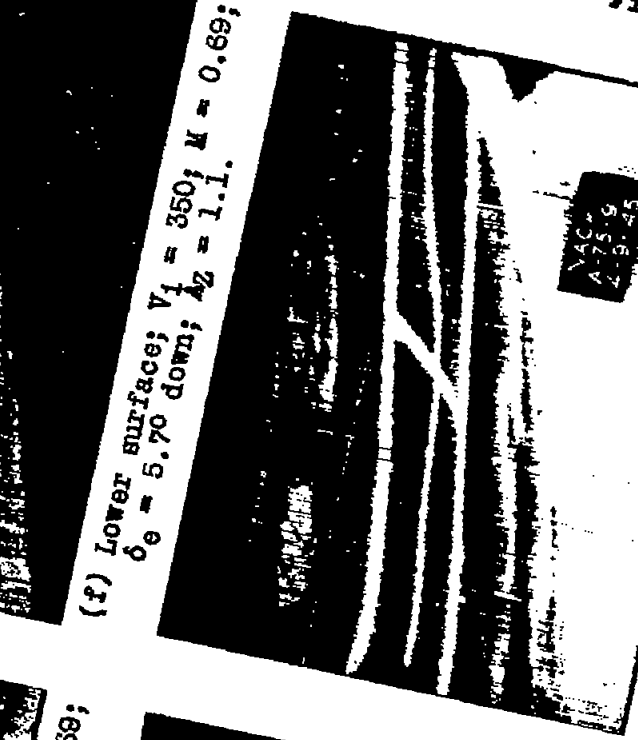

(g) Upper surface; V_1 = 454; M = 0.72; δ_e = 5.4° down; A_Z = 6.0.

(h) Lower surface; V_1 = 454; M = 0.72; δ_e = 5.4° down; A_Z = 6.0.

Figure 7.- Concluded.

Fig. 7e,f,g,h

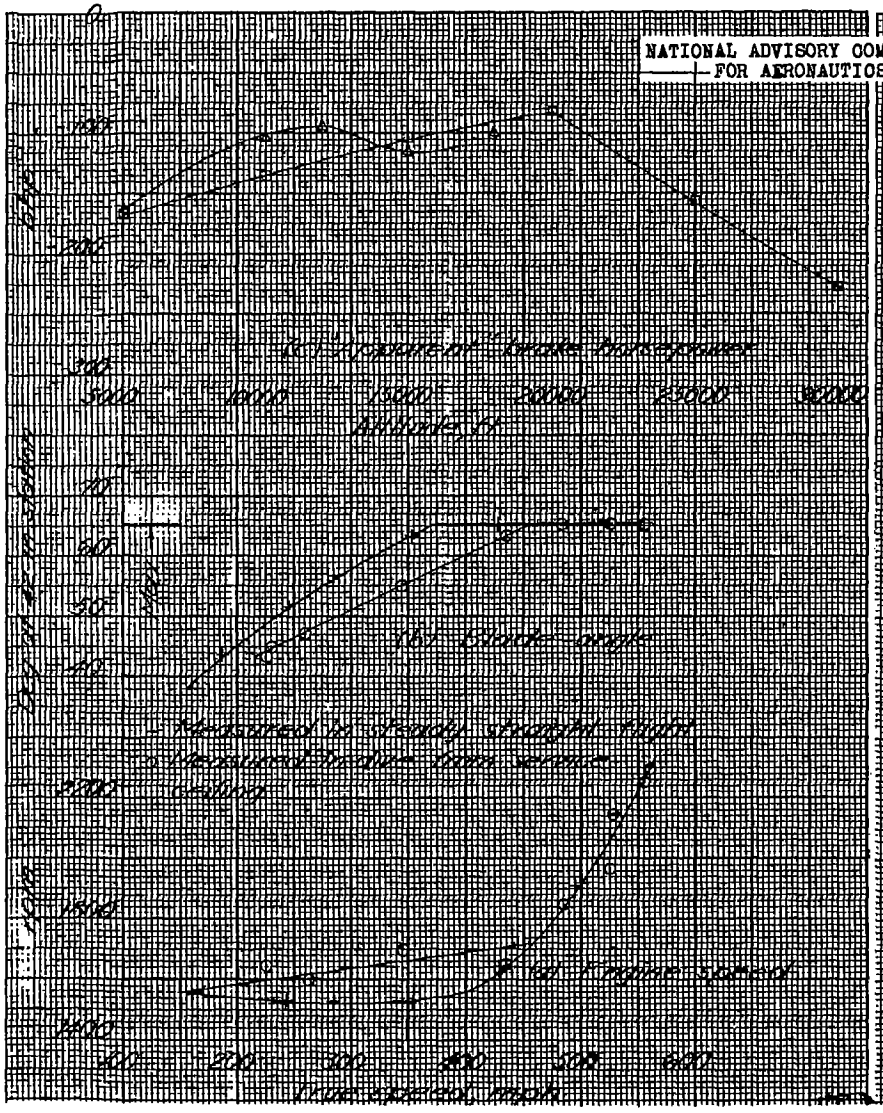

Figure 8.- Engine speed, propeller-blade angle, and brake horsepower for the engine-throttled, propeller-in-high-pitch power setting of the test airplane.

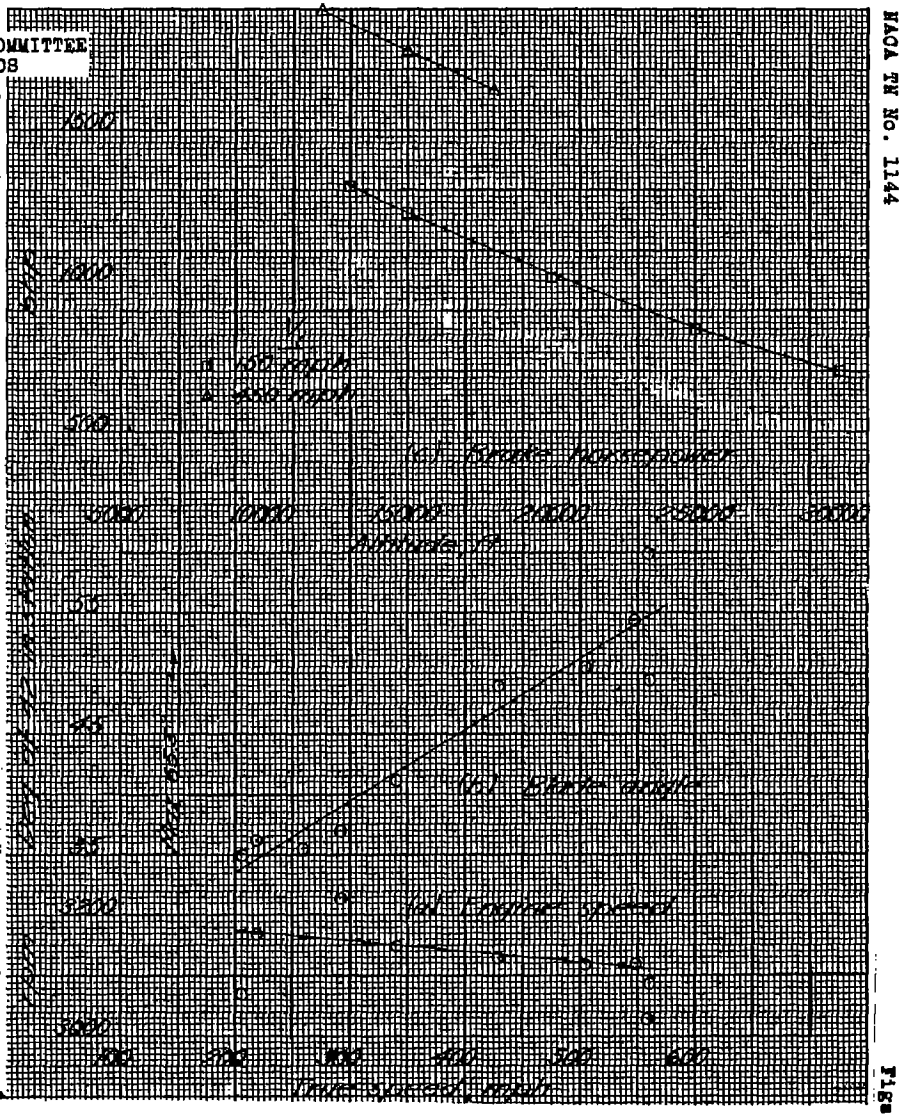

Figure 9.- Engine speed, propeller-blade angle, and brake horsepower for a power setting of full throttle and 3000 rpm of the test airplane.

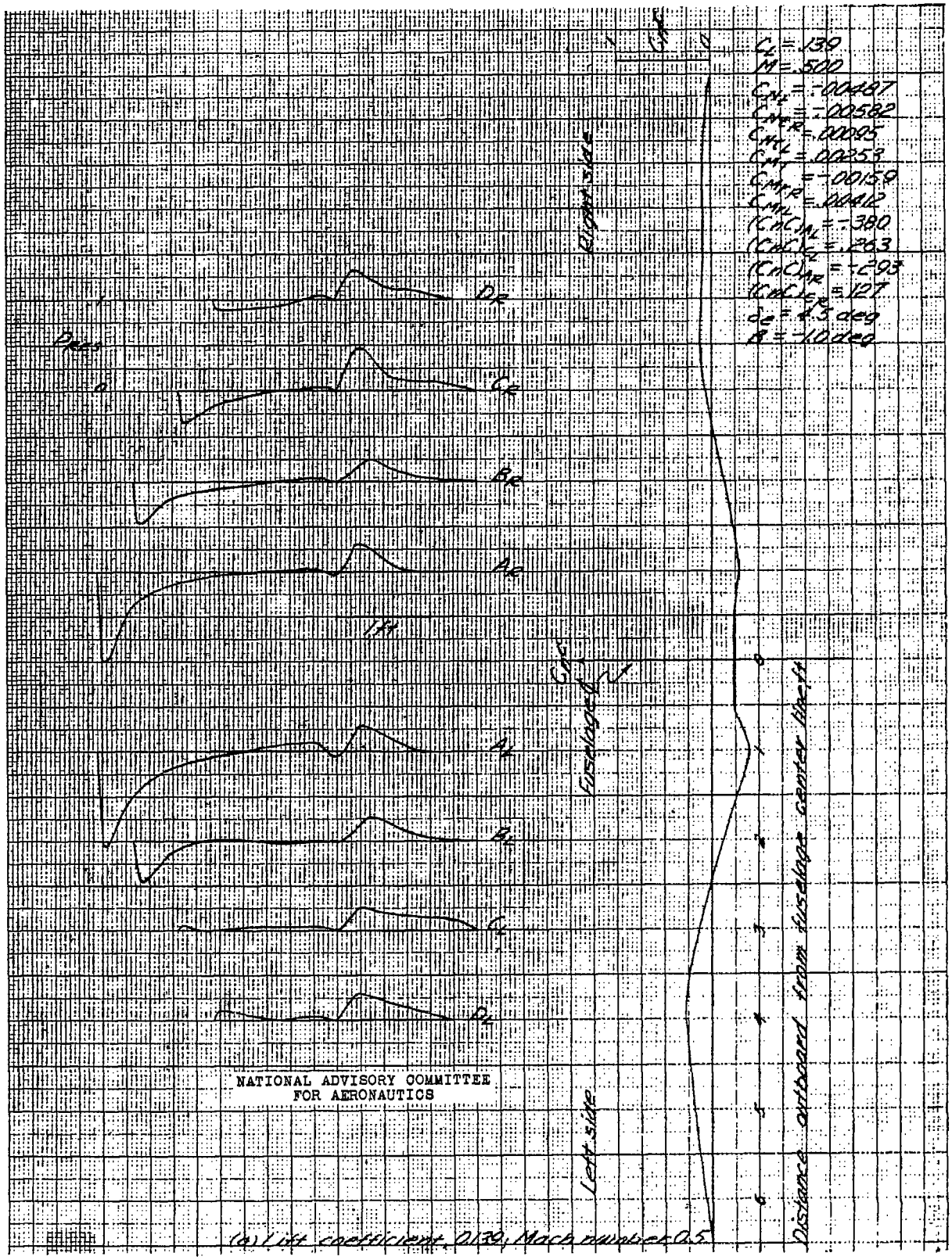

Figure 10(a-n).- Pressure distribution on the horizontal tail in power-on flight. Test airplane.

Fig. 10b

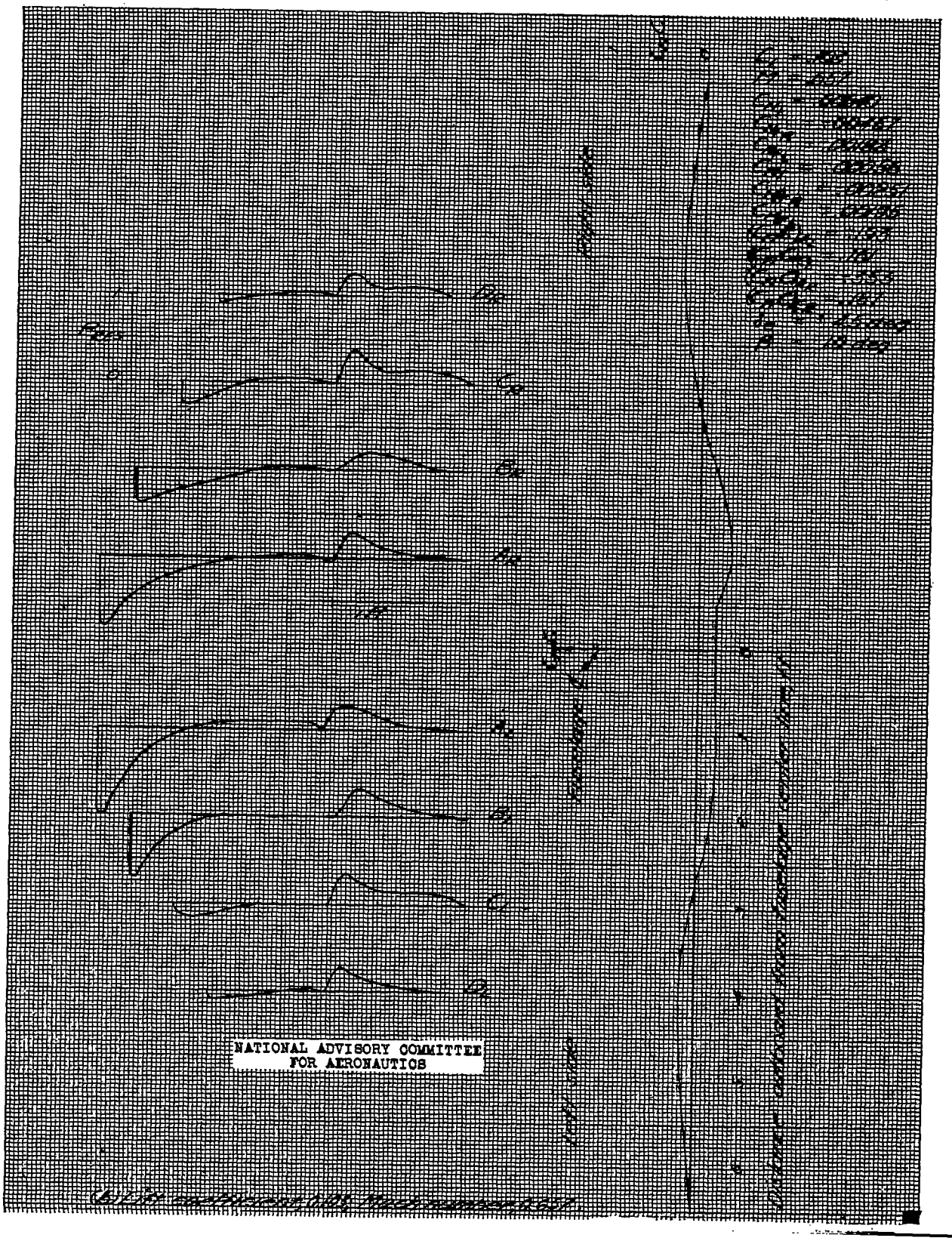

Figure 10.- Continued.

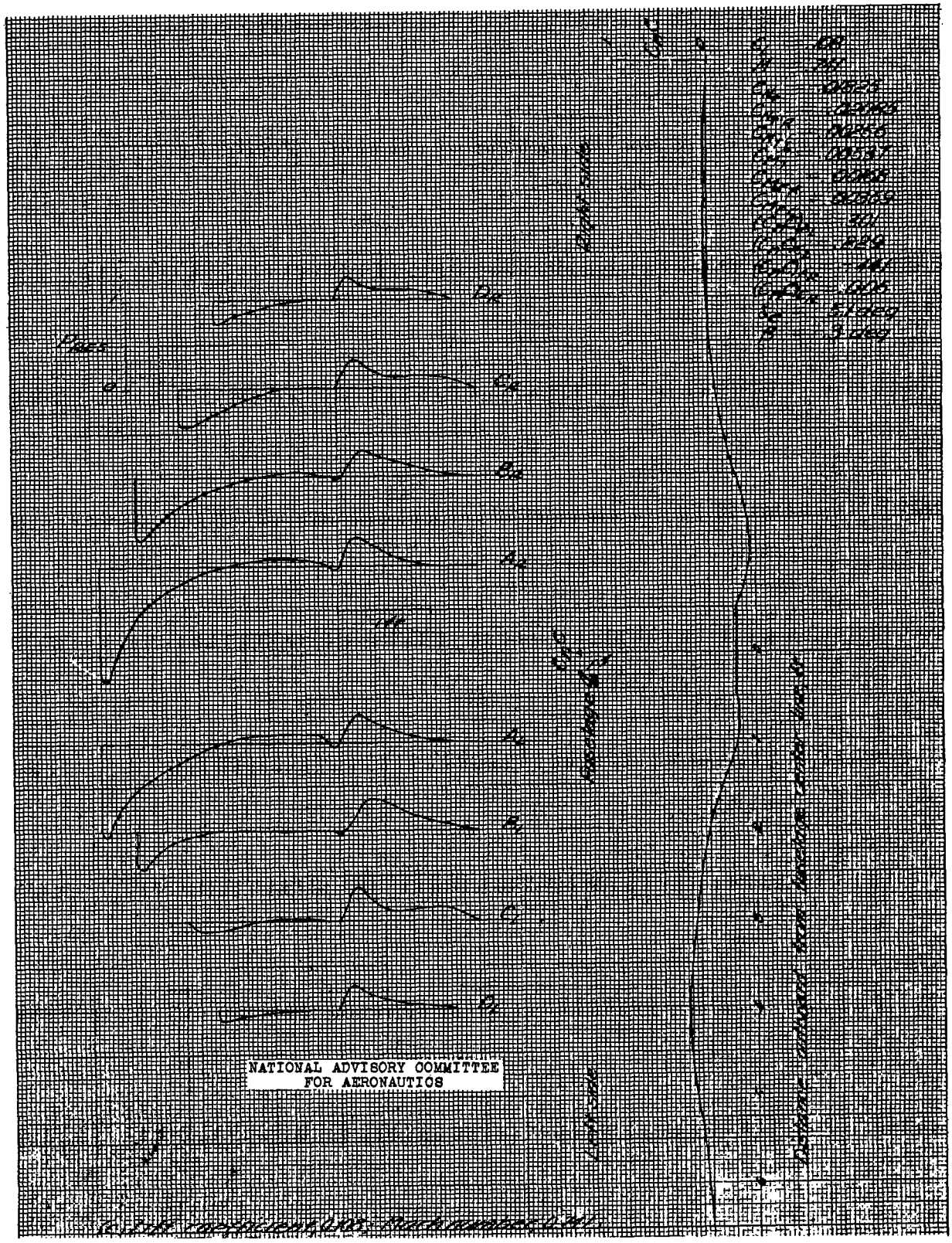

Figure 10.- Continued.

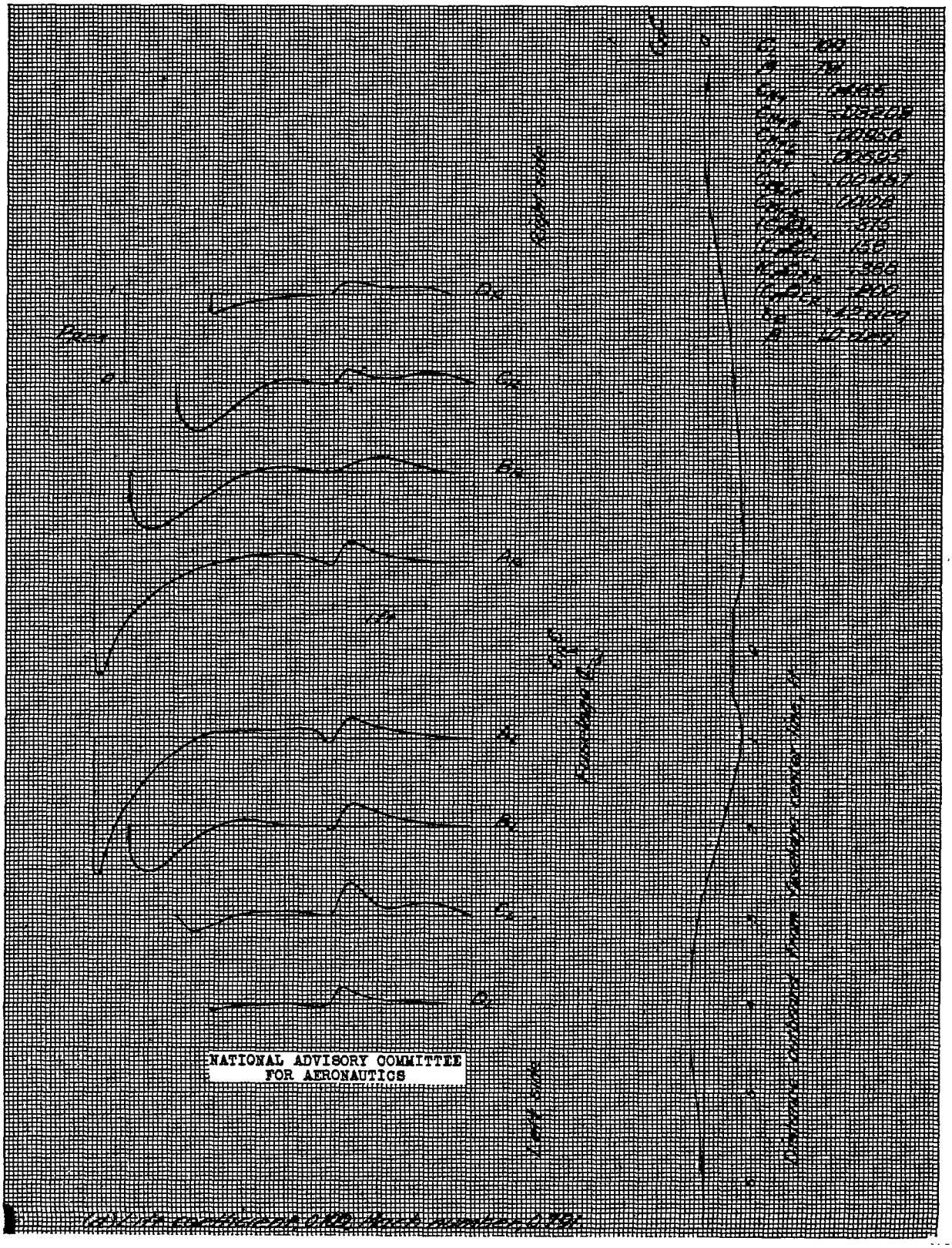

Figure 10.- Continued.

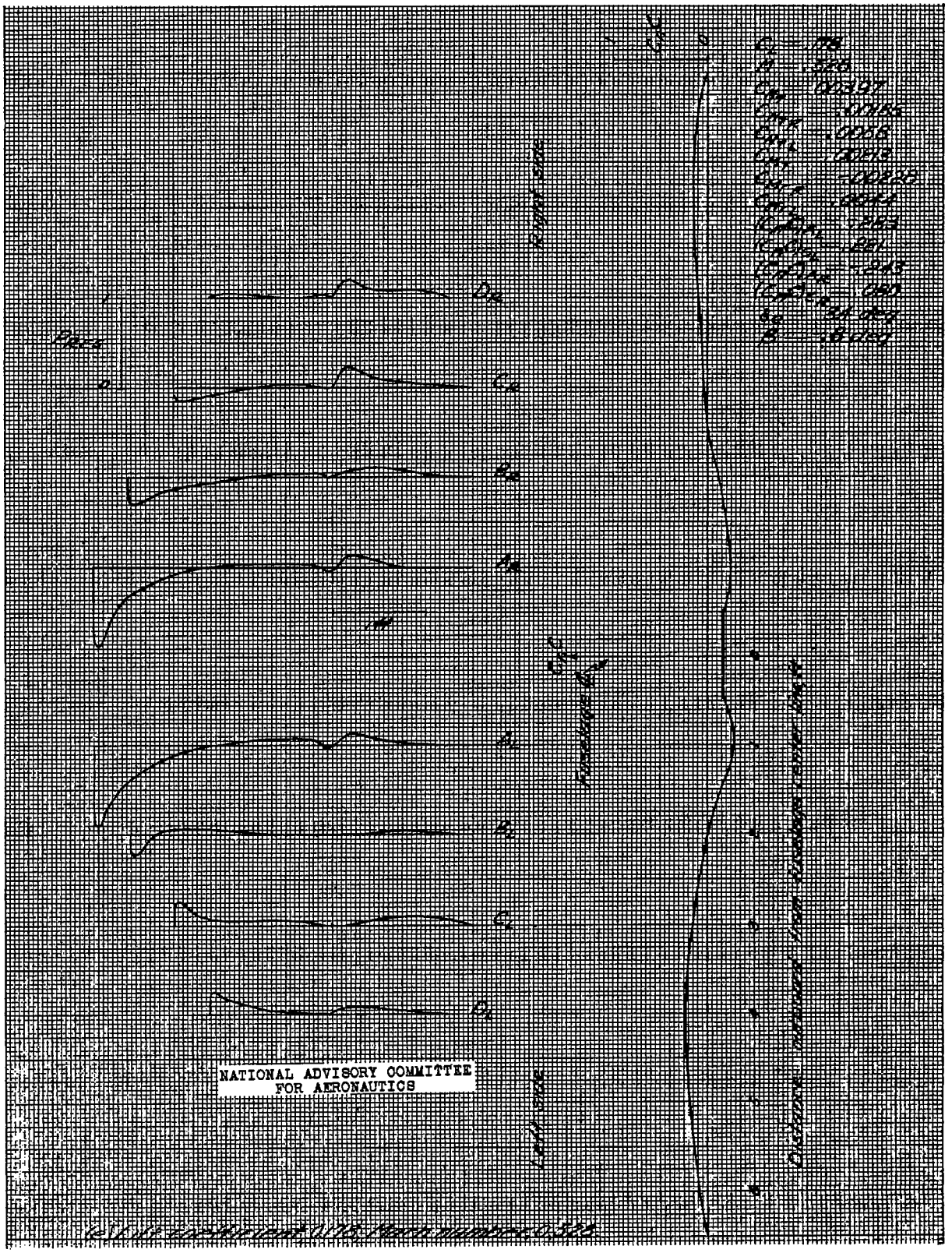

Figure 10.- Continued.

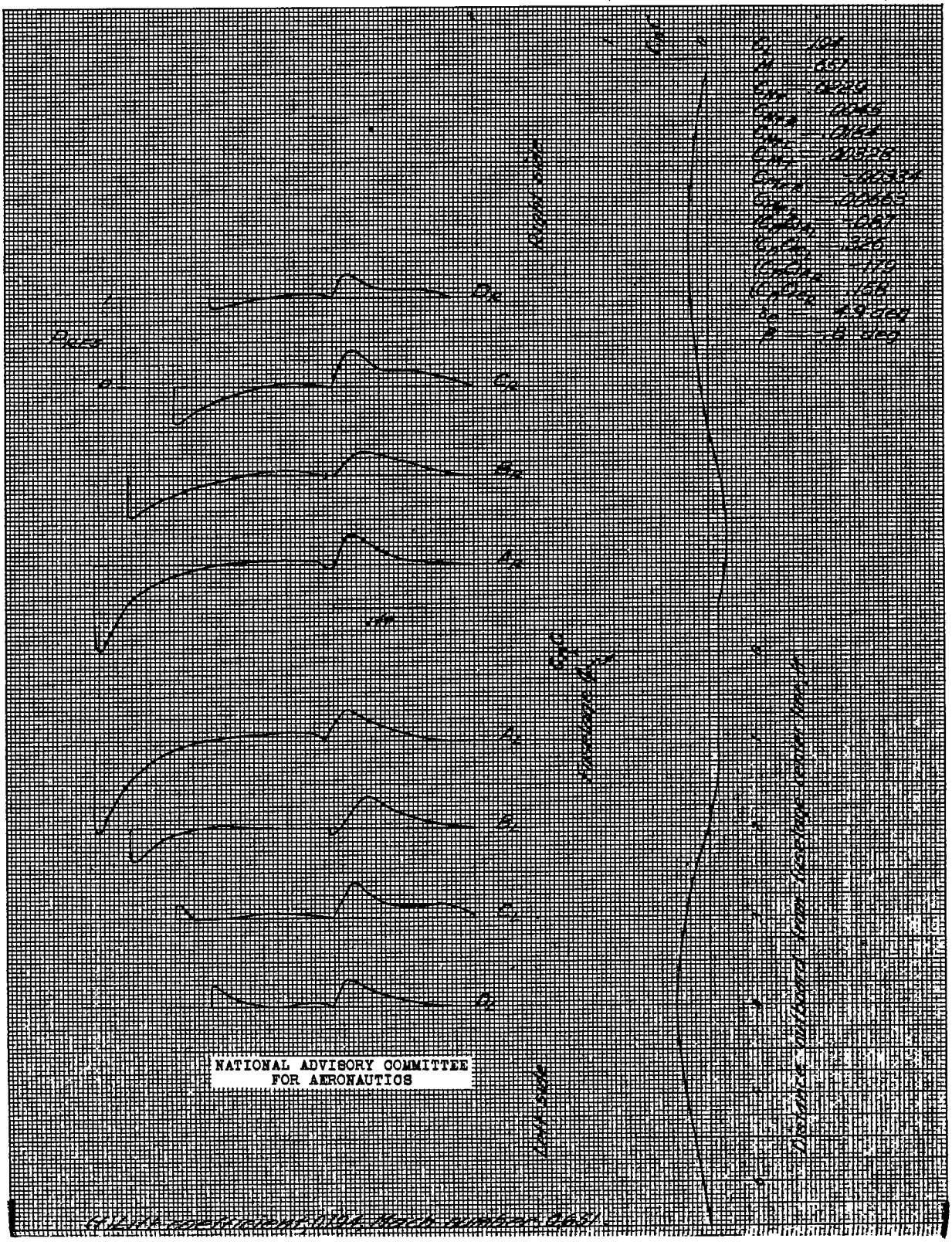

Figure 10.- Continued.

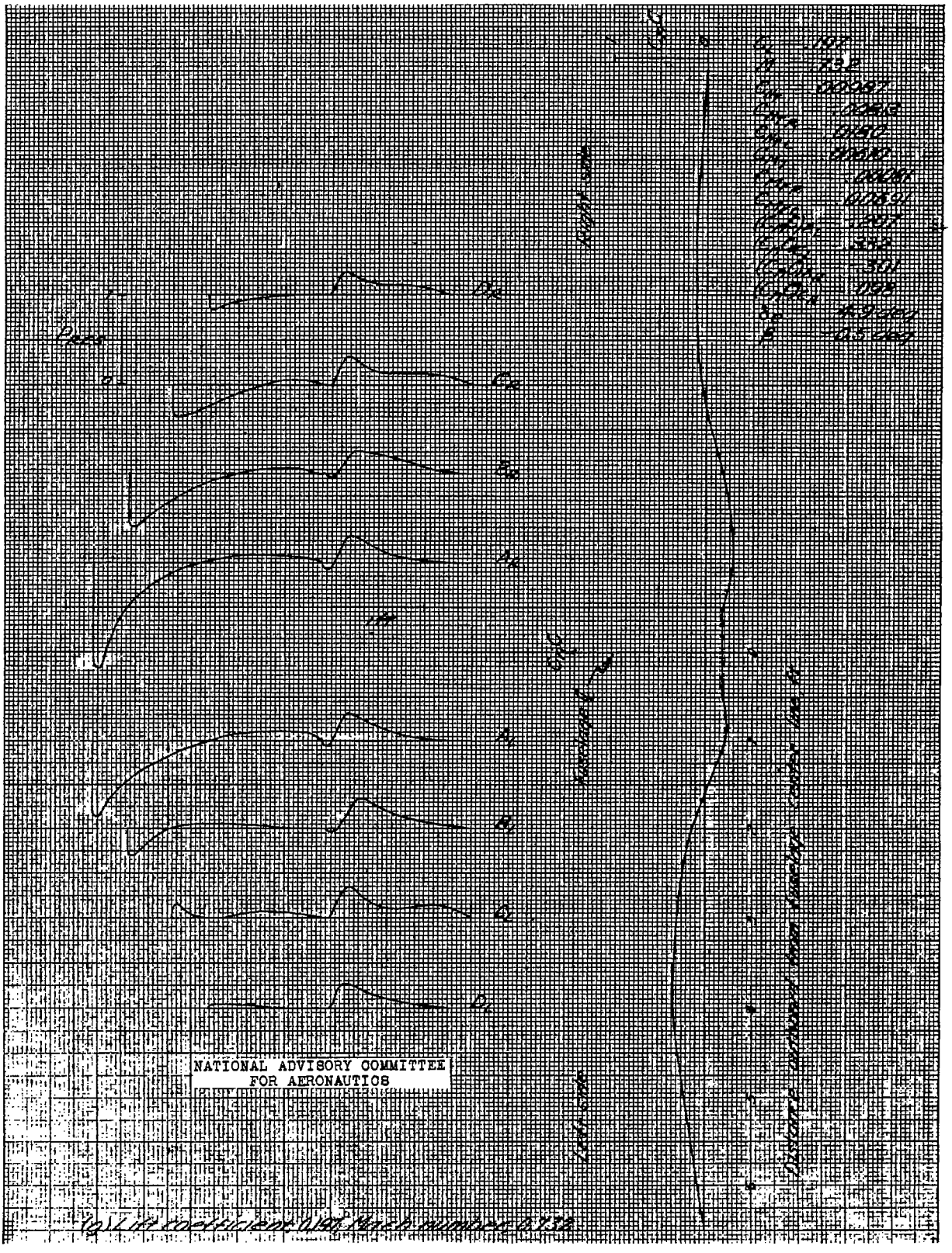

Figure 10.- Continued.

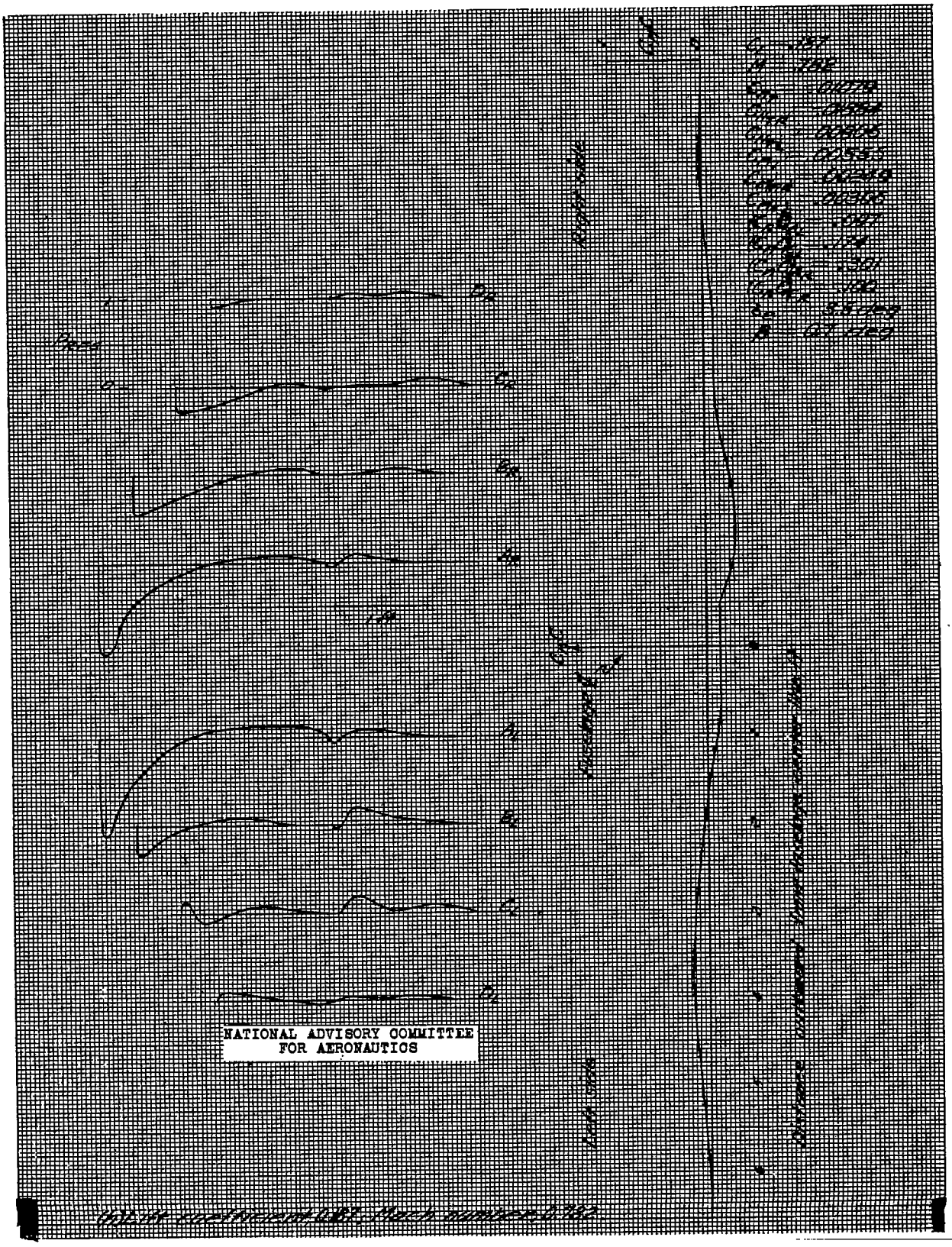

Figure 10.- Continued.

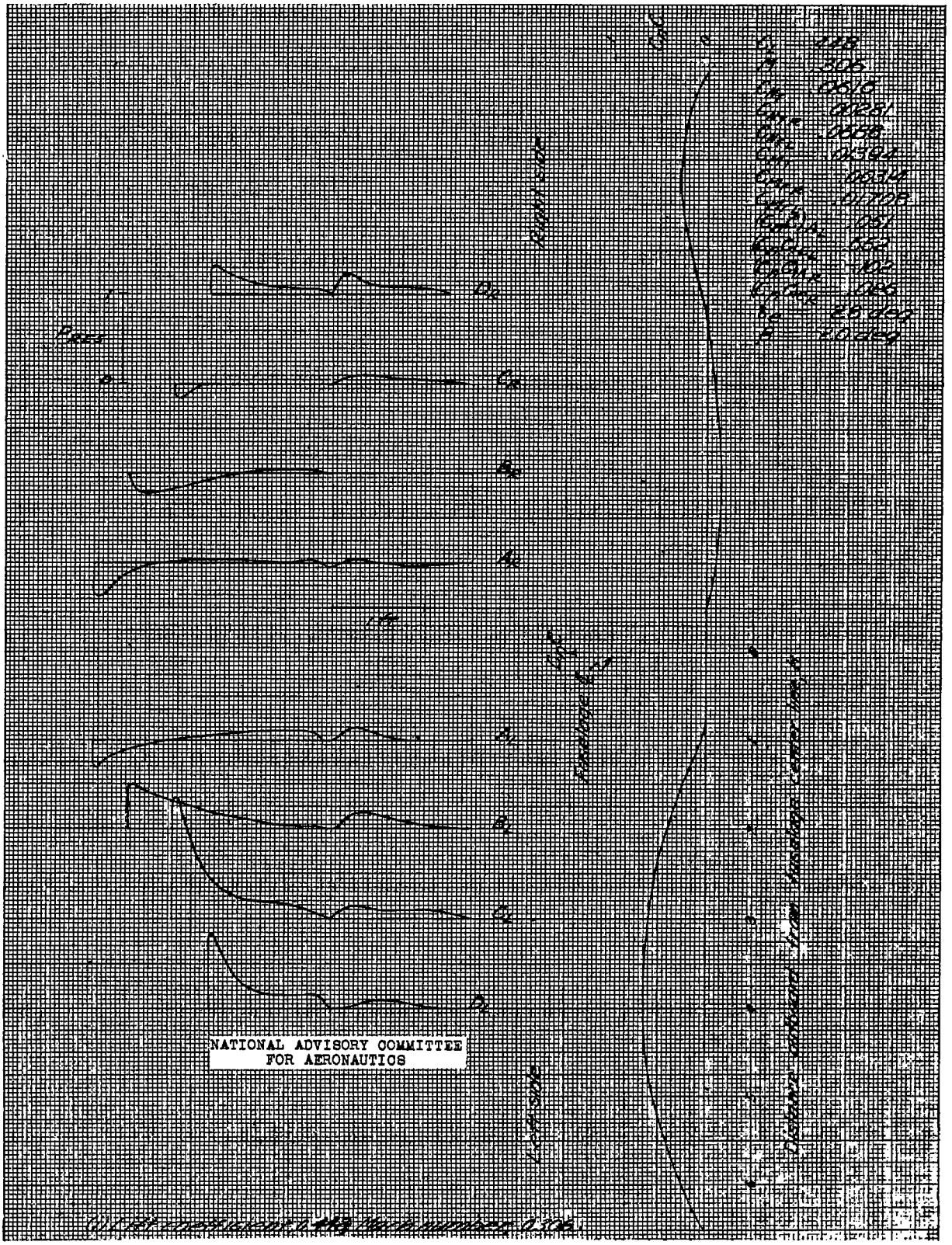

Figure 10.- Continued.

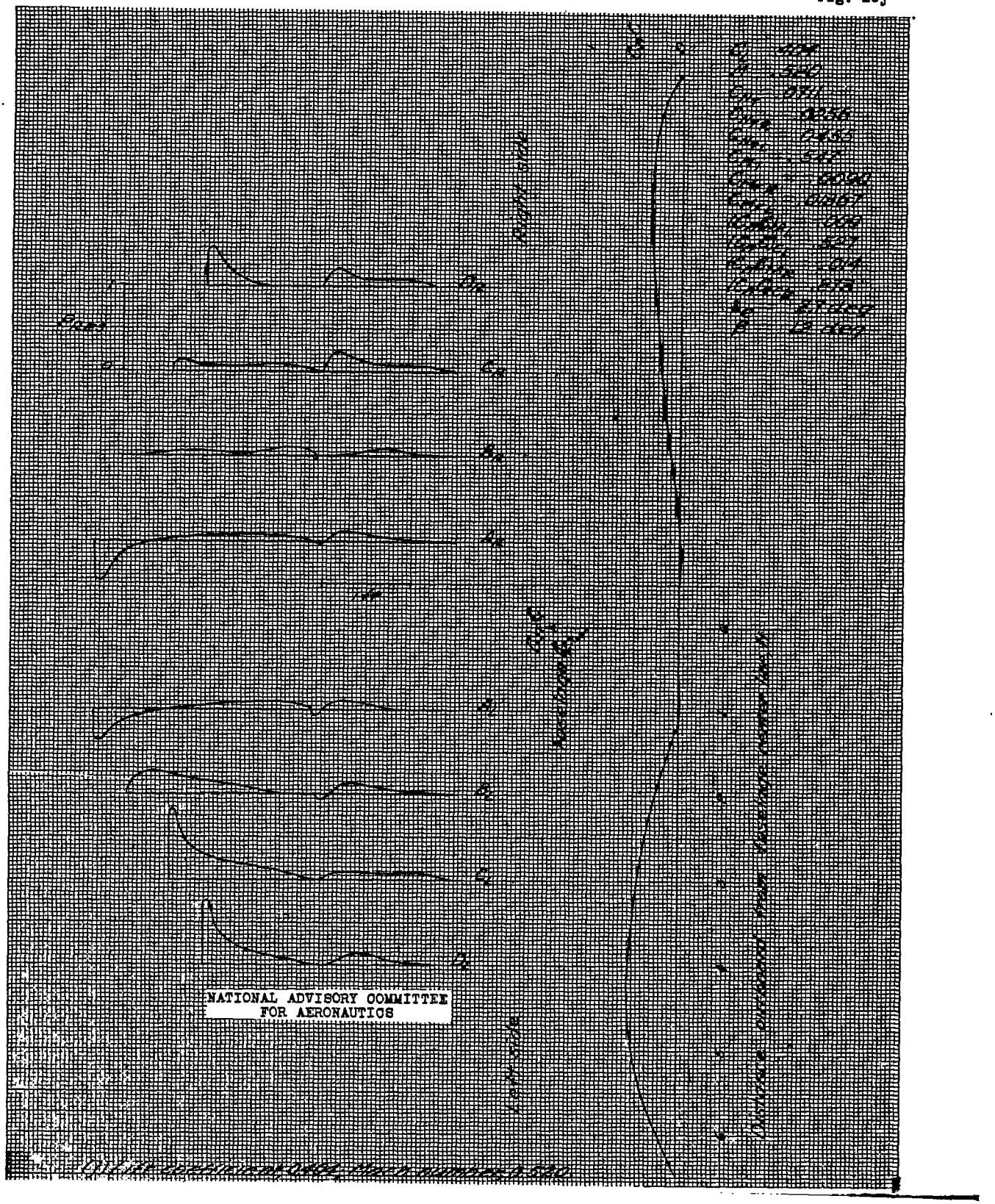

Figure 10.- Continued.

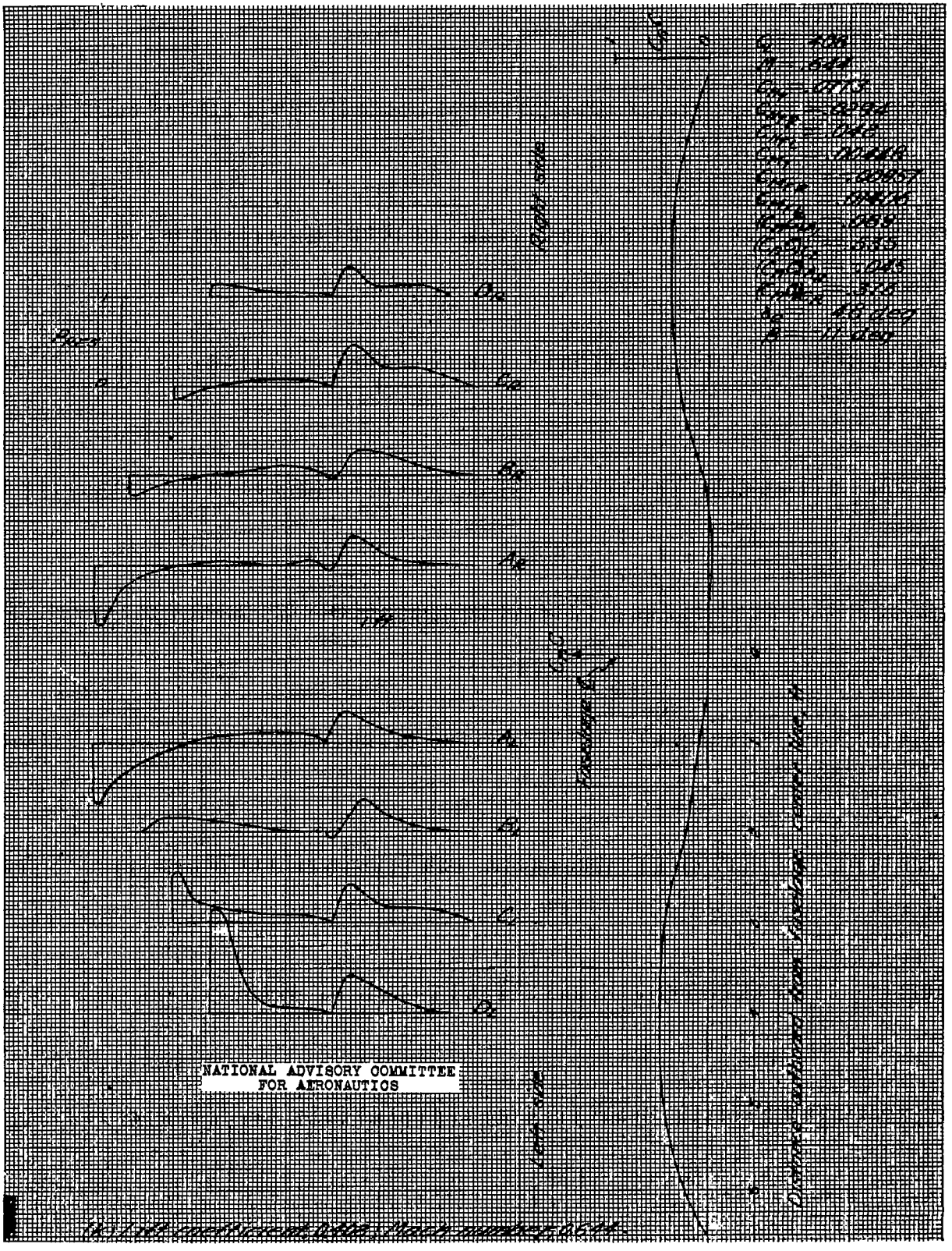

Figure 10.- Continued.

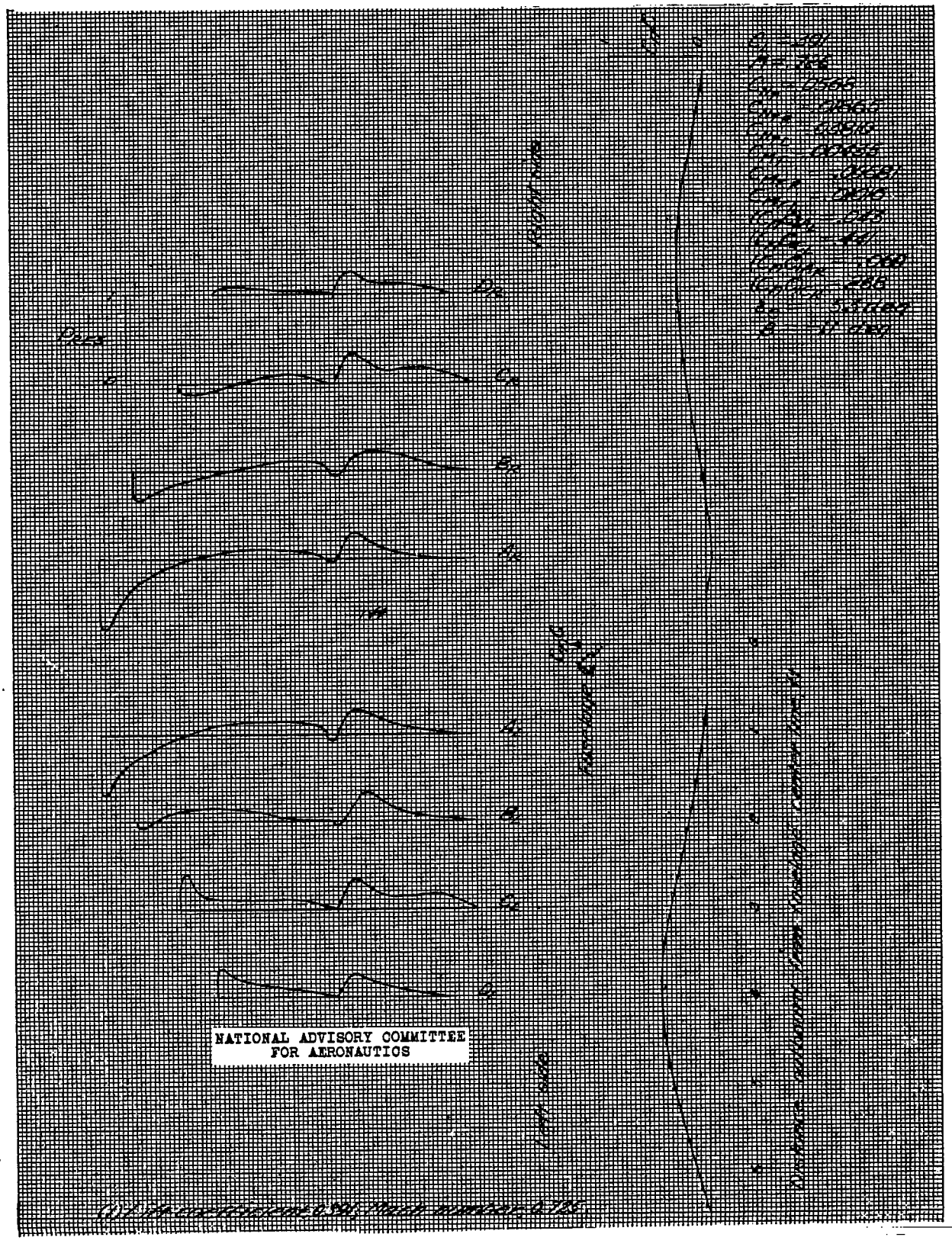

Figure 10.- Continued.

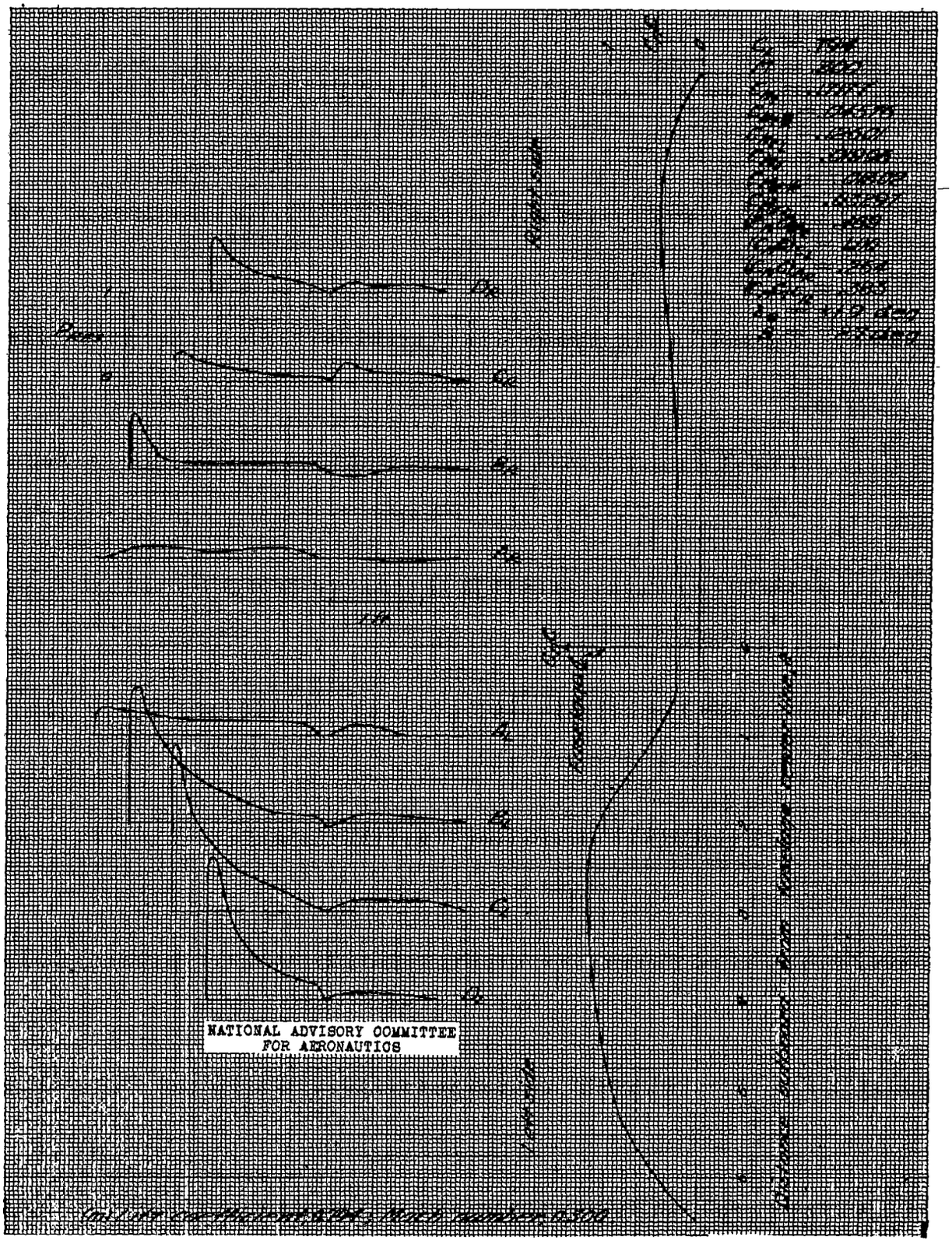

Figure 10.- Continued.

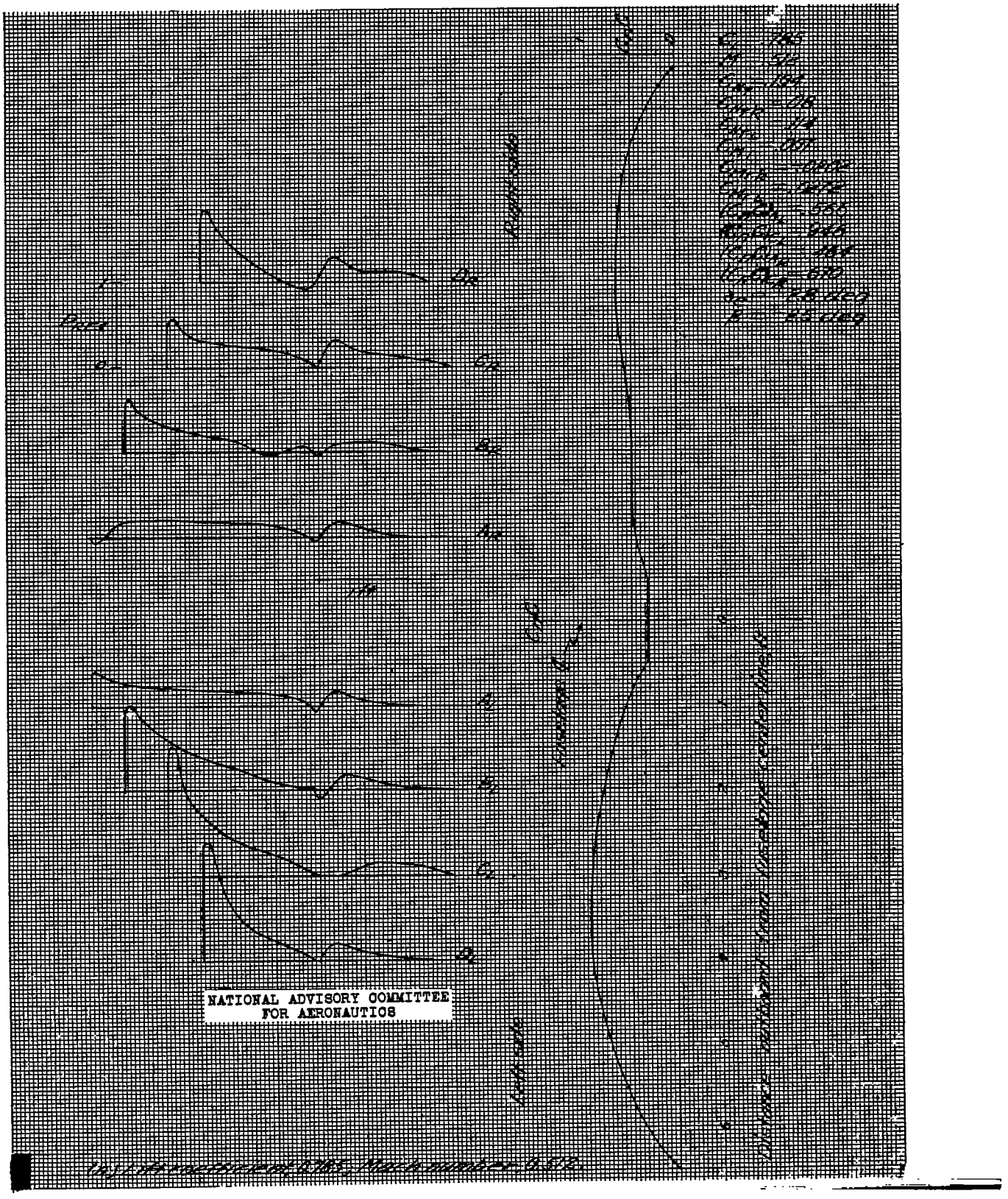

Figure 10.- Concluded.

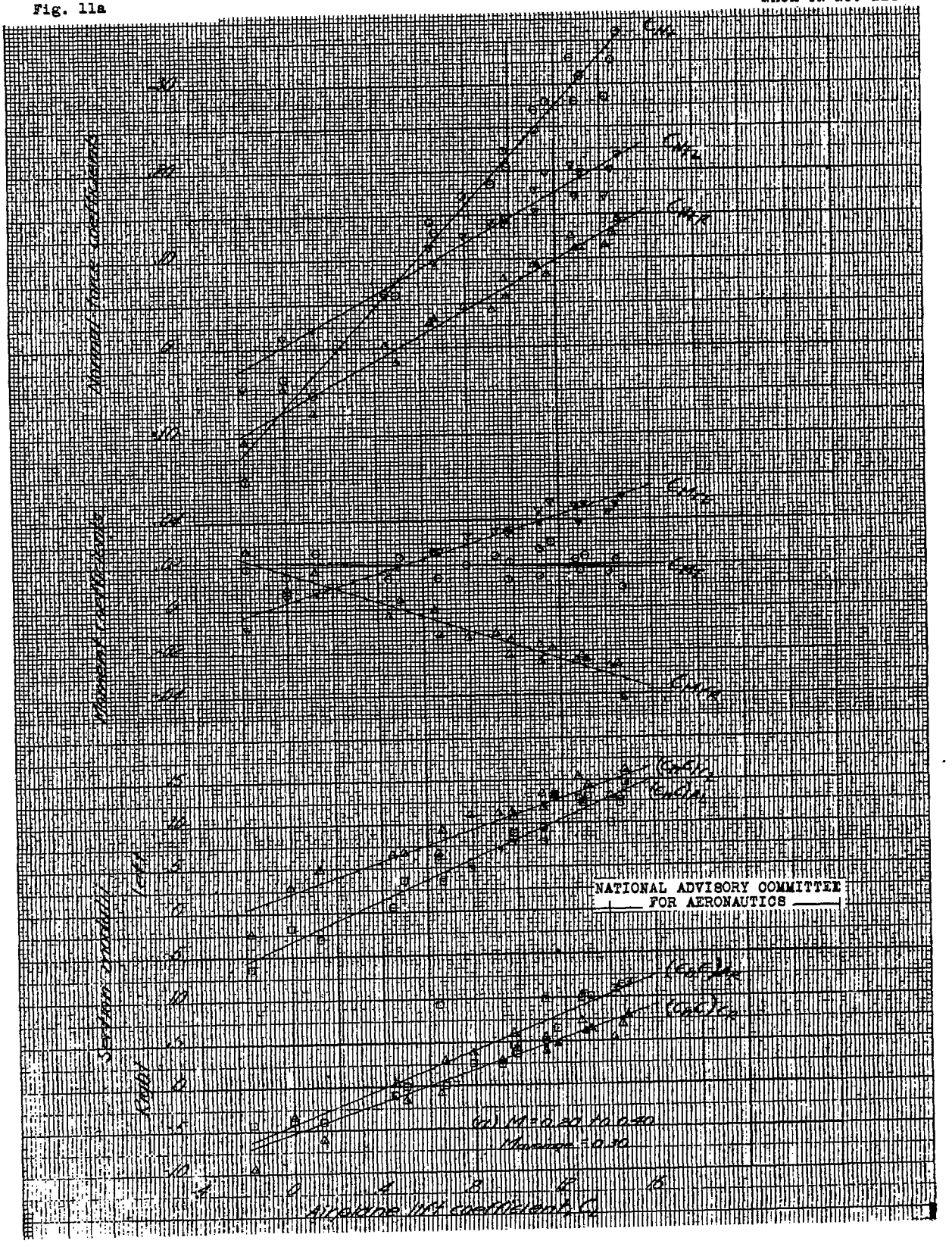

Figure 11(a-d).- Basic power-on data plotted as a function of airplane lift coefficient for several values of Mach number. Test airplane.

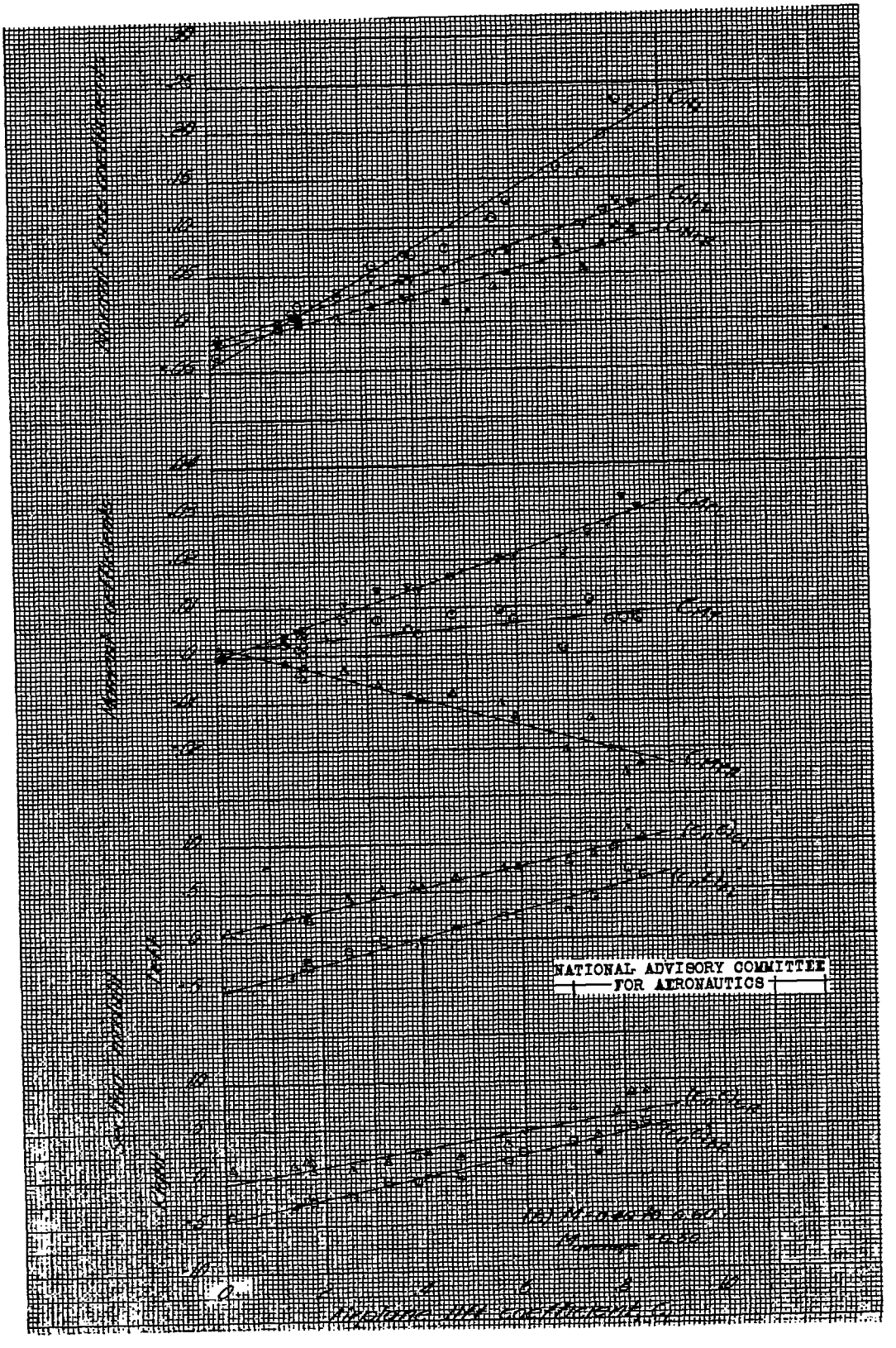

Figure 11.- Continued.

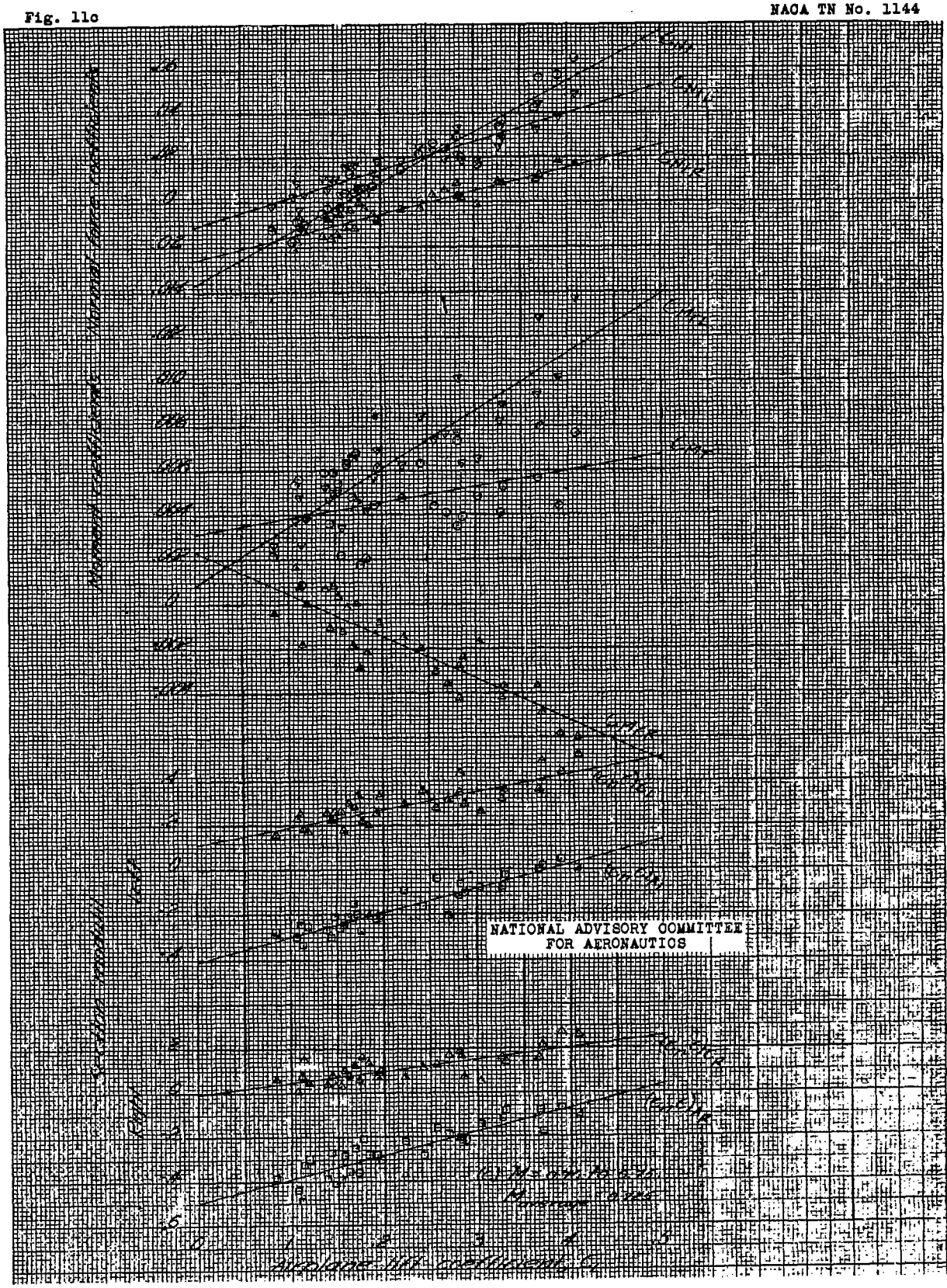

Figure 11.- Continued.

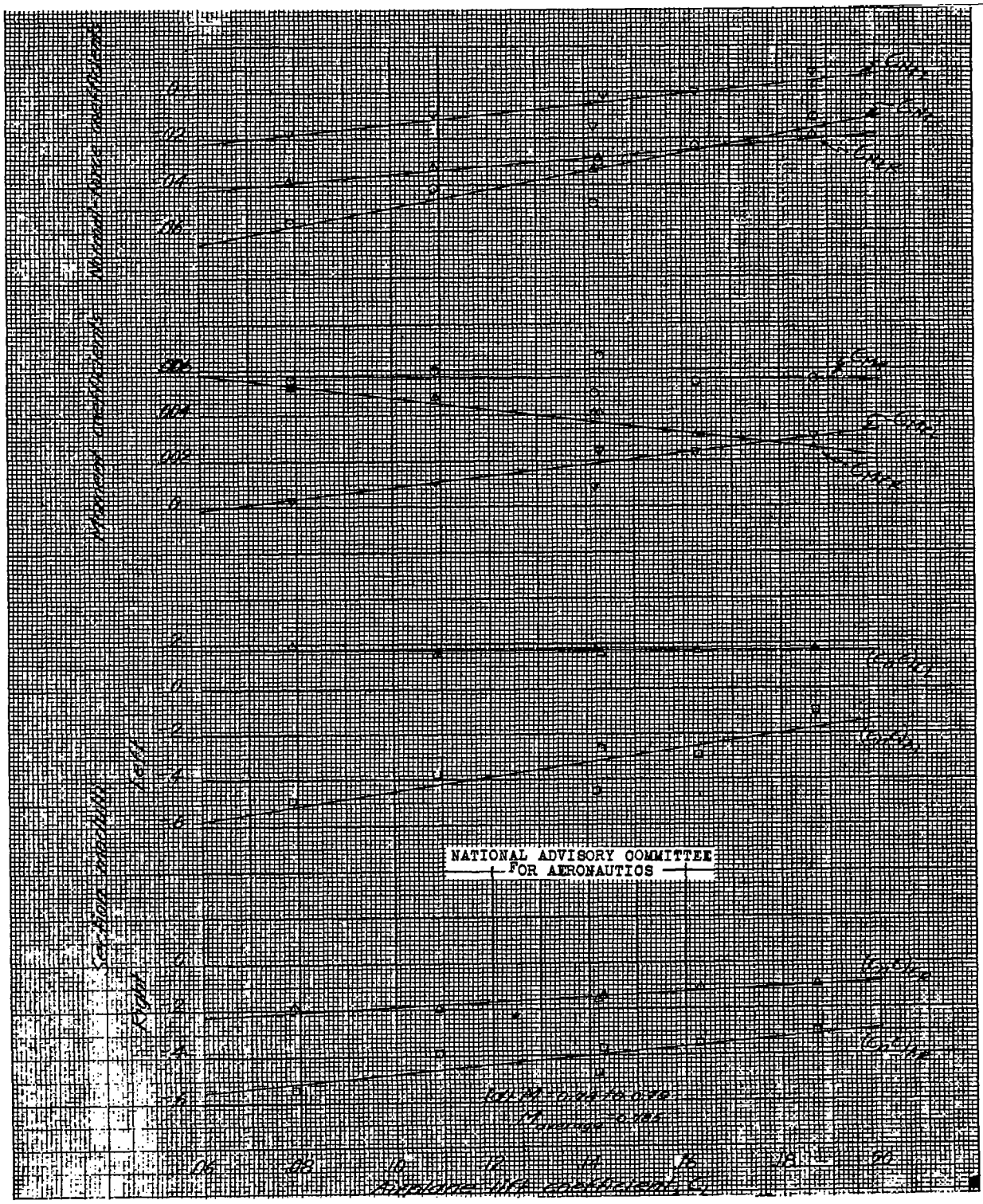

Figure 11.- Concluded.

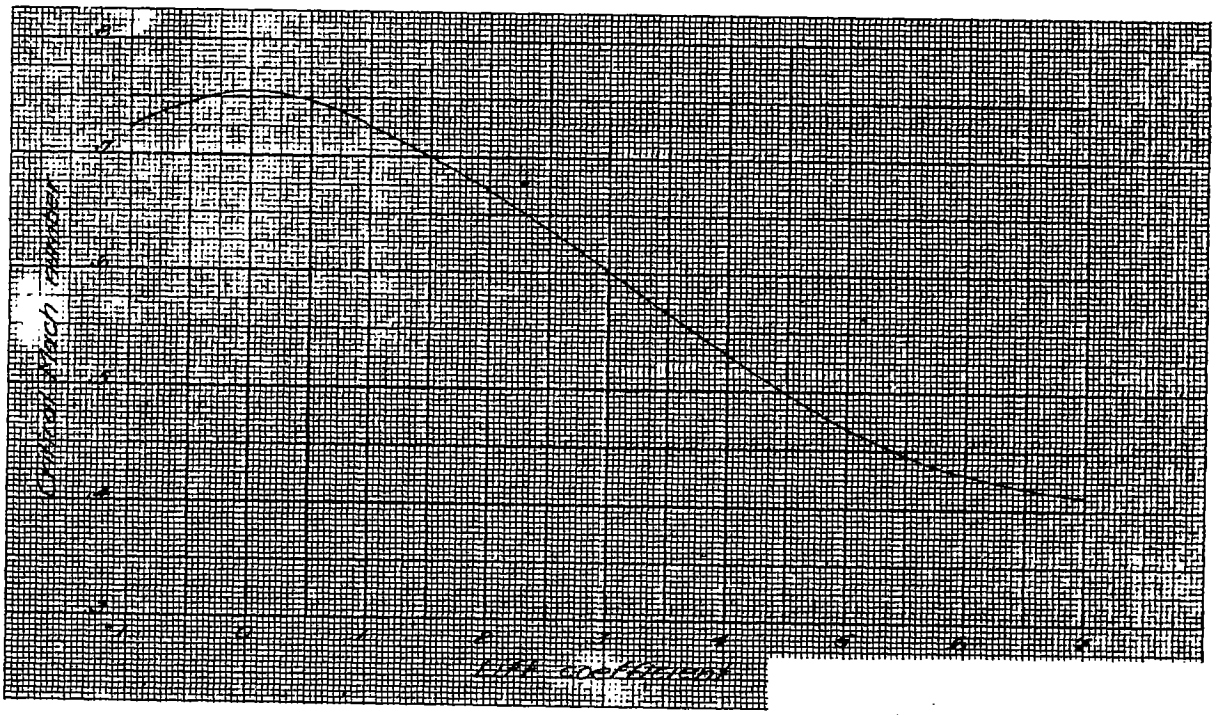

Figure 12.- Variation of the calculated value of critical Mach number with lift coefficient for a symmetrical 9-percent-thick airfoil section. (Data taken from reference 3).

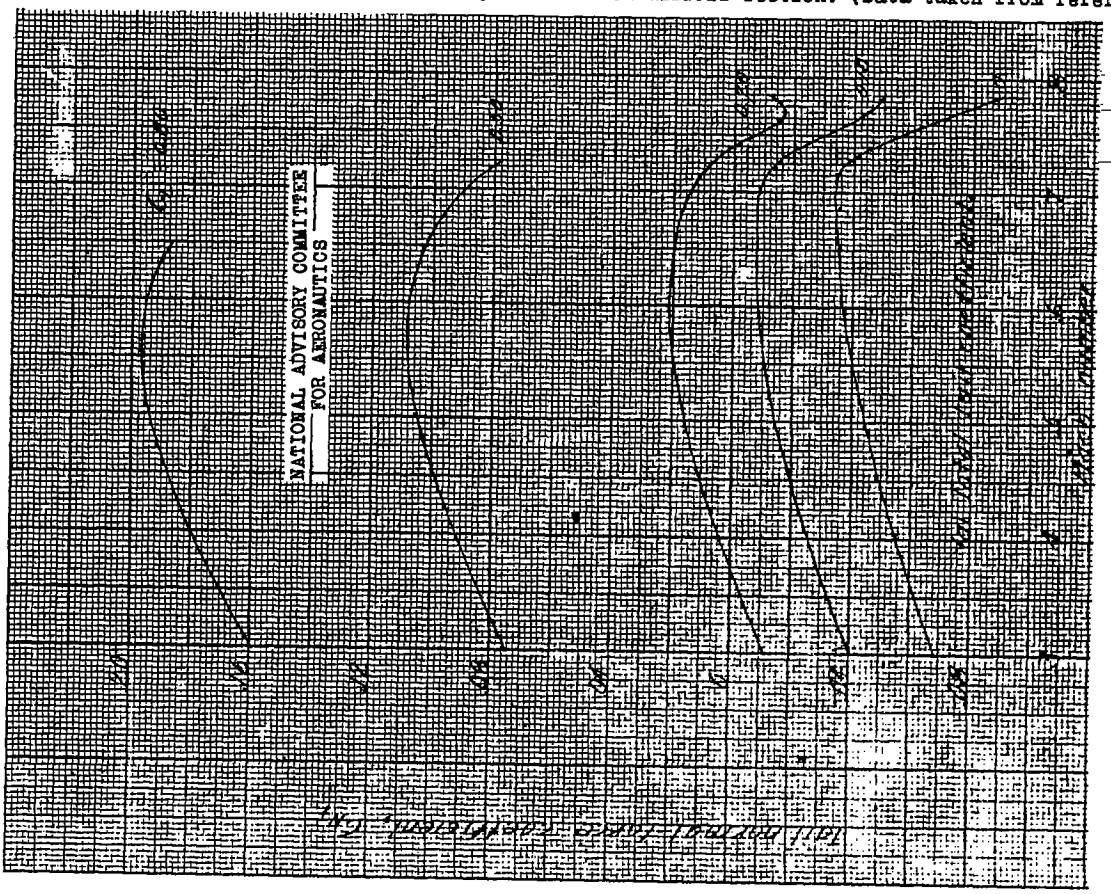

Figure 13(a-c).- Variation of tail normal-force coefficients with Mach number at several values of airplane lift coefficient.

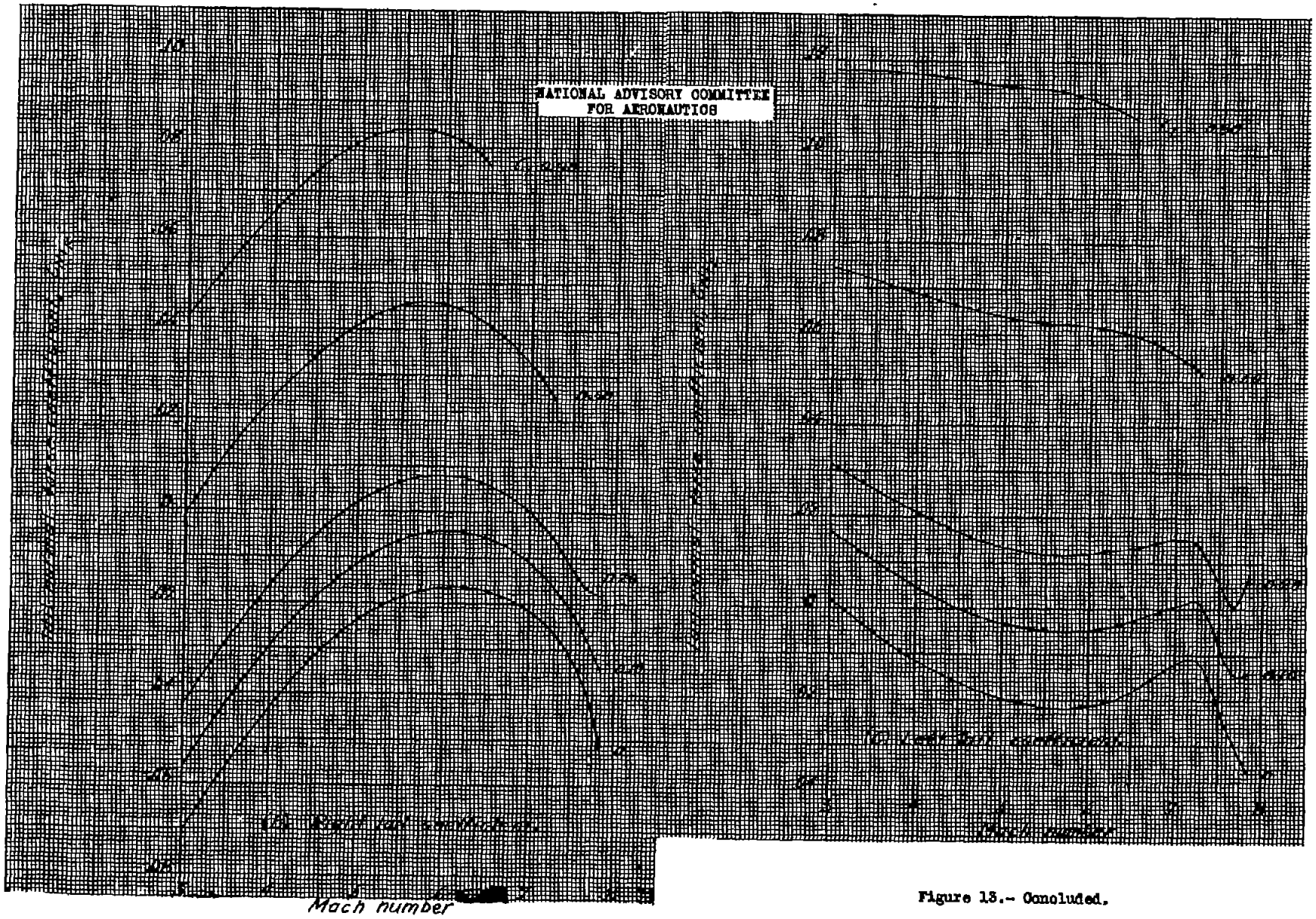

Figure 13.- Continued.

Figure 13.- Concluded.

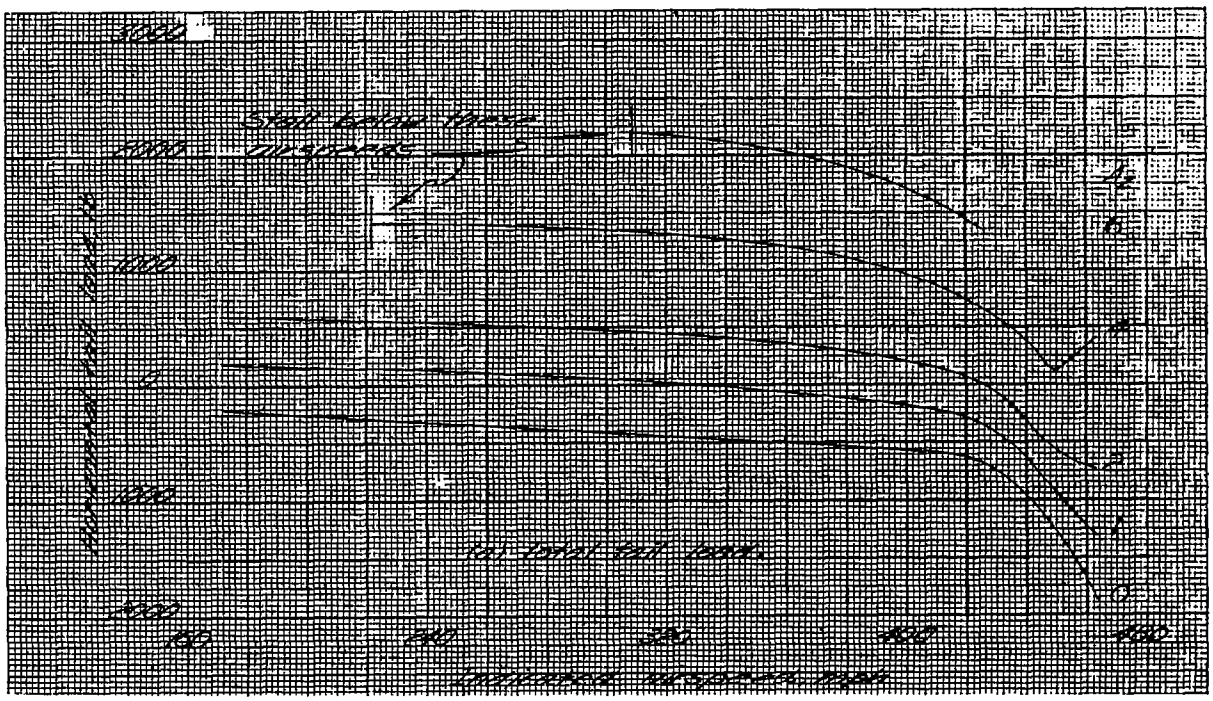

Figure 14(a-c).- Variation with indicated airspeed of horizontal-tail loads at several values of acceleration factor; pressure altitude 15000 feet. Test airplane.

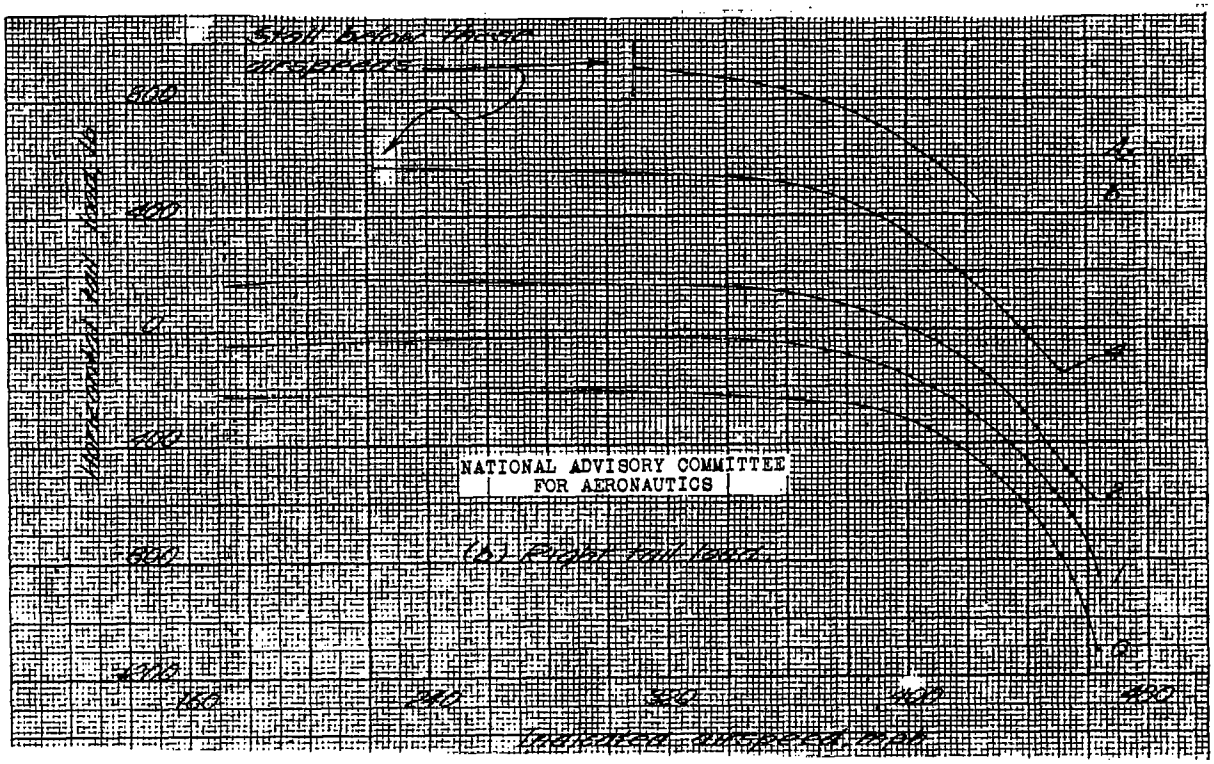

Figure 14.- Continued.

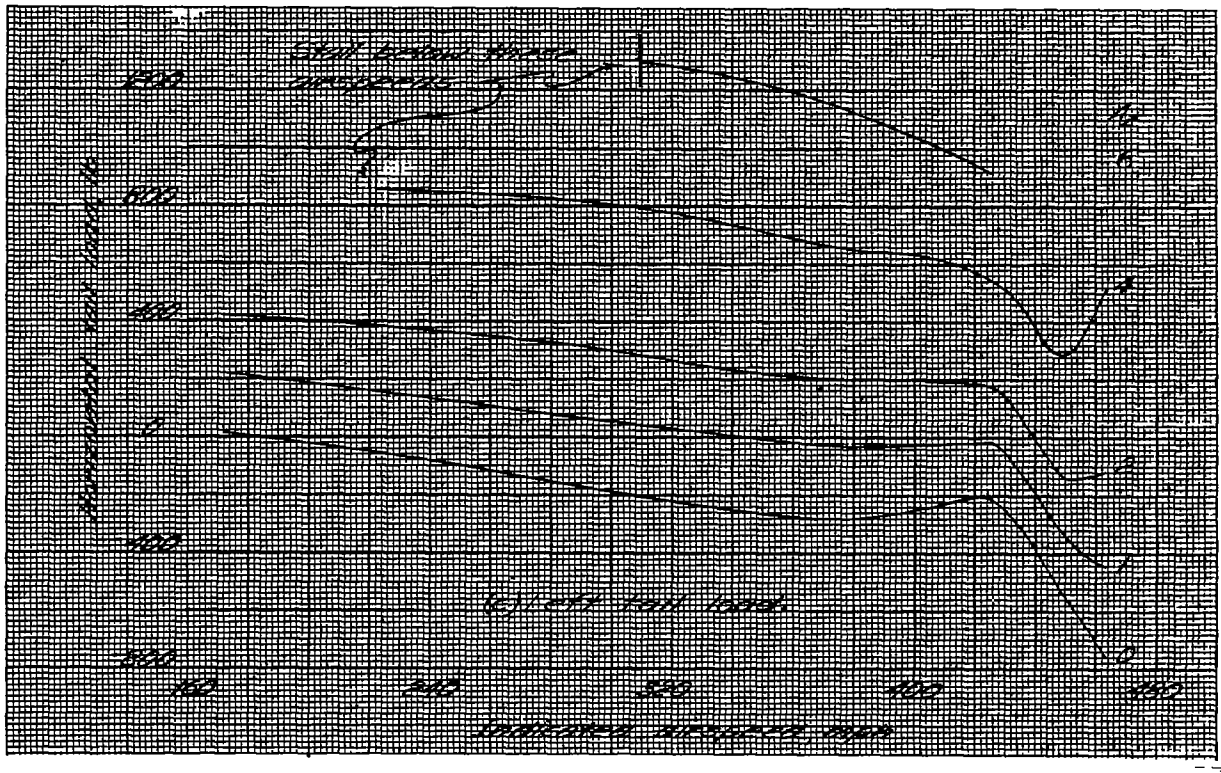

Figure 14.- Concluded.

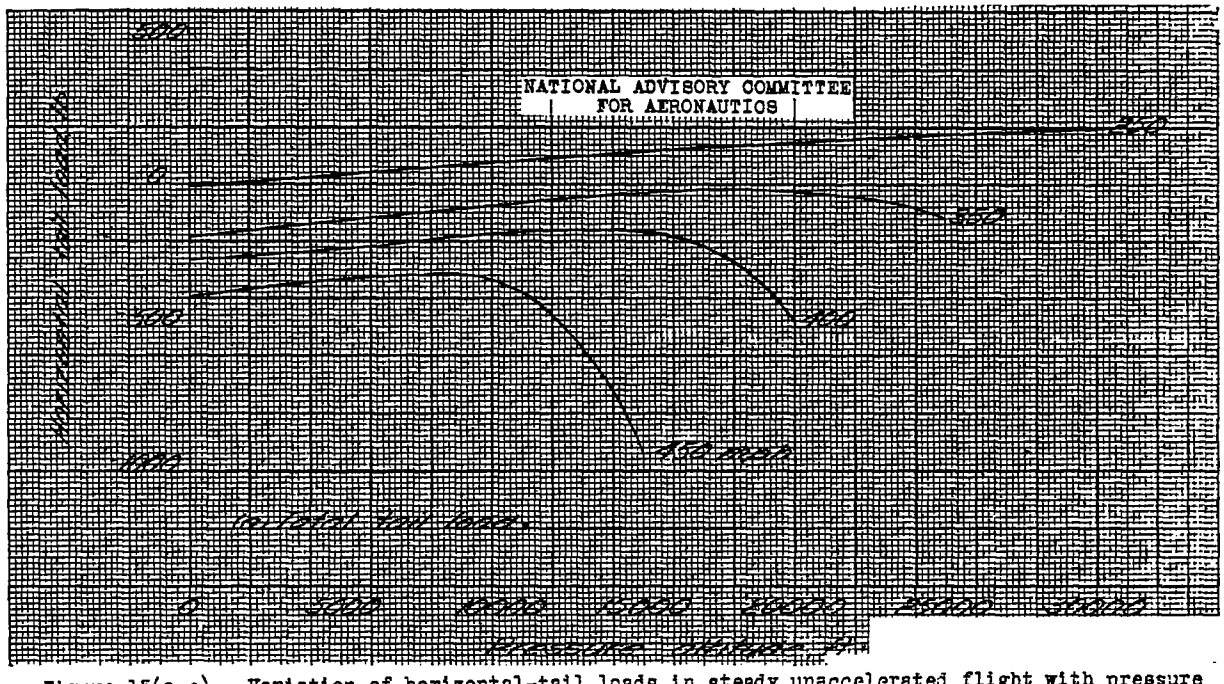

Figure 15(a-c).- Variation of horizontal-tail loads in steady unaccelerated flight with pressure altitude at several values of indicated airspeed. Test airplane.

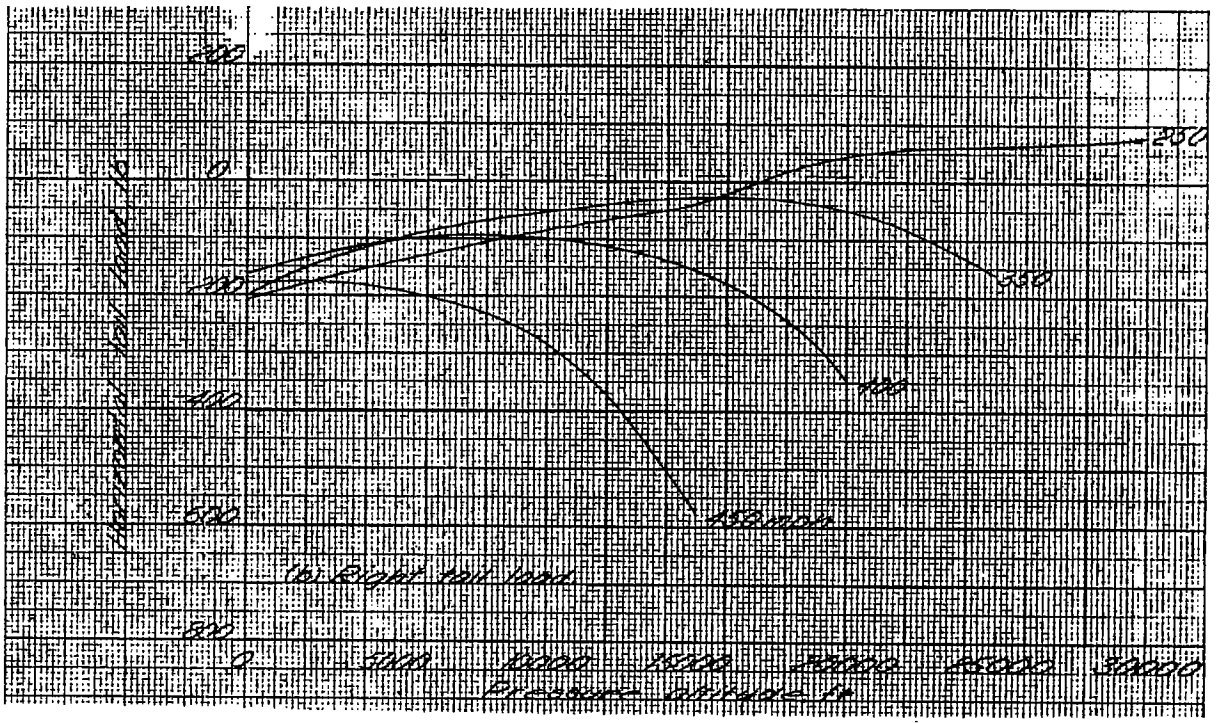

Figure 15.- Continued.

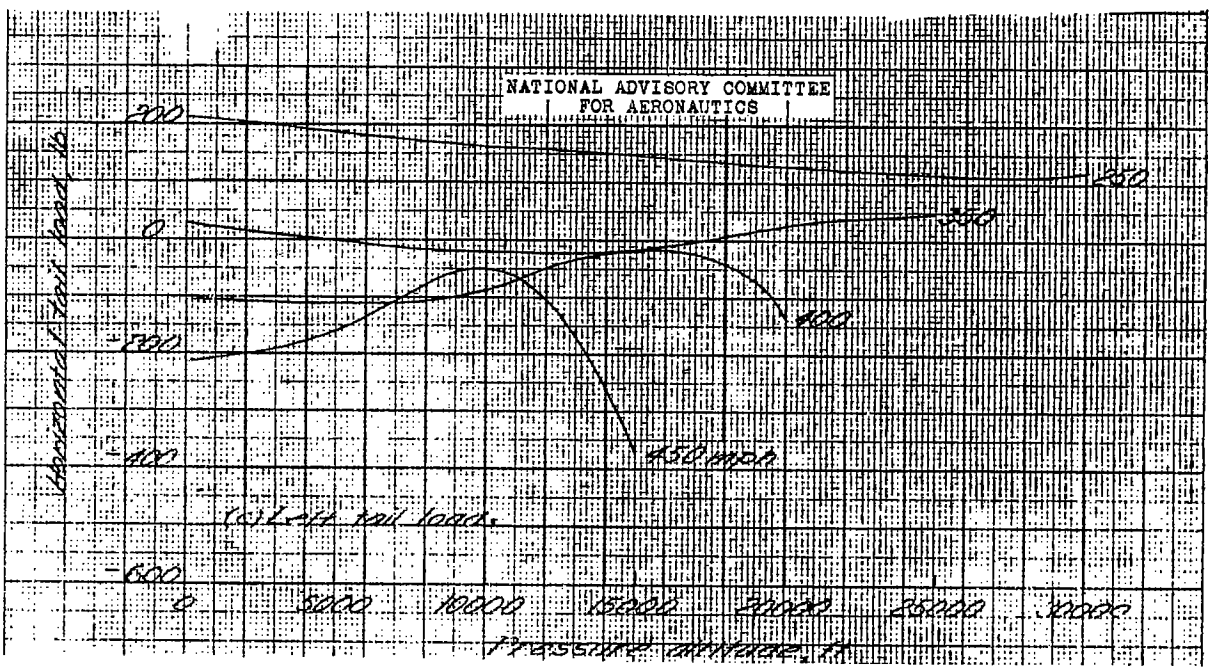

Figure 15.- Concluded.

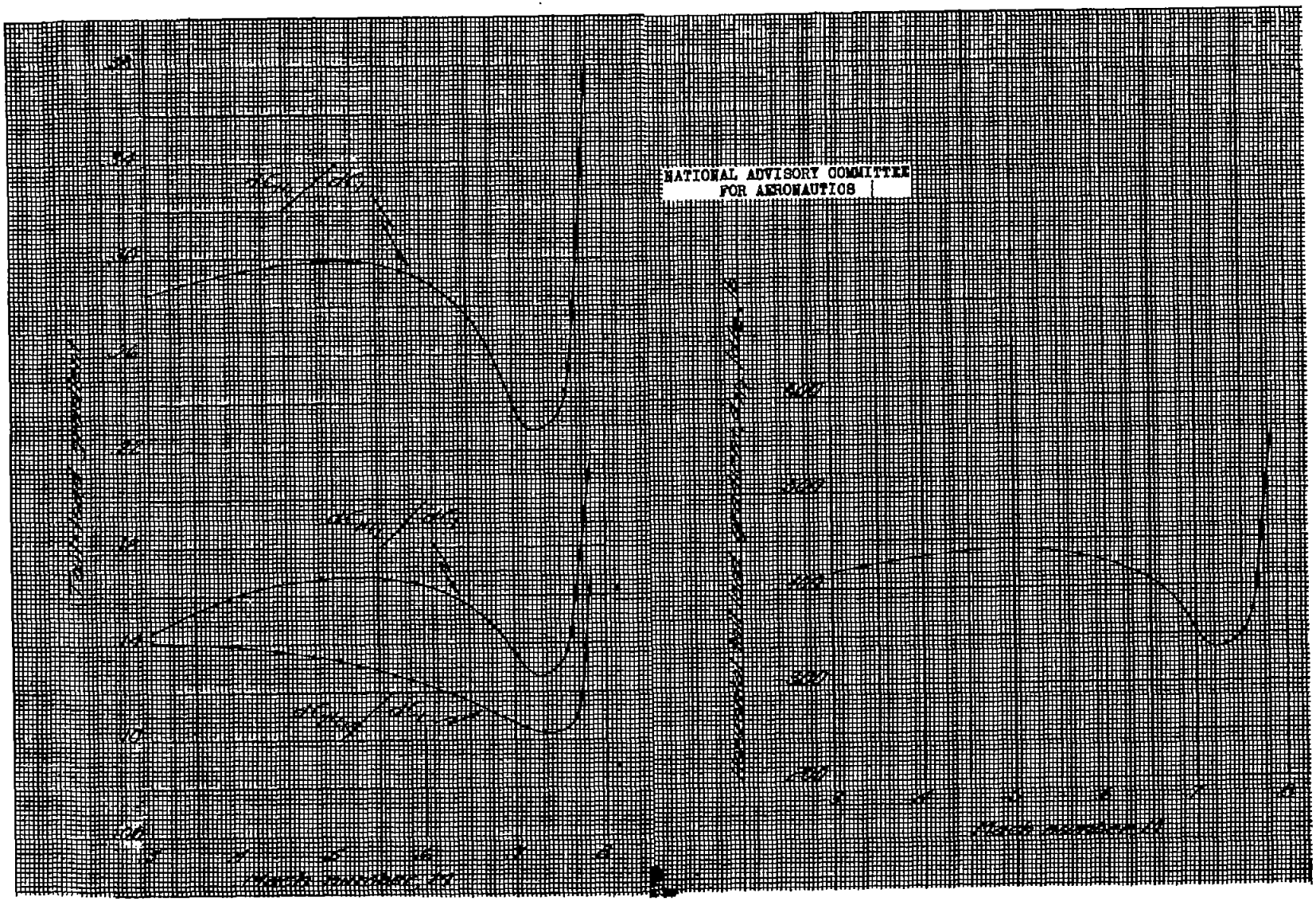

Figure 16.- Variation with Mach number of rate of change of tail normal-force coefficient with airplane lift coefficient. Test airplane.

Figure 17.- Variation of tail-load gradient with Mach number. Test airplane.

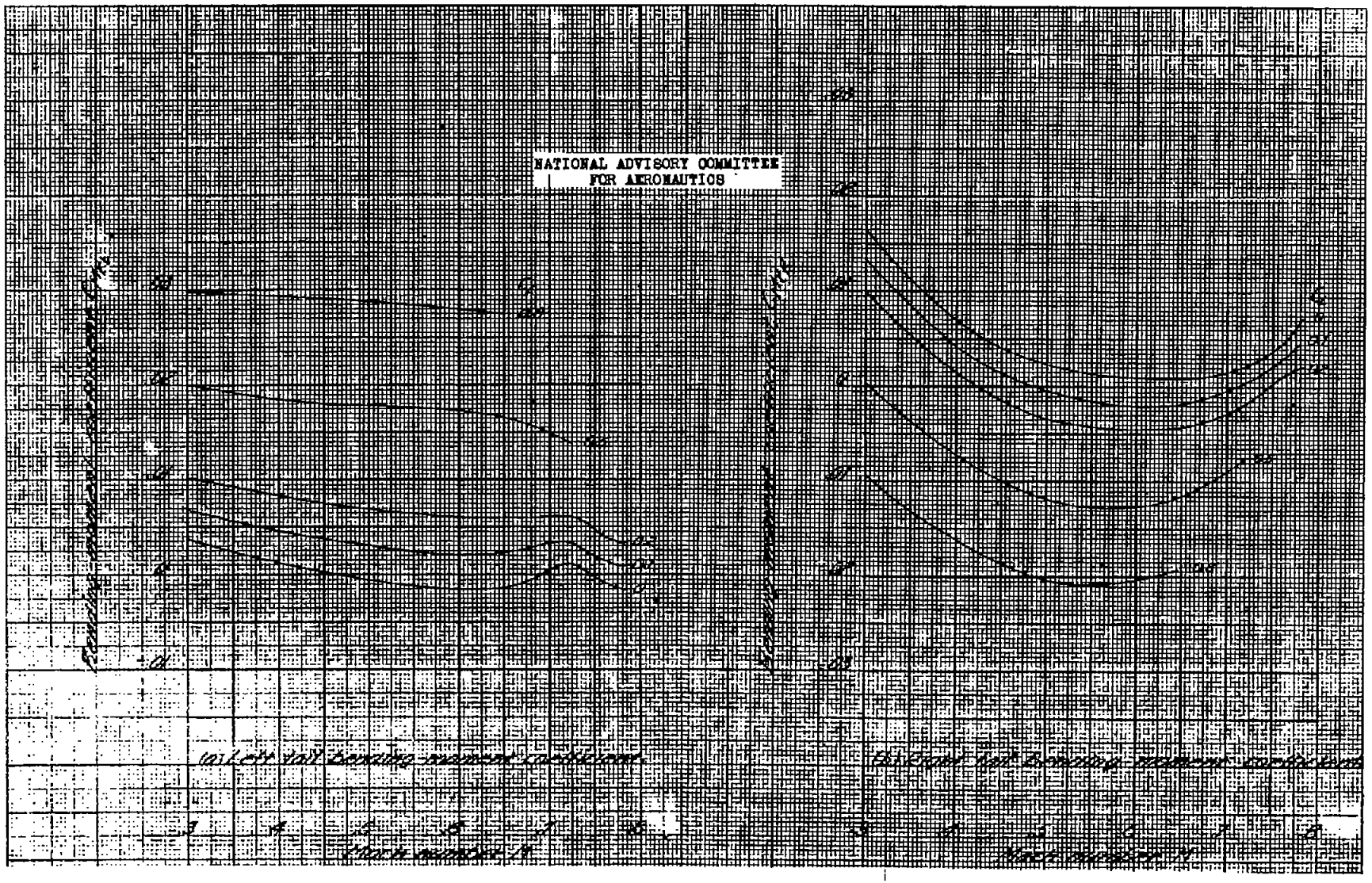

Figure 18(a-c).- Variation of root bending-moment coefficients and fuselage torsional-moment coefficient with Mach number at several values of airplane lift coefficient. Test airplane.

Figure 18.- Continued.

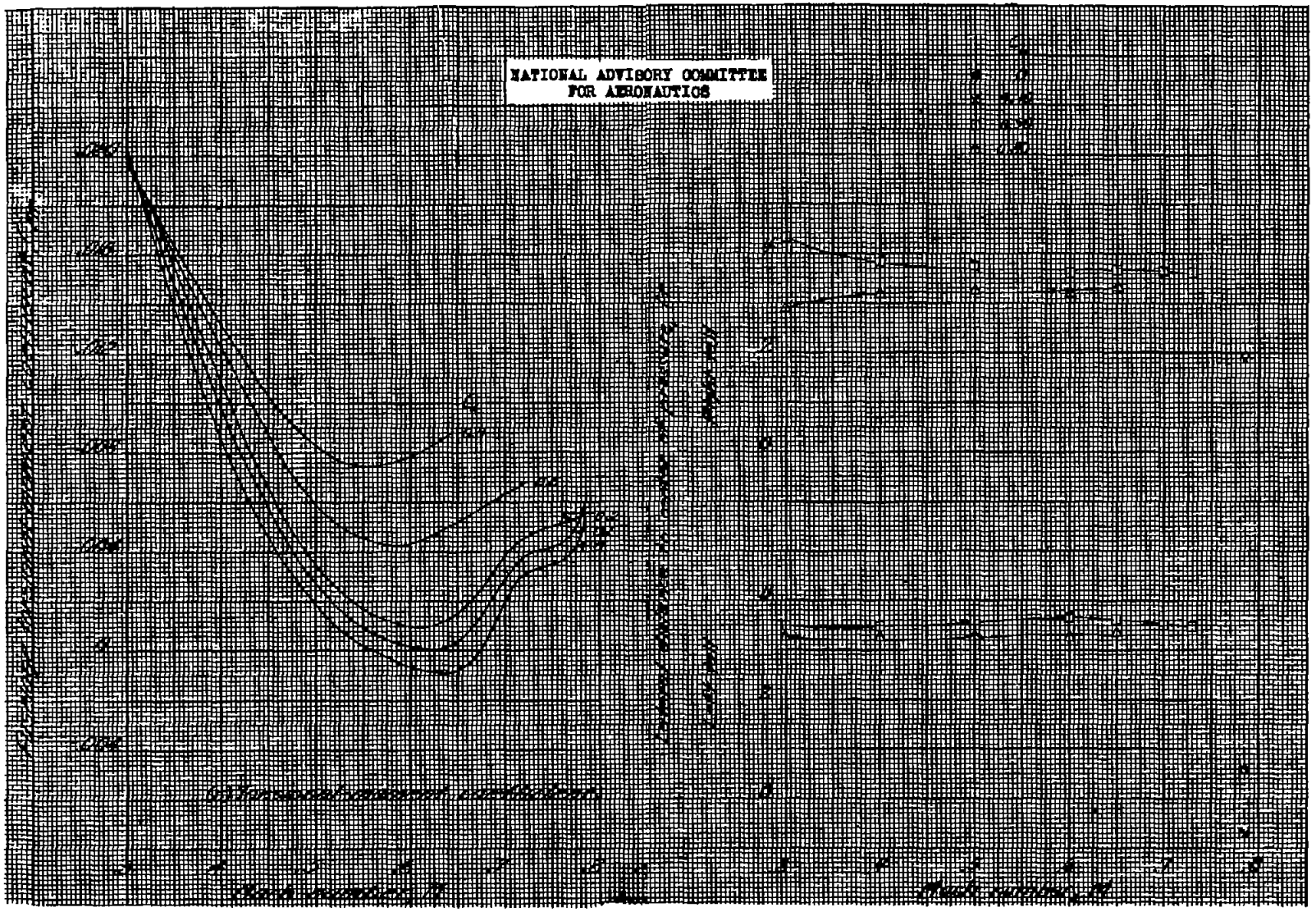

Figure 18.- Concluded.

Figure 19.- Variation of lateral distance to center of pressure on right and left tail with Mach number. Test airplane.

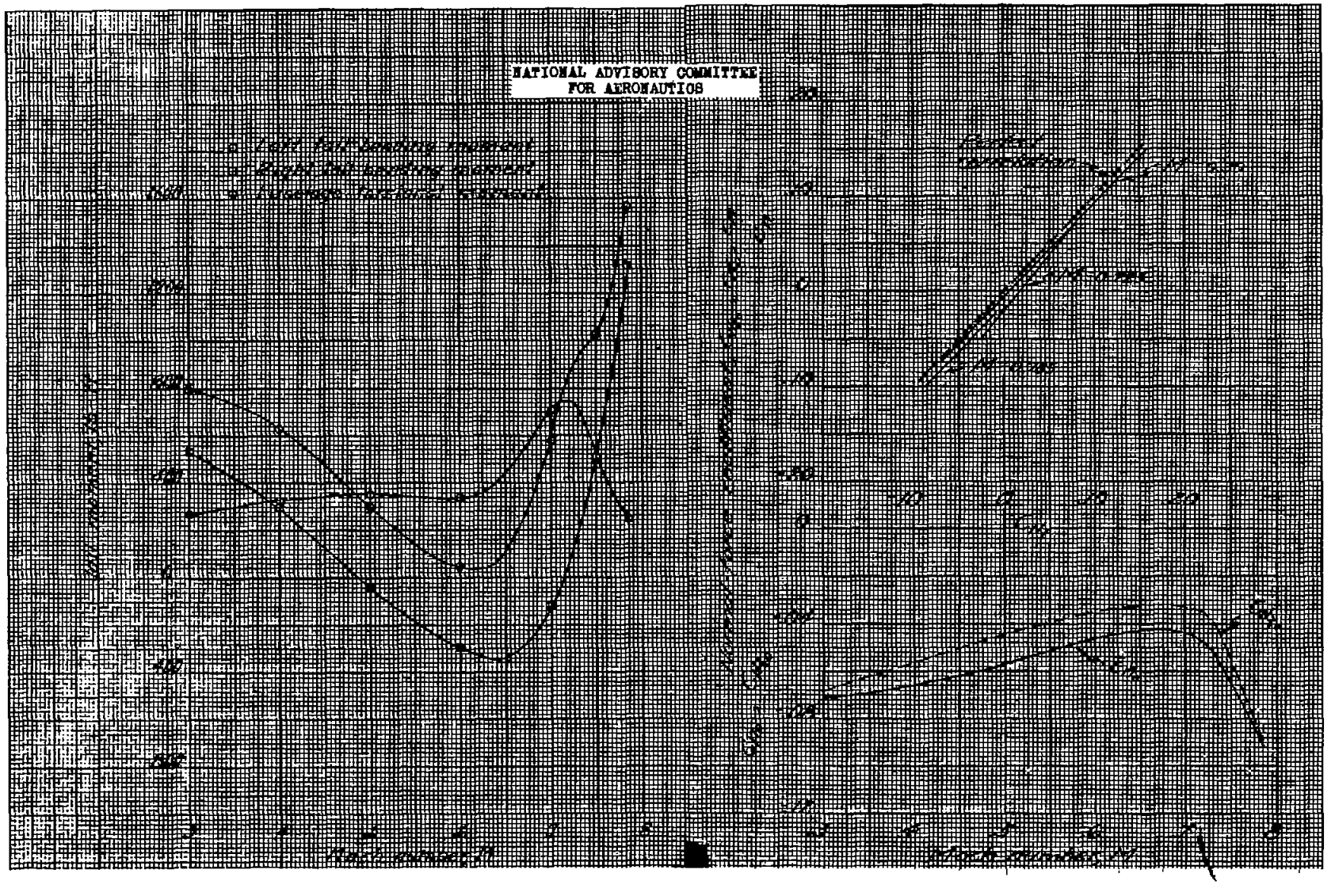

Figure 20.- Variation of left and right tail root bending moments and fuselage torsional moments with Mach number at an airplane lift coefficient of 0.10. Test airplane.

Figure 22.- Comparison of the average of the section characteristics with the total tail characteristics. Test airplane.

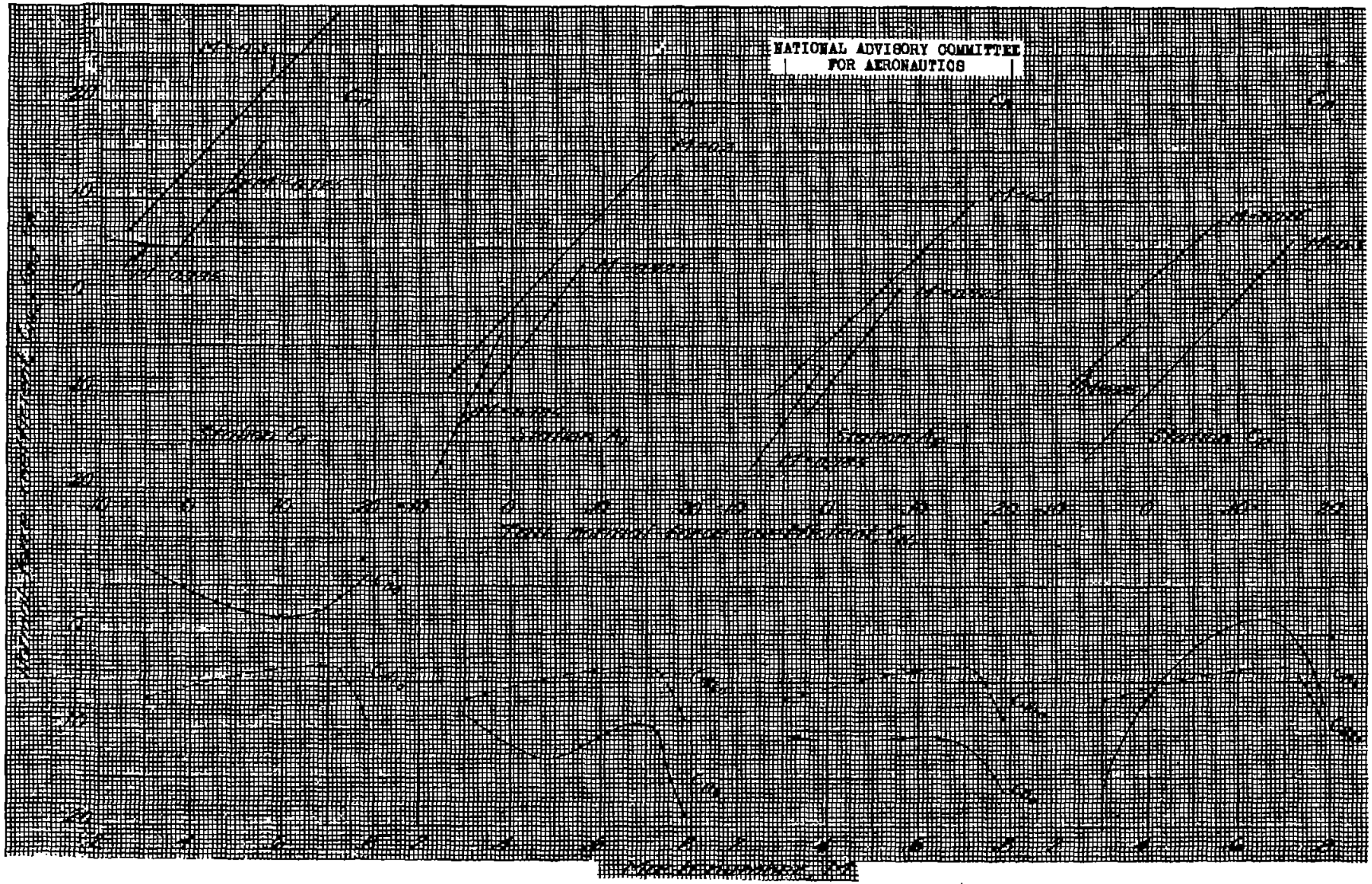

Figure 21.- Comparison of section characteristics with total tail characteristics. Test airplane.

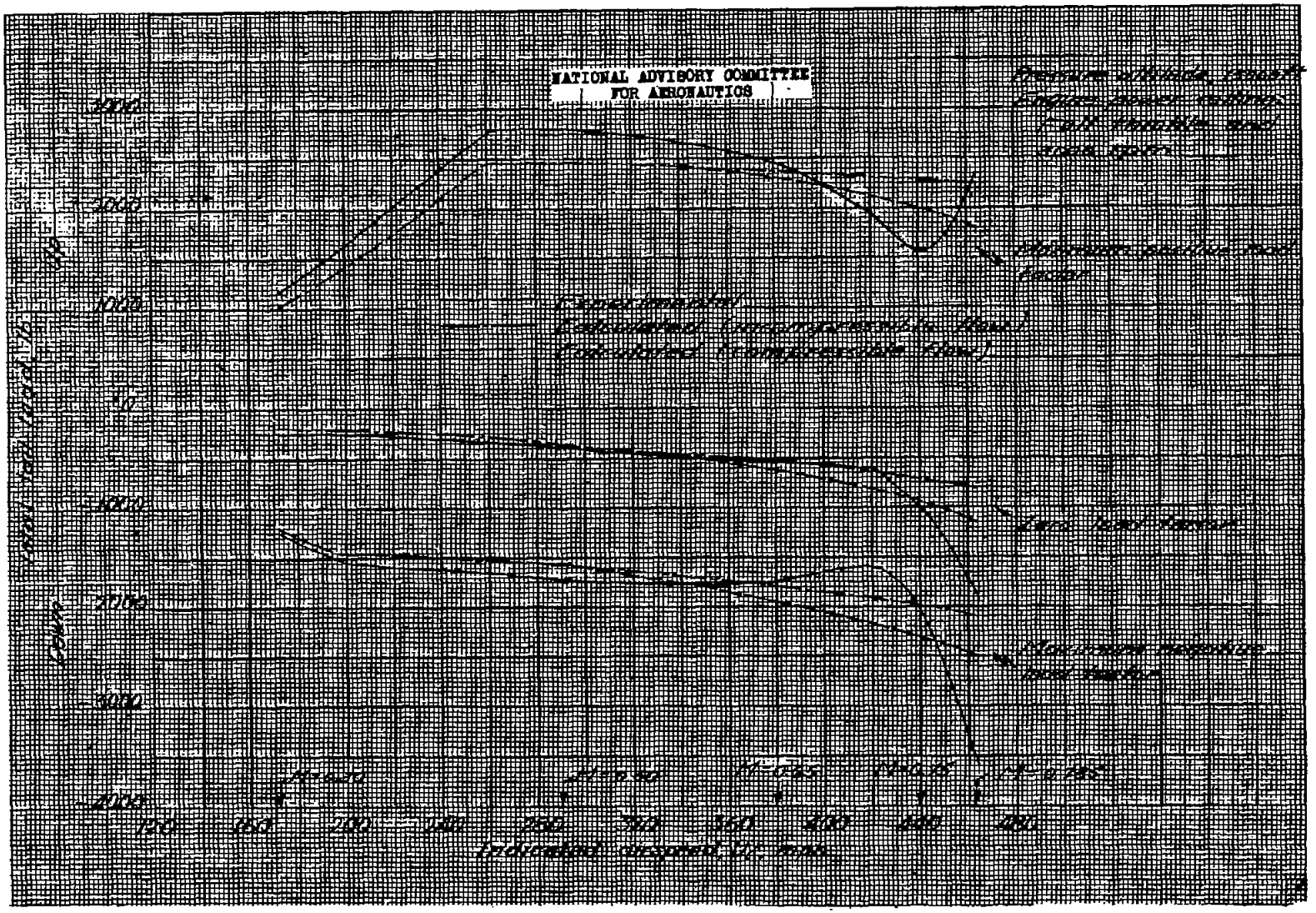

Figure 23.- Comparison of calculated with experimental balancing tail loads at maximum positive, zero and maximum negative load factors. Test airplane.

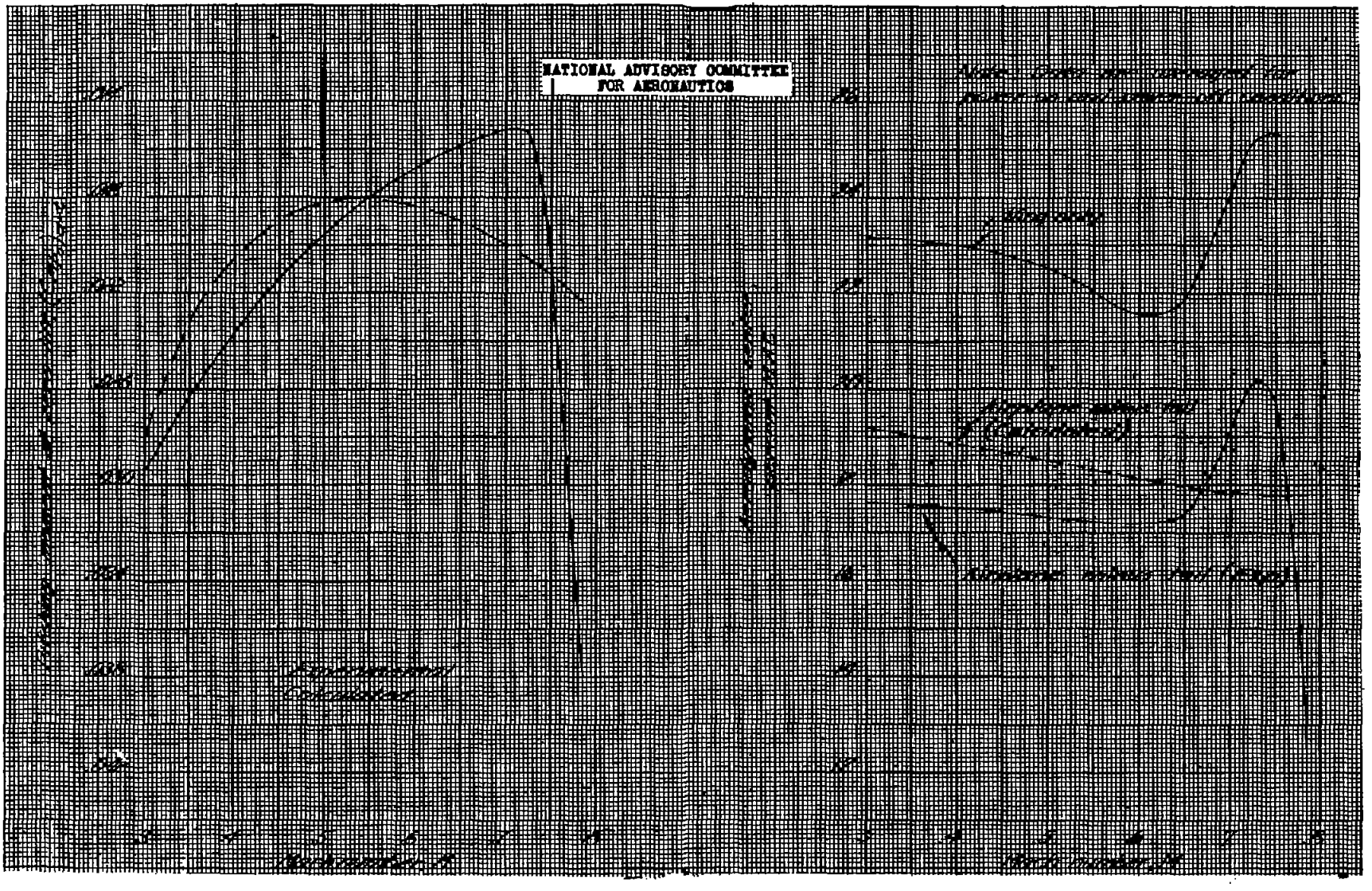

Figure 24.- Variation of pitching moment at zero lift of airplane minus tail with Mach number. Test airplane.

Figure 25.- Variation with Mach number of the aerodynamic center of the wing and the wing-fuselage-propeller group. Test airplane.

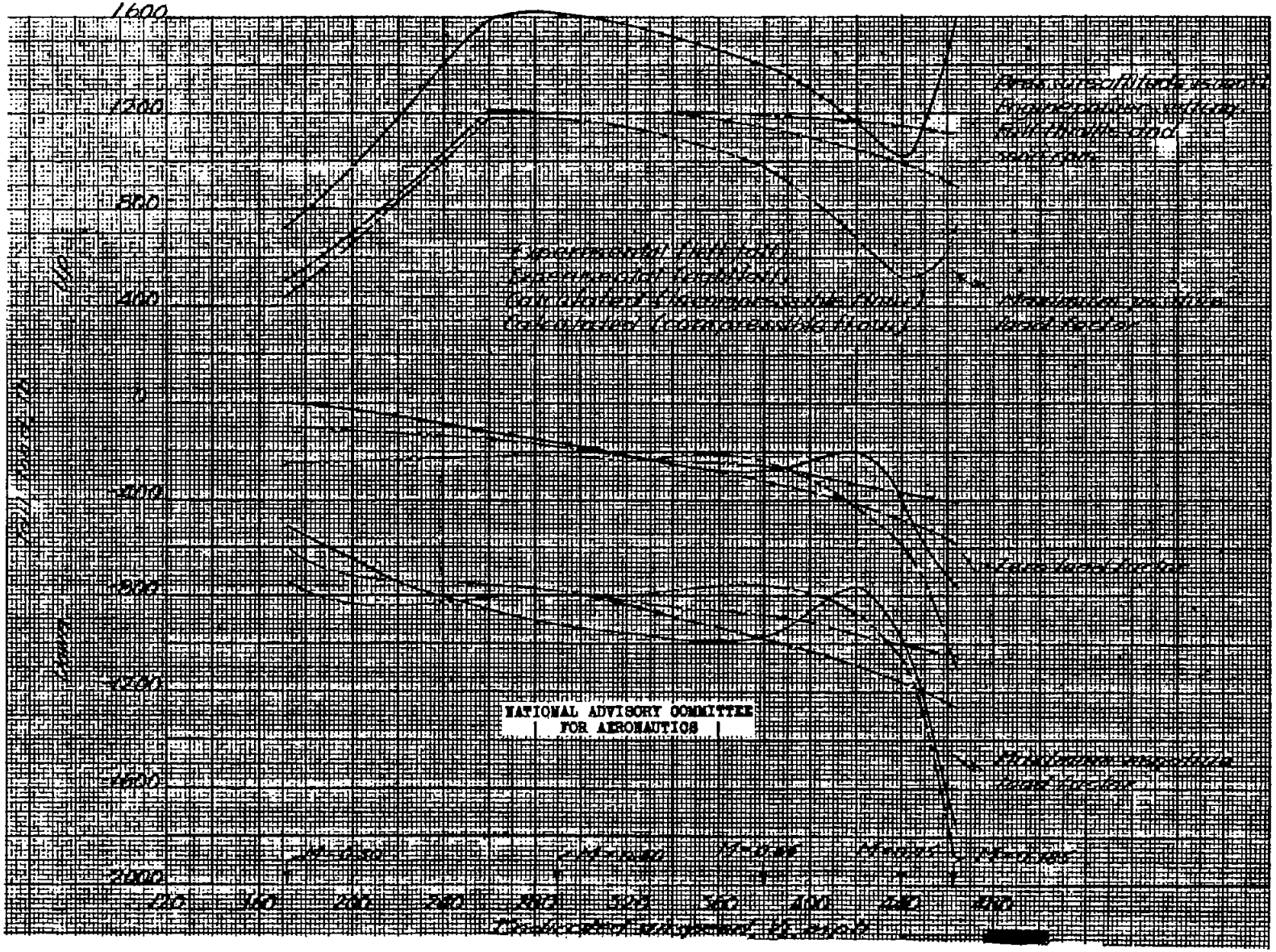

Figure 26.- Comparison of the calculated left (or right) tail loads with the experimental values at maximum positive, zero and maximum negative load factors. Test airplane.

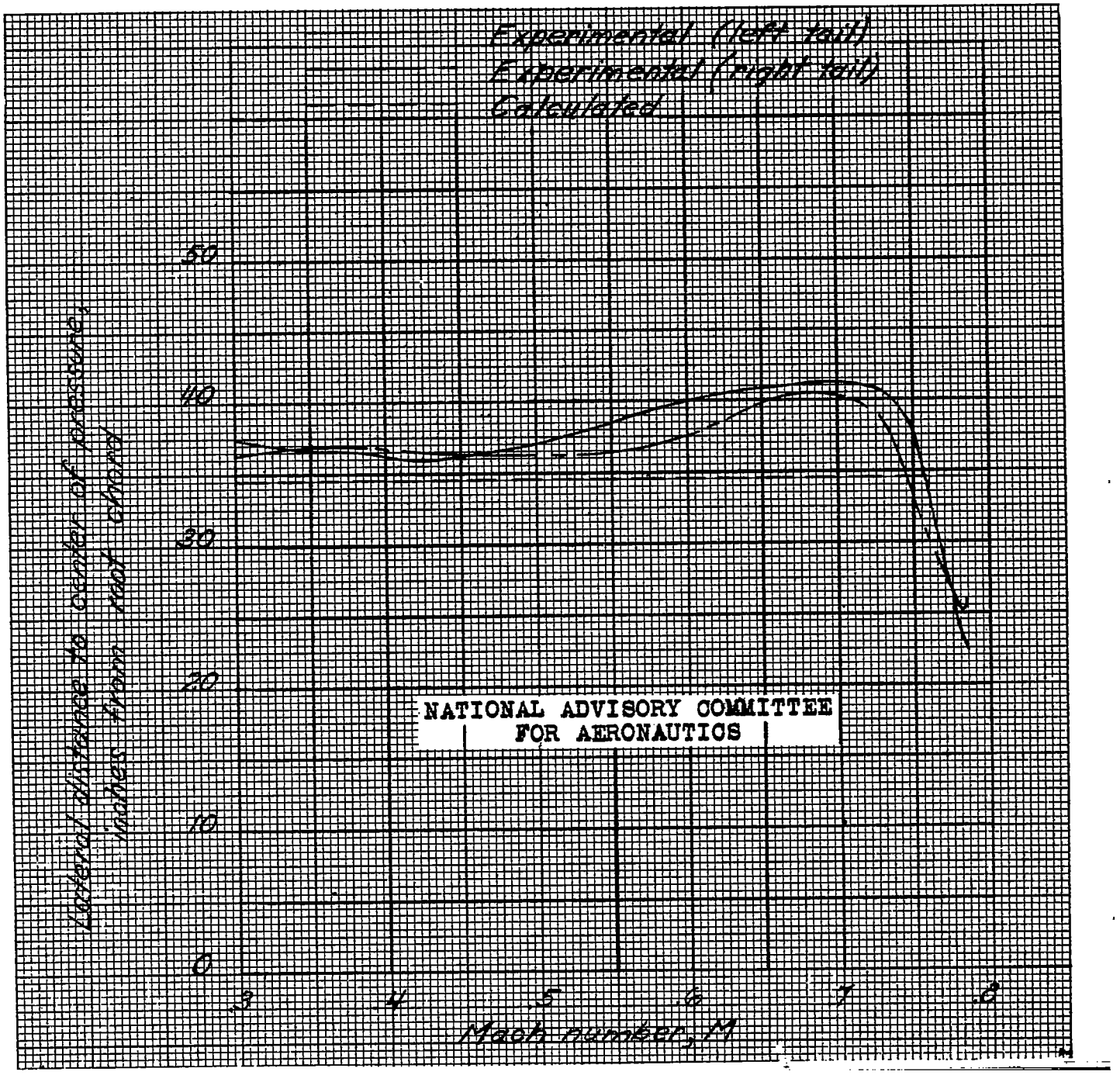

Figure 27.- Variation of lateral distance to center of pressure at maximum positive load factor with Mach number. Test airplane.

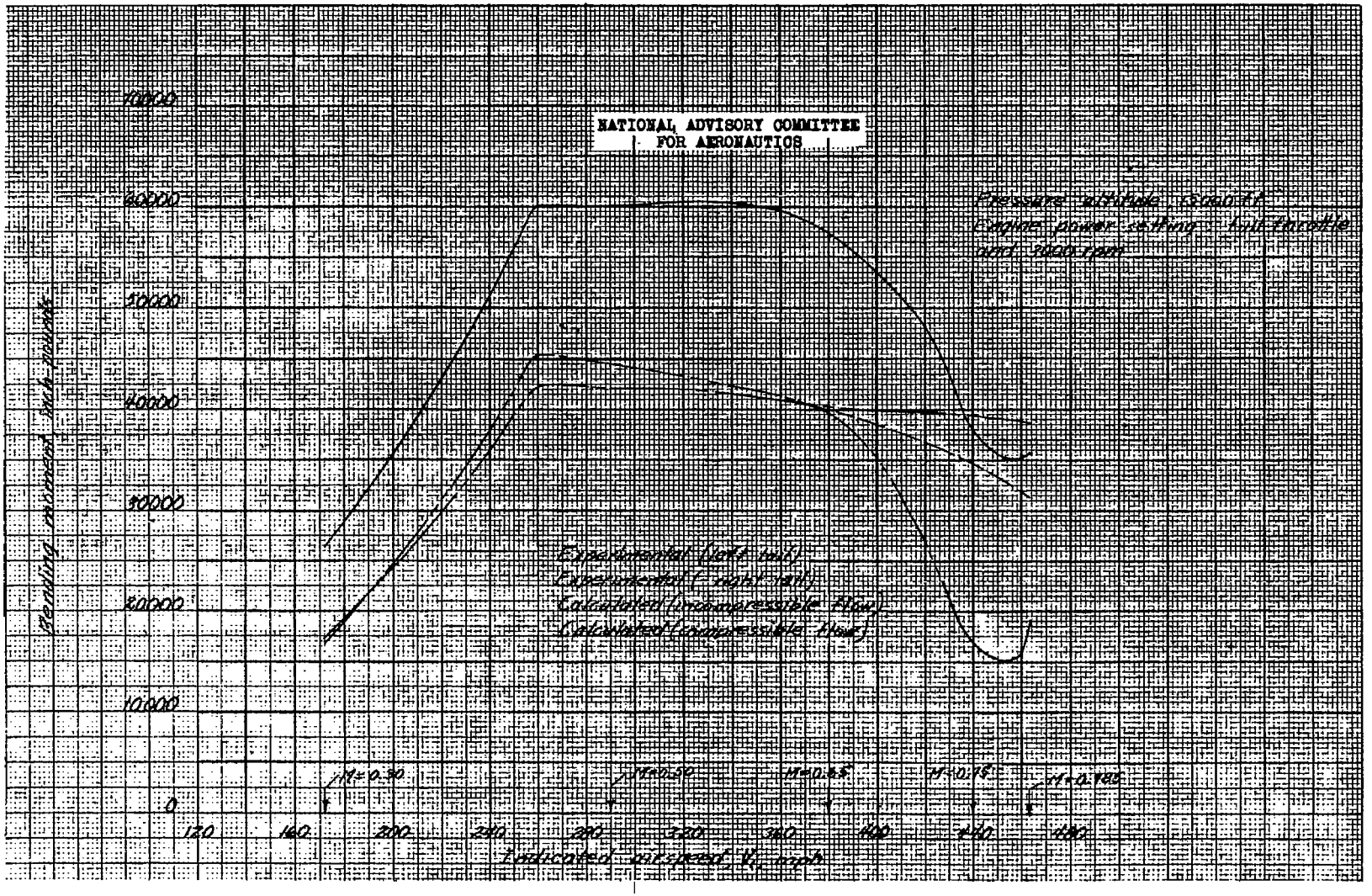

Figure 28.- Comparison of the calculated with the experimental left and right tail bending moments at maximum positive load factor. Test airplane.

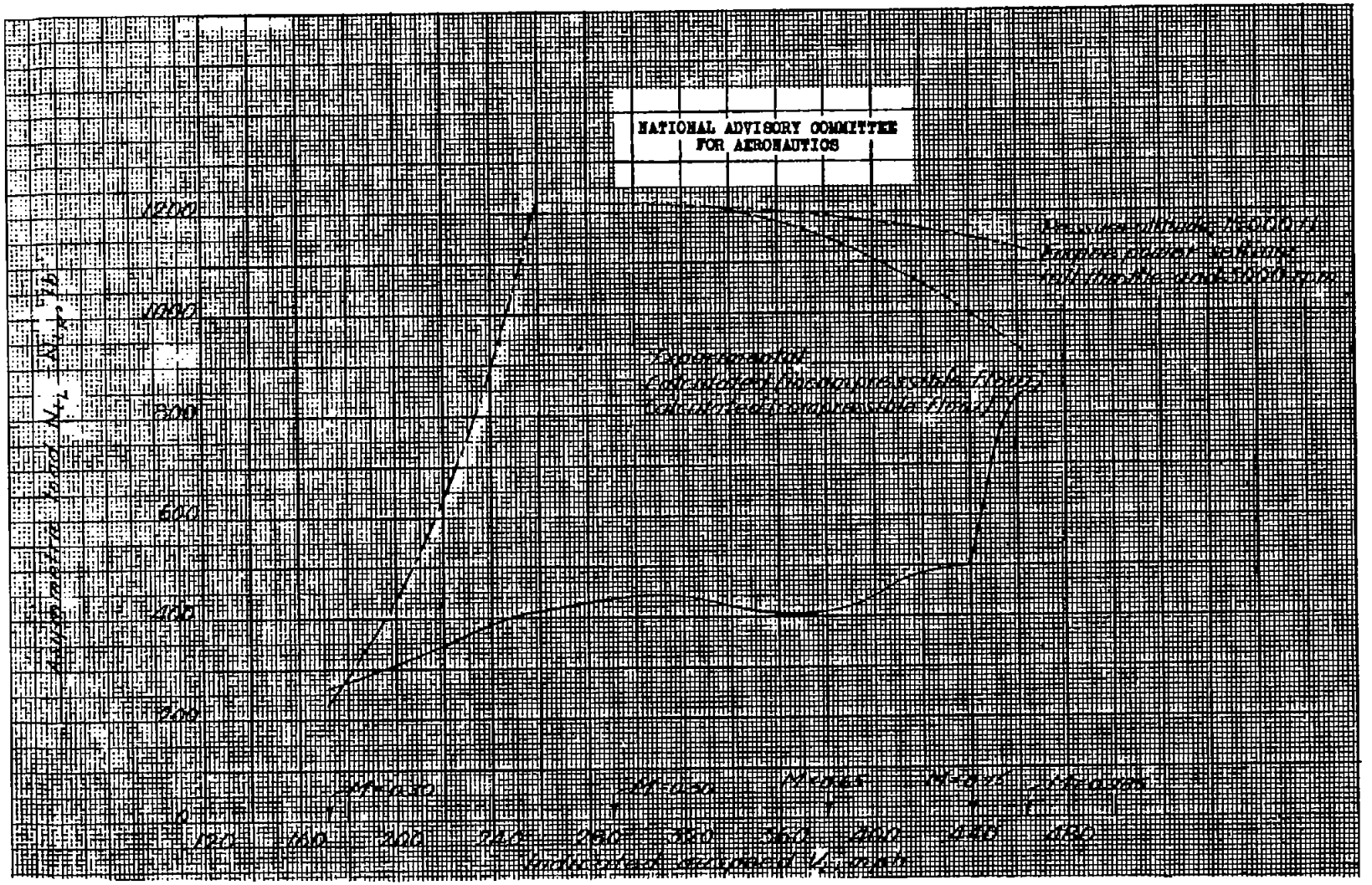

Figure 29.- Comparison of calculated with experimental asymmetric loads at maximum positive load factor. Test airplane.

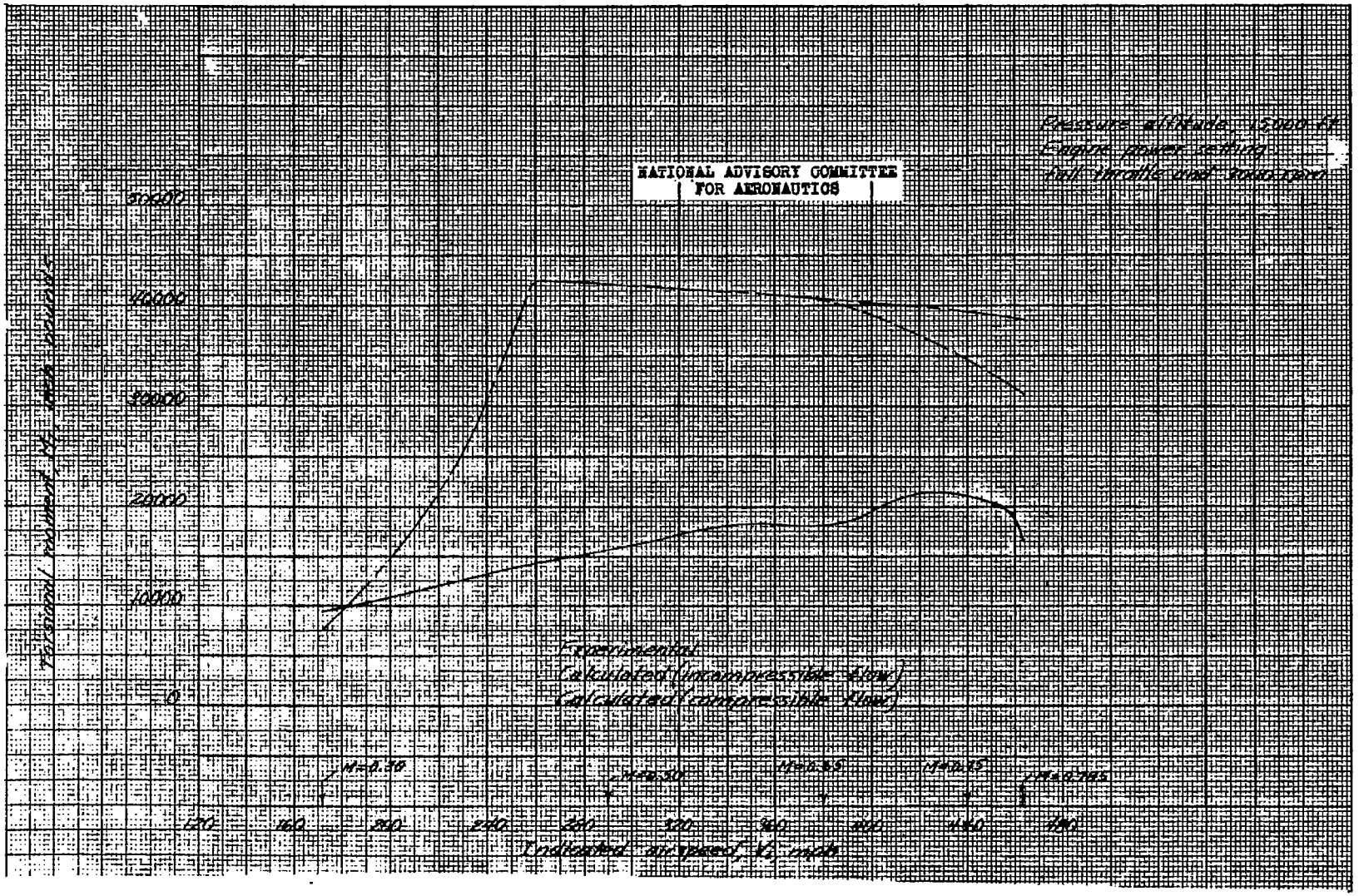

Figure 30.- Comparison of calculated with experimental torsional moments at maximum positive load factor. Test airplane.

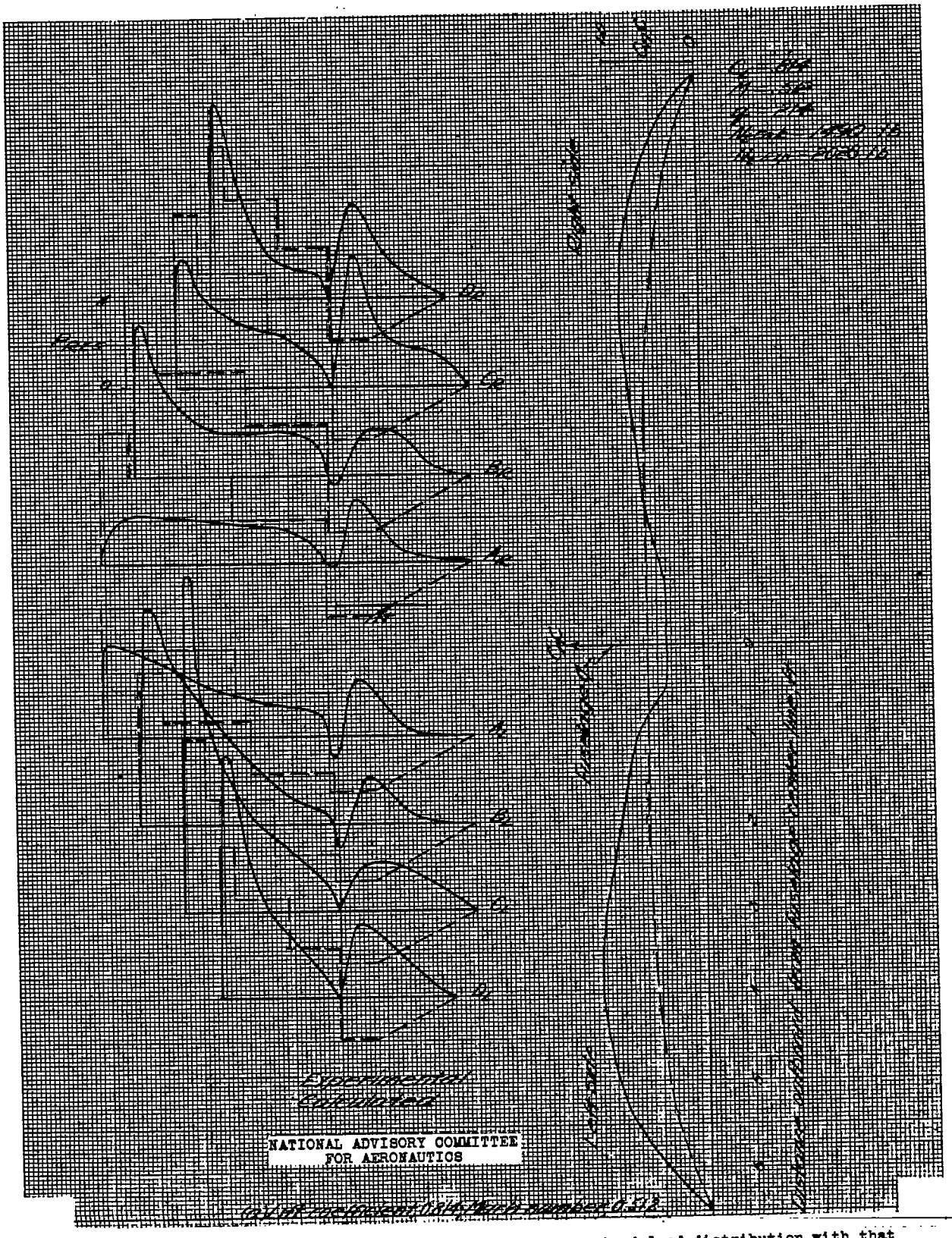

Figure 31(a-d).- Comparison of the experimentally determined load distribution with that calculated by methods outlined in current Army specifications. Test airplane.

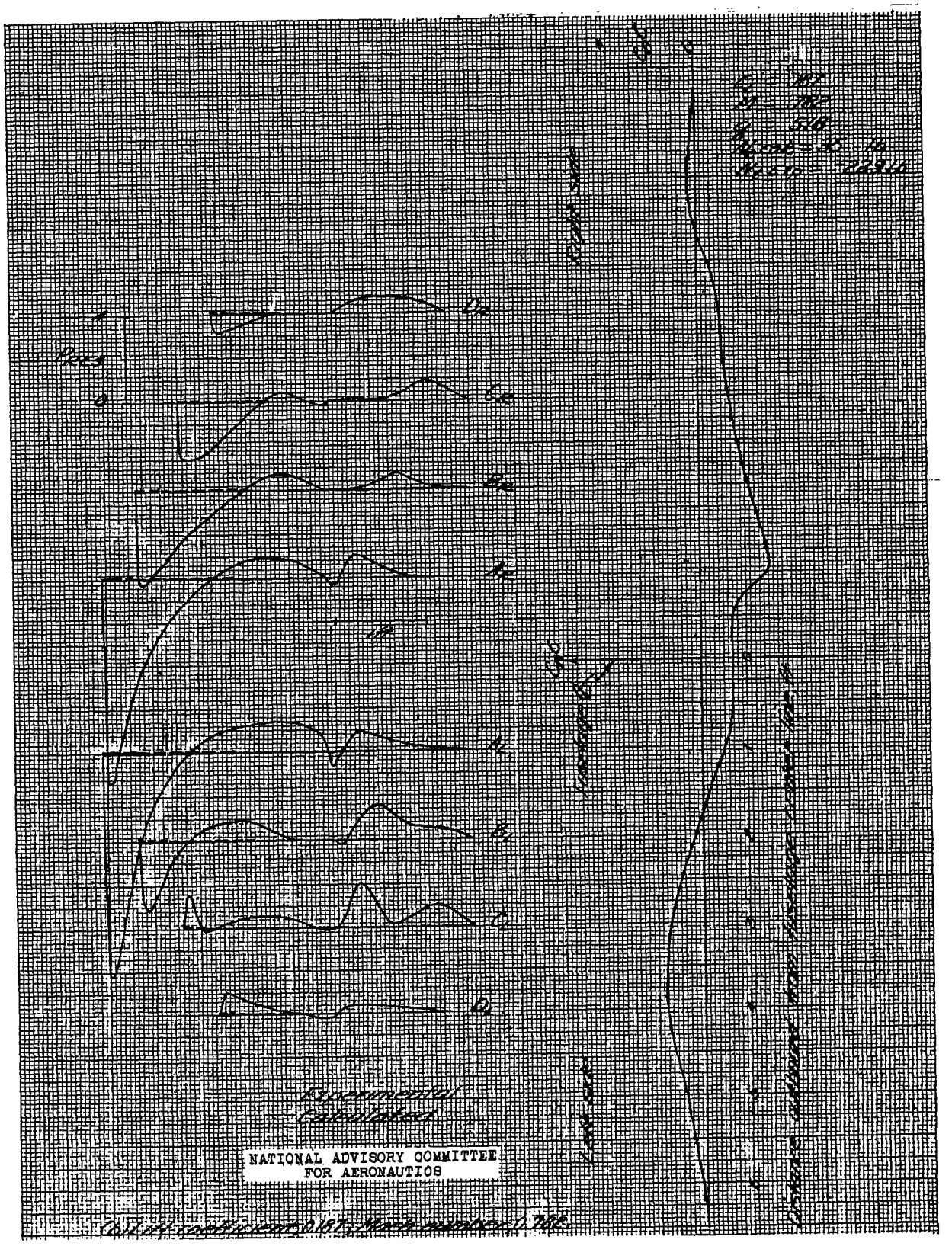

Figure 31.- Continued